**Project No. 410018**
**INE/AUTC 13.01**

# GEOPHYSICAL APPLICATIONS FOR ARCTIC/SUBARCTIC TRANSPORTATION PLANNING

## FINAL REPORT

Prepared for

**Alaska University Transportation Center**


William E. Schnabel[1]
Richard Fortier[2]
Mikhail Kanevskiy[1]
Jens Munk[3]
Yuri Shur[1]
Erin Trochim[1]

[1]University of Alaska Fairbanks
Water and Environmental Research Center
Fairbanks, Alaska

[2]Laval University
Center for Northern Studies
Quebec City, Quebec

[3]University of Alaska Anchorage
School of Engineering
Anchorage, Alaska


**July 2014**

## ACKNOWLEDGMENT OF SPONSORSHIP

This work was sponsored by the Alaska University Transportation Center, in cooperation with the U.S. Department of Transportation Research and Innovative Technology Administration and the Alaska Department of Transportation and Public Facilities.

## DISCLAIMER

**CONTENTS**

## LIST OF FIGURES

## LIST OF TABLES

## AUTHOR ACKNOWLEDGMENTS

The research reported herein was performed under AUTC Project Number 410018 by the Water and Environmental Research Center (WERC) at the University of Alaska Fairbanks (UAF) and by the School of Engineering at the University of Alaska Anchorage (UAA). The Water and Environmental Research Center was the contractor for the study, with the Alaska University Transportation Center serving as the Fiscal Administrator.

Dr. William E. Schnabel, P.E., Director of WERC, was the Project Director and co-Principal Investigator. The other authors of this report are Dr. Richard Fortier, Professor of Geology and Geological Engineering at Laval University, co-Principal Investigator; Dr. Mikhail Kanevskiy, Associate Professor of Research at the UAF Institute of Northern Engineering, co-Principal Investigator; Dr. Jens Munk, Professor of Electrical Engineering at the UAA School of Engineering, co-Principal Investigator; Dr. Yuri Shur, Professor of Civil Engineering at the UAF Department of Civil and Environmental Engineering, co-Principal Investigator; and Erin Trochim, Ph.D. candidate in Remote Sensing and Hydrology at UAF.

This work, which was coordinated and conducted through the integrated efforts of the co-Principal Investigators and overseen by Billy Conner, P.E., Director of AUTC, was performed in collaboration with the Alaska Department of Transportation and Public Facilities (ADOT&PF), with expert advice and technical coordination provided by Steve Masterman of the ADOT&PF Northern Region Design and Engineering Services. In addition, Kevin Bjella of the U.S. Army Corps of Engineers Cold Region Research and Engineering Laboratory contributed equipment, field assistance, and technical guidance towards the successful completion of this project. Finally, Bob McHattie of GZR Engineering provided expert technical review of the final report.

## ABSTRACT

This report describes a series of geophysical surveys conducted in conjunction with geotechnical investigations carried out by the Alaska Department of Transportation and Public Facilities. The purpose of the study was to evaluate the value of and potential uses for data collected via geophysical techniques with respect to ongoing investigations related to linear infrastructure. One or more techniques, including direct-current resistivity, capacitive-coupled resistivity, and ground-penetrating radar, were evaluated at sites in continuous and discontinuous permafrost zones. Results revealed that resistivity techniques adequately differentiate between frozen and unfrozen ground, and in some instances, were able to identify individual ice wedges in a frozen heterogeneous matrix. Capacitive-coupled resistivity was found to be extremely promising due to its relative mobility as compared with direct-current resistivity. Ground-penetrating radar was shown to be useful for evaluating the factors leading to subsidence in an existing road. Taken as a whole, the study results indicate that supplemental geophysical surveys may add to the quality of a geotechnical investigation by helping to optimize the placement of boreholes. Moreover, such surveys may reduce the overall investigation costs by reducing the number of boreholes required to characterize the subsurface.

## EXECUTIVE SUMMARY

The use of geophysical methods as a supplement to conventional geotechnical investigations for arctic and subarctic linear infrastructure was evaluated. Historically, geotechnical investigations have been based on borehole data that provide unequivocal subsurface information at discrete points along an alignment. These borehole data are usually supplemented and their locations guided by the process of terrain unit mapping. The terrain unit maps are based on interpretations of airphotos and satellite images. Terrain unit mapping assumes that the geomorphic, geological, and geotechnical properties of landforms are related and that they were affected by the same processes during their development.

In general, geophysical methods represent a suite of noninvasive instrumental techniques that can provide information that is more definitive than terrain unit maps alone, but less definitive than boreholes. Geophysical methods have the potential to increase the quality of a geotechnical investigation by positioning boreholes at locations that provide the most useful subsurface information. Geophysical methods also have the potential to reduce the cost of geotechnical investigations by decreasing the overall number of boreholes required.

Geophysical methods were selected to address problems related to permafrost. Questions deemed important included distinguishing between frozen and unfrozen ground, evaluating permafrost thickness, addressing the ice content of soils including the location of massive ice, identifying areas of saline soil, and delineating between different soil textures including bedrock. Hence, electrical profiling was selected as the primary geophysical method for use in this study. Electrical profiling can be used to detect changes in electrical resistivity based on water content, soil composition, thermal state, temperature, and soil cryostructure. Electrical profiling was completed via two types of electrical resistivity tomography (ERT): direct-current resistivity using galvanic contact (DCR-ERT) and capacitive-coupled resistivity (CCR-ERT). In addition, ground-penetrating radar (GPR) was evaluated for use in characterizing frost impacts on an existing road.

A defining characteristic of this study is its focus on the use of geophysical methods in areas underlain by continuous or discontinuous permafrost. Consequently, considerable effort was made to observe and describe the frozen subsurface using conventional borehole techniques. This approach was intended not only to provide the research team with ground truth information for the geophysical results, but also to provide the reader with detailed background information on permafrost properties. Understanding permafrost characteristics is an essential precursor for appropriate interpretation of geophysical results.

Permafrost was described using the cryofacies method, which quantifies permafrost formation using the close relationship between shape, size, and spatial pattern of ice inclusions in the soil. This information determines whether the permafrost is epigenetic (formed after soil aggradation) or syngenetic (formed at the same time as soil development). Epigenetic permafrost is typically ice-rich in the near surface, while syngenetic permafrost is typically silty (70–80% silt) and extremely ice-rich (may exceed 100–200% gravimetric water content). Ice wedges may be found through the entire thickness of syngenetic permafrost.

Concerns for highway infrastructure development are especially pertinent when building over yedoma, which is extremely ice-rich late Pleistocene syngenetic permafrost. Yedoma is

found in various areas of Alaska including the North Slope, Yukon River drainage basin, and Seward Peninsula. Near-surface permafrost properties including active layer development must be considered, since they directly relate to and control the development of hazardous processes including thermokarst and thermal erosion. Moreover, permafrost contains an ice-rich transition zone just below the average active layer. Minimal disturbance of this layer is important, as it plays a critical role in preventing underlying massive ice from thawing.

Two methods of drilling were used to obtain soil samples. The most common method used was augering (solid-stem). The advantage of this technique is that it is relatively inexpensive and fast, but it cannot be used to describe permafrost structure and properties in detail. Augering can detect massive ice, but only provides general information about soil texture due to periodic rather than continuous sampling. The alternative drilling method used was continuous coring, which is more time-consuming to obtain and analyze, but which provides high-quality information on cryostratigraphy. Continuous coring should be used selectively in studies where it is most beneficial to determine the nature of ground ice. Other typical quantitative measures include grain-size analysis, volumetric moisture content, and thaw strain analysis.

Four sites were analyzed: 9-Mile, Anaktuvuk, UAF Farm, and Goldstream Road. At the 9-Mile site, hollow-stem drilling was performed by the Alaska Department of Transportation and Public Facilities (ADOT&PF) and the Alaska University Transportation Center (AUTC) using a rig. These data were used to evaluate wedge-ice occurrence and distribution. Ground-penetrating radar, DCR-ERT, and CCR-ERT transects were performed on-site. At Anaktuvuk, hollow-stem drilling by University of Alaska Fairbanks (UAF) researchers was completed using a hand-operated Snow, Ice and Permafrost Research Establishment (SIPRE) corer. The geophysical technique used at Anaktuvuk was DCR-ERT. At the UAF Farm, DCR-ERT and CCR-ERT transects were collected with no complementary borehole information. At the Goldstream Road site, drilling and logging was completed by ADOT&PF; the geophysics data collected by this project were limited to GPR. Analysis of the Goldstream Road site was supplemented by CCR-ERT information collected by the U.S. Army Cold Regions Research and Engineering Laboratory (CRREL).

The data from 9-Mile were collected over a 5-year period (2 years of information from this study, and ancillary information collected during a previous study). The 9-Mile site allowed comparison of all three geophysical methods along a transect where permafrost was well characterized by information obtained from a dense array of boreholes. The CCR-ERT technique using a dipole-dipole array was found to be an efficient method at this site. Transects were successfully collected on top of the seasonal snowpack using a tracked all-terrain vehicle. In contrast, the DCR-ERT results were comparable but more time-consuming to obtain. The advantage of DCR-ERT is that it allows a greater degree of flexibility with respect to array configuration once contact is established. At the 9-Mile site, a Wenner array was used with DCR-ERT, but a dipole-dipole array was also possible. Results indicated that the array choice was an important component in characterizing ice-wedge distribution. A dipole-dipole array is more efficient in delineating vertical structures (used in CCR-ERT), while the Wenner is best suited for horizontal variations (DCR-ERT). Since the ice wedges in this region were more strikingly vertical features, the dipole-dipole results were a better representation. The GPR was not as useful at the 9-Mile site because the depth of penetration was limited to the near surface (1

to 2 m). This limitation could be resolved by using a lower frequency antenna system (with the trade-off of lower resolution) and/or obtaining measurements over a frozen surface to minimize conductivity.

At Anaktuvuk, fieldwork at four main alignment areas associated with the ADOT&PF Foothills West project was completed in September 2011. The only geophysical technique applied was DCR-ERT using a Wenner array and various spacing of electrodes to alter spatial resolution and depth of penetration. Drilling was completed along the survey transects to ground truth the geophysical results. DCR-ERT was able to separate regions of permafrost and nonpermafrost in and around floodplains and thermokarst areas. The coarser-resolution transects were not able to delineate individual areas of ice-rich permafrost in yedoma. DCR-ERT was affected by use of the Wenner array, where the variation was primarily vertical rather than horizontal. At higher resolutions where depth of penetration is shallowest, individual ice wedges could be isolated.

The UAF Farm site was used to compare CCR-ERT and DCR-ERT, obtained simultaneously at a well-studied location in March 2012. Unlike other sites, DCR-ERT was acquired using both a Wenner and a dipole-dipole array. CCR-ERT and DCR-ERT, both of which used the dipole-dipole array, had high lateral sensitivity that would be useful for ice wedges.

During spring 2012, GPR was collected in the Goldstream Road study area and compared against drilling completed by ADOT&PF the previous winter. Drainage conduits were visible in the GPR from Miles 5 to 6. In this section, the base of the asphalt concrete pavement could be inferred, and the lack of linearity suggested frost heaving over time. This interpretation was consistent with CCR-ERT data obtained by CRREL in a parallel project. CCR-ERT also indicated the presence of ice lenses. Miles 6 to 7 had lower overall values, likely a result of frozen ground instead of massive ice. The upper and lower boundaries of the road grade were visible in the GPR data. The nonconformity evident by differences between their relative positions suggests that subsidence has occurred.

This report is organized into four chapters. Chapter 1 provides a general summary of geotechnical investigative techniques applicable to arctic and subarctic conditions. This review is supplemented by a description of the types and origins of permafrost in Alaska to aid future technicians in the interpretation of geophysical results. Chapter 2 provides a detailed description of activities conducted and the technical results of this research. Chapter 3 contains a description of how geophysical methods similar to the ones used in this study can be integrated into future geotechnical investigations conducted by entities such as ADOT&PF. Chapter 3 also contains recommendations regarding which methods should be used to collect which types of data, general cost considerations, and possible benefits. Chapter 4 provides a synthesis of the data collected to present a set of conclusions and recommendations for further action.

# CHAPTER 1 – INTRODUCTION AND BACKGROUND

## INTRODUCTION

Exploratory geotechnical drilling methods tend to be relatively expensive and provide data for only a limited number of points along a linear transect. Geophysical methods such as electrical resistivity tomography (ERT) and ground-penetrating radar (GPR) have the potential to lower exploration costs, reduce the impacts of exploration, and investigate a considerably higher volume of the subsurface compared with drilling methods. Such geophysical methods are currently underutilized by transportation agencies including the Alaska Department of Transportation and Public Facilities (ADOT&PF), but could become important non-invasive subsurface investigation tools in the future as regionally specific protocols are developed for collecting and interpreting data.

While boreholes are still the most reliable form of subsurface investigation, they can be prohibitively expensive in cases where delineating small but significant ground features that could affect the performance of infrastructure is important for the design of linear infrastructure (Kawasaki and Osterkamp, 1984). Although geophysical methods will not likely replace borehole sampling as the primary means by which planners investigate the geological conditions beneath planned infrastructure components (ADOT&PF, 2007), ERT and GPR profiling can identify and provide the spatial extent of anomalous zones to guide and optimize the placement of boreholes. Thus, a geophysical investigation can help planners to decrease the cost of the drilling process by indicating the location and density of boreholes required in a given area. As ERT and GPR profiling represent low-cost and high-production-rate geophysical methods for assessing the spatial distribution of permafrost conditions and talik occurrence, these methods are well suited for arctic and subarctic linear projects such as roads, pipelines, and runways prior to borehole investigation.

This project explored the use of ERT and GPR techniques as means of optimizing borehole drilling during arctic/subarctic subsurface geotechnical investigations. In particular, the focus of this project was on the response and characteristics of frozen soil as they relate to geophysical methods. Since previous studies indicate that the presence of frozen soil confounds geophysical data during characterization of the subsurface (Golder, 2002), our intention was to evaluate frozen soil response.

This report provides a general description of methods of geotechnical investigations in cold regions, followed by a comprehensive presentation and discussion of field results obtained over the course of the study. The information is employed in a later chapter to develop a set of geophysical guidelines for practitioners in arctic/subarctic subsurface investigations. The report concludes with recommendations for further study and development. Additional data are provided in the appendix.

## METHODS OF GEOTECHNICAL INVESTIGATIONS

The existing approach to geotechnical investigations for highways in Alaska is based mostly on data obtained from drilling. The space between boreholes usually varies from 200 to 500 ft, a distance that can be shortened if needed (ADOT&PF, 2007). Although drilling with

such spacing may be acceptable for projects such as road renovation, it can be unfeasible for new construction of extensive roads. For example, a road 300 miles long requires more than 4000 boreholes. Our opinion is that the number of boreholes can be decreased significantly by using complementary methods of geotechnical investigations including geophysical surveys before the drilling campaign.

The ultimate goal of geotechnical investigations in the permafrost region is to provide comprehensive information on permafrost and geological conditions. This information should be sufficient for selection of the best route and for design of a stable and economically sound structure. A complex of methods that includes analysis of existing information and the preliminary terrain, geophysical surveys, and subsurface exploration has been developed through contemporary engineering science and practice in reaching this goal. Subsurface exploration usually in the form of drilling is the final step in the geotechnical investigation. In selecting a road alignment, studies preliminary to drilling are particularly important and should not be overlooked. Sources of preliminary information on terrain characteristics, surface geology, permafrost, and geotechnical conditions of an area of interest include topographic and geologic maps, especially maps of surface geology and engineering geology developed by the U.S. Geological Survey (USGS) and the Alaska Division of Geological and Geophysical Surveys (DGGS). For some areas such as the Beaufort Sea Coastal Plain, the Copper River Basin, and the Trans-Alaska Pipeline corridor, numerous reports and publications provide valuable preliminary information on permafrost and soil.

**Terrain Unit Mapping**

Interpretation of airphotos and satellite images is widely used in contemporary geotechnical investigations of permafrost regions because of the close relationship between permafrost properties and surface features. Many successful and economical geotechnical investigations, such as those for the Trans-Alaska Pipeline and numerous gas pipelines in Russia's arctic region, have been based on thorough airphoto interpretation of pipeline corridors and development of landform maps along the proposed pipeline route. Landforms differ along an extensive route, shaped by the hydrography and geologic history of a terrain. The assembly of landforms typical of the Arctic Coastal Plain is different from the assembly of landforms of the Arctic Foothills, and both differ from the landforms of the Brooks Range. On the other hand, the Arctic Foothills have landforms in common with landforms of the northern part of the Seward Peninsula. A preliminary map of landforms based on airphoto interpretation should be verified in the field by air reconnaissance and/or ground truthing. With sufficient preliminary information on permafrost and geology, a map of landforms can be used for development of a preliminary engineering-geology map.

Landform analysis is based on the ultimate assumption that geomorphic, geologic, and geotechnical properties of terrain patterns are closely related and that terrain patterns formed during the same time in the same climatic conditions, and affected by similar processes, have identical properties. Terrain pattern formation during identical climate is especially important in studying the permafrost region. For example, in Alaska, textures of soils of the contemporary floodplains in the continuous and discontinuous permafrost zones can be identical, but permafrost properties of soils including thermal state, ground ice content, existence of massive ice, and permafrost-related processes can be different. On the other hand, geotechnical

conditions of floodplains in the continuous permafrost zones of Arctic Alaska and East Siberia are identical.

As stated by the American Association of State Highway and Transportation Officials *Manual on Subsurface Investigations* (AASHTO, 1988, page 34),

> Two main types of surficial maps represent the state-of-the art engineering geological mapping for transportation systems: engineering unit maps and engineering maps. Both techniques recognize that the landform observed is the key to the nature and origin of the rock or soil material underlying the ground surface at that point, and that lateral and vertical extent of the units indicated by the form and lateral boundaries of each landform unit… Individual DOT regions may have established the general geomorphological and stratigraphic relations of the physiographic regions in which they operate.

Similarities in terrain pattern properties have been known to permafrost scientists and engineers for a long time (Yanovsky, 1933; Tumel, 1945), but a practical interest in landform analysis increased with the wide availability of aerial photographs and satellite imagery. Adaptation of these tools in landform analysis had a revolutionary effect on methods used for geotechnical investigations. The use of aerial photographs and satellite imagery developed into one of the most important parts of geotechnical investigations, becoming a preliminary stage in the process, preceding fieldwork. Interpretation of aerial photographs with identification of landforms results in a preliminary landform map. In areas where a similar approach has been used on other projects, such a map can be converted into terrain unit maps with a preliminary evaluation of geotechnical conditions including permafrost properties of landforms. It is often stated that geotechnical properties of soils can be directly identified by interpretation of aerial photographs. In reality, the success of this method is rather the exception than the rule. Such identification is only possible if an interpreter has knowledge of a region and experience in aerial photograph interpretation. Even then, important features such as individual, large ice masses (such as along Tok Cutoff) can be missed.

The term *landform* has several definitions, one of which is "A landform may be defined as a portion of the earth surface differing by its shape and their structural features from the neighboring portions. Mountains, valleys, plains and even swamps are landforms" (Krynine and Judd, 1957, page 81).

Two approaches are used in terrain analysis in contemporary geotechnical practice in permafrost regions: (1) Evaluation of geotechnical conditions of sites and routes based on airphoto interpretation and existing geotechnical information, and (2) development of a landform map as a base for geotechnical investigations at "key" sites of typical landforms and extrapolation of geotechnical data on other identical landforms. The first approach is useful at the preliminary stage of planning and at the design stage. The second approach is especially valuable for areas with limited or zero preliminary geotechnical information. The difference between these approaches has led to different understandings and uses of *landform*, as summarized by Kreig and Reger (1976, page 58):

> Some earth scientists and geographers prefer that this term (*landform*) be restricted to the description of topographic features, i.e., mountains, valleys, and

basins. But this particular use of “landform” is only of limited value in a geotechnical investigation, because it does not include a consideration of such three-dimensional properties as soil characteristics and other physical and environmental conditions at the surface and at depth. Although the word “form” indicates shape only, it has become generally acceptable to use the term “landform” to describe not only surface topography, but also the deposits comprising the feature.

This understanding of landforms is in agreement with the first approach of terrain analysis, which requires preliminary knowledge of geotechnical conditions of typical units identified by airphoto interpretation. Without such information (Approach 2), the airphoto interpretation reveals only a surface manifestation of landforms and patterns of their distribution in the area of interest.

An experienced interpreter of airphotos can evaluate some permafrost and soil features such as ice-wedge polygons, pingos, yedoma surfaces and their remnants, sand dunes, and slope slides. Airphoto interpretation can reveal features that may not be detected while working on the ground. Though particularly helpful in areas of tundra, airphoto interpretation provides useful information in forested areas as well.

A landform map developed by airphoto interpretation is an expression of the soil surface presented as an assembly of repeated landforms typical of a study area. Some landforms occupy most of an area; others occur at a few sites only. A correlation between landforms manifested on the soil surface and their subsurface properties can be effectively studied at so-called key sites.

A key site is the area that represents typical landforms. Figure 1,Figure 2, andFigure 3 show the landform map, the engineering-geological section, and the engineering-geological map of a key site. Detailed geophysical and subsurface investigations at a key site provide data on permafrost conditions and soil properties, and are used for calibration of geophysical methods by subsurface coring data. Geotechnical information obtained at key sites can be extrapolated on identical landforms. Geophysical investigations calibrated at key sites can be confidently used for continuous geophysical survey along a route.

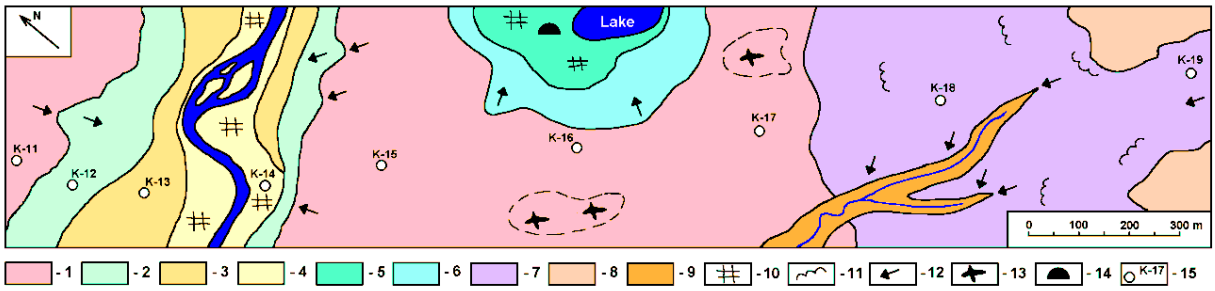


Figure 1. Landform map

1 – old alluvial terrace; 2 – slope of the alluvial terrace; 3 – abandoned floodplain; 4 – active floodplain; 5 – bottom of thaw-lake basin; 6 – slope of thaw-lake basin; 7 – solifluction slope (hillside); 8 – flat hilltop surface; 9 – thermal-erosional gully; 10 – active ice wedges forming low-centered polygons; 11 – solifluction; 12 – thermal erosion; 13 – thermokarst (partial ice-wedge degradation resulted in high-centered polygons formation); 14 – pingo; 15 – boreholes

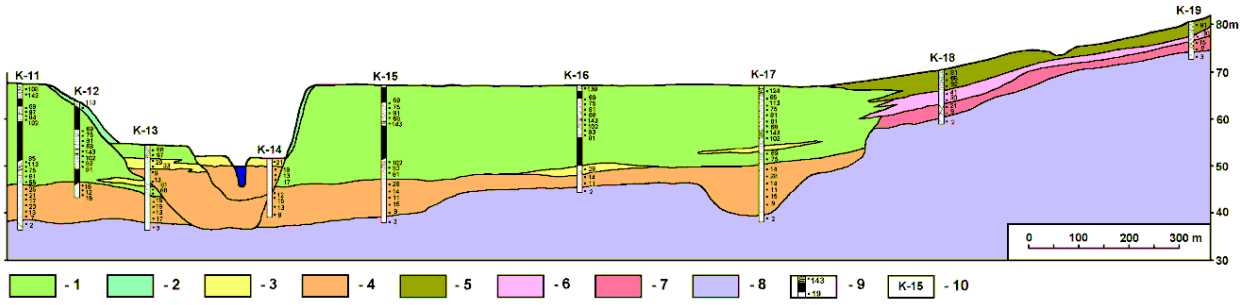


Figure 2. Engineering geological section

1 –ice-rich silt with syngenetic ice wedges; 2 – ice-poor silt; 3 – ice-poor sandy silt and silty sand; 4 – ice-poor sand and sandy gravel; 5 – ice-rich gravelly silt; 6 – ice-poor gravel with silt and sand; 7 – weathered bedrocks (schist, sandstone); 8 – competent bedrocks (schist, sandstone); 9 – cryostructure (ice is black) and gravimetric moisture content, %; 10 – borehole number

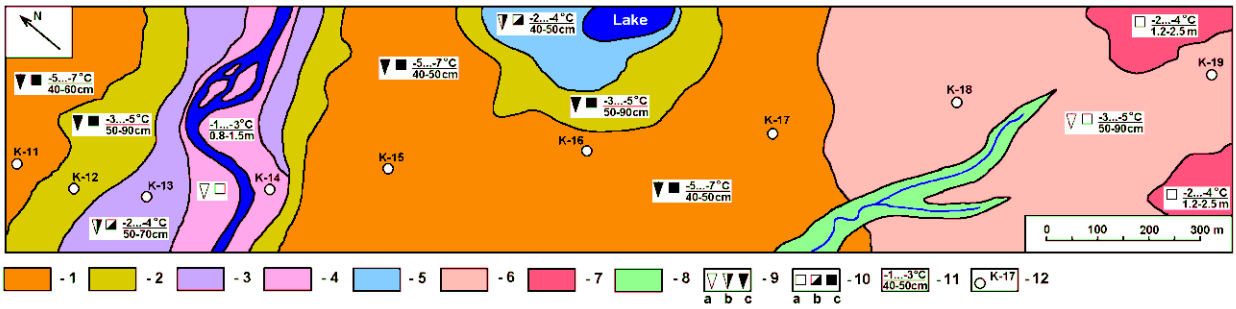


Figure 3. Engineering geological map

1 – Late Pleistocene ice-rich alluvial and reworked eolian silt with mostly inactive syngenetic ice wedges up to 20 m tall, underlain by alluvial sand and gravel; 2 – Holocene colluvial ice-poor silt up to 3 m thick, underlain by alluvial ice-rich silt with syngenetic ice wedges; 3 – Holocene ice-rich alluvial silt and silty sand with inactive and active syngenetic ice wedges up to 5 m tall, underlain by alluvial sand and gravel; 4 – modern ice-poor alluvial silt and silty sand with thin active epigenetic ice wedges up to 3 m tall, underlain by alluvial sand and gravel; 5 – Holocene and modern ice-rich peat with active syngenetic ice wedges up to 4 m tall, underlain by ice-poor lacustrine silt and thawed and refrozen alluvial silt; 6 – Holocene and modern ice-rich colluvial gravelly silt 3–4 m thick, underlain by ice-poor gravel and weathered bedrocks; 7 – Mesozoic weathered bedrocks (schist, sandstone); 8 – Holocene and modern colluvial and fluvial gravelly silt, underlain by ice-rich alluvial silt or ice-poor gravel and weathered bedrocks; 9 – ice-wedge volume: a < 5%, b – 5–15%, c – 15–35%; 10 – excess volume of segregated ice: a < 10%, b – 10–30%, c – 30–60%; 11 – permafrost temperature/active layer thickness; 12 – boreholes

## Geophysical Methods

The main goal of a geophysical survey as part of a geotechnical investigation is evaluation of the homogeneity of a studied geological body and the uncovering of heterogeneities in it. Experience with applications of geophysical methods in permafrost regions shows that these methods are effective in the following ways:

- Evaluation of areal distribution of perennially frozen and unfrozen soils and the boundaries between them.
- Evaluation of the permafrost table depth (especially in areas with a lowered permafrost table).
- Evaluation of permafrost thickness.
- Mapping of areas with high ice content of soils.
- Detection of areas with massive ice and its distribution.
- Detection of areas with saline soil.
- Finding boundaries between fine-grained soils, coarse-grained soils, and bedrock.
- Finding potential borrow material.

Geophysical methods used in geotechnical investigations in the permafrost region—electrical, seismic, magnetic, and gravity—uncover differences between properties of geological bodies in the earth's crust, and use of these methods is time- and cost-efficient. In general, geophysical methods are indirect. Direct evaluation of soil properties by geophysical methods is limited. To make a direct conclusion, geophysical data should be calibrated by using information on soil obtained by direct methods, such as trenching and drilling. The application of geophysical methods at a key site can be used for calibration, and the application of calibrated geophysical methods can be used for extrapolation of geotechnical data on similar landforms and for design of a drilling program. Geophysical methods, theoretically, can greatly reduce the number of boreholes.

The widest application of geophysical methods is electric profiling, which is based on the detection of changes in electrical resistivity of soil due to change in its composition, thermal state, temperature, and soil cryostructure (Table 1, Table 2, and Table 3 and Figure 4, Figure 5, and Figure 6). Soil particles are practically nonconductive, and the electrical properties of soils are controlled by water in unfrozen soils and by unfrozen water in frozen soils. The amount of unfrozen water depends mainly on the texture, temperature, salinity, and cryogenic structure (cryostructure) of a frozen soil.

Table 1. Typical electrical resistivity of (unfrozen) earth materials (from Engineer manual 1110-1-1802)

| Soil or rock | Electrical resistivity ohm*m |
|---|---|
| Clay | 1–20 |
| Sand, wet to moist | 20–200 |
| Shale | 1–500 |
| Porous limestone | 100–1,000 |
| Dense limestone | 100–1,000,000 |
| Metamorphic rocks | 50–1,000,000 |
| Igneous rocks | 100–1,000,000 |

Table 2. Electrical resistivity (ohm-m) of non-saline soils in West Siberia (from Melnikov and Dubikov, 1986)

| | | Frozen soil with cryostructure | |
|---|---|---|---|
| Soil | Unfrozen soil | Massive (pore ice) | Ataxitic (suspended) |
| Silty clay | 20–100 | 100–800 | 300–20,000 |
| Peat | 200–600 | | 1,000–100,000 |
| Sand | 100–100,000 | 500–200,000 | |

Table 3. Observed electrical resistivity of rocks and soils (from Frolov, 2005)

| | ρ, K ohm*m | | Temperature |
|---|---|---|---|
| Rock and soil | Unfrozen ground | Frozen ground | of frozen ground, °C |
| **Bedrock** | | | |
| Granite, gneiss, shale: | | | |
| *highly fractured* | 0.15–1 | 1.5–10 | 0 to -2 |
| *slightly fractured* | 12–30 | 50–100 | 0 to -3 |
| Dolomite, limestone, marl | | | |
| *fractured* | 0.5–2 | 5–10 | 0 to -2 |
| *dense* | 6–9 | 19–36 | |
| Sandstone | | | |
| *fractured* | 0.1–0.5 | 0.9–1 | 0 to -2 |
| *solid* | 1.0–1.5 | 3–15 | |
| **Soil** | | | |
| Sand with silt and some gravel (pore ice) | 0.1–0.12 | 0.7–1.0 | -0.5 |
| Gravel (pore ice) | 0.07–0.18 | 3–15 | -1 to -5 |
| Silty clay (layered and reticulate cryostructure) | 0.05–0.1 | 2–5 | -1 |
| Silty clay: | | | |
| *pore ice* | 0.02–0.1 | 0.2–3 | -0.2 to -7 |
| *reticulate cryostructure* | | 0.2–40 | -1.0 to -8 |
| *ataxitic (suspended)* | | 3.0–100 | -0.2 to -7 |
| Silty sand (lenticulate cryostructure) | | 0.5–5 | -0.2 to -7 |
| Coarse sand: | | | |
| *with pore ice* | | 0.8–100 | -0.2 to -7 |
| *with segregated ice* | | 20–300 | -0.2 to -6 |
| Peat | | 0.2–40 | -0.2 to -3 |
| Ground ice | | $3*10^3$ | -2 |
| River ice | | $0.6*10^3$ | -6 |
| Sea ice of different age and structure | | 0.03–0.35 | -2 to -8 |

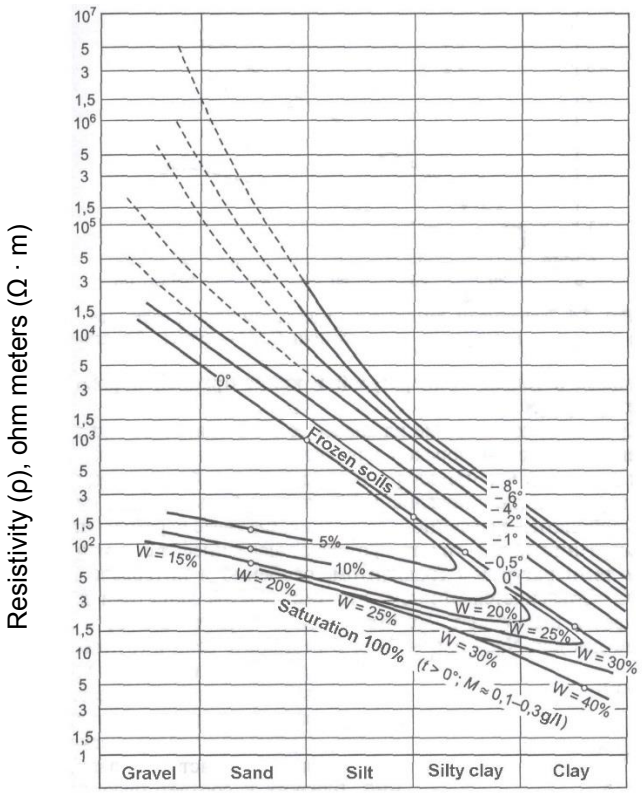


Figure 4. Electrical resistivity of unfrozen and frozen soils as a function of water content and temperature (from Zykov, 2007)

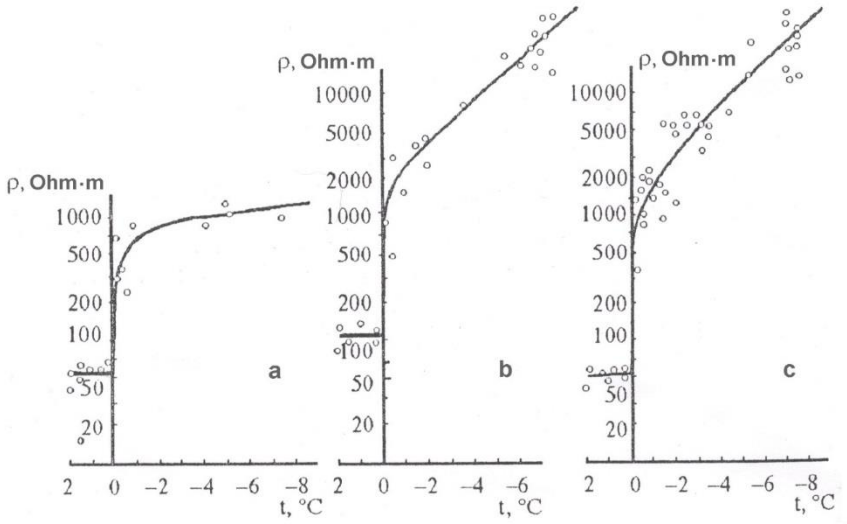


Figure 5. Electrical resistivity of soils as a function of temperature (from Frolov, 2005) a) Silt and silty clay with pore ice, b) Silty sand with pore ice, and c) Silty clay with segregated ice

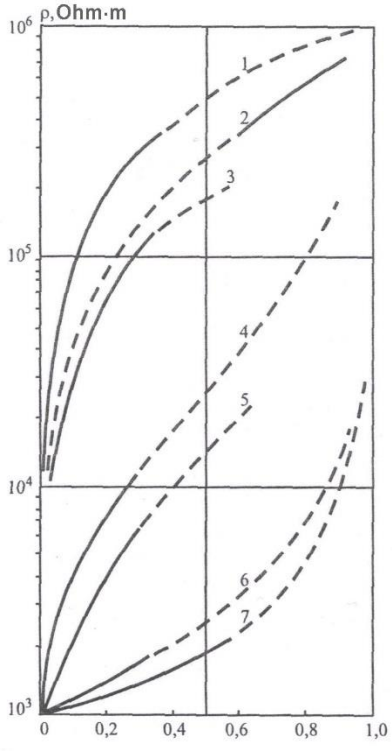


Figure 6. Electrical resistivity of frozen soils as a function of volumetric ice content and cryostructure (from Zhestkova and Shur, 1982)

1– layered cryostructure (current perpendicular to ice layers); 2 – ataxitic (suspended) cryostructure; 3 – reticulate cryostructure; 4 – lenticular cryostructure; 5 – incomplete reticulate cryostructure; 6 – porphyritic cryostructure; 7 – layered cryostructure (current along ice layers). Solid parts of lines show most common range of volumetric ice content for soils with cryostructure

Data in Table 1, Table 2, and Table 3 show that the electrical resistivity of soil and rocks varies widely. Conductivity is the reciprocal of resistivity; both measurements indicate the ability of a material to conduct electrical current. The wide variation is due to (1) the different volume of water in unfrozen soil and the different volume of unfrozen water and cryostructure in the frozen state, and (2) the difference between the electrical conductivity of soil as a physical property of soil and the apparent electrical conductivity derived from field geophysical surveys. Both of these causes limit the application of published data to specific projects, which is why a field calibration by geophysical methods at a key site greatly increases their value.

Use of geophysical methods can be extremely valuable in areas with saline soil. Geophysical methods can identify pockets of brine in permafrost. The soil in pockets of brine is much weaker than the surrounding soil. Miller and Johnson (1990) described settlement of the State Courthouse in Barrow, Alaska, as weak spots in the foundation soil due to brine pockets that were not identified during geotechnical investigations. Electrical resistivity of saline soil is shown in Figure 7. At the Barrow site, the salinity of pore water was from 20 to 60 ppt (or g/l). According to Figure 7, electrical resistivity of soil with such salinity should be less than 100 ohm*m. Such soil could be easily detected by electrical profiling.

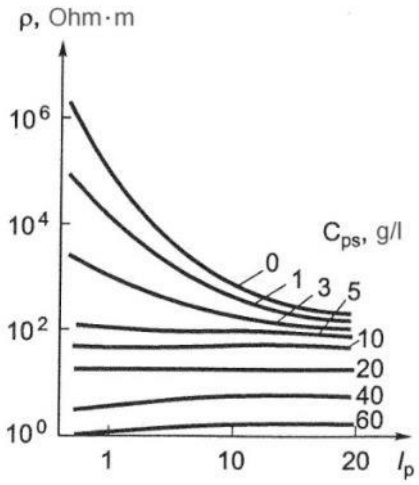


Figure 7. Dependence of electrical resistivity of saline permafrost soil on concentration of pore water and soil; Plasticity Index at soil temperature -5°C (from Zykov, 2007)

**Drilling and Logging**

In areas where natural or artificial permafrost exposures are rare, drilling becomes a main source of geotechnical information. The common practice of geotechnical investigation in permafrost areas of Alaska includes augering (solid-stem drilling) as a main drilling method and sampling of frozen soils with split spoons. Solid-stem drilling is relatively inexpensive and very fast, but soil description and samples obtained from the auger cuttings cannot be used for appropriate evaluation of permafrost structure and properties. This method of drilling detects massive ground ice distribution in boreholes, but it provides general information only on the soil texture and moisture content. In many boreholes, core samples are obtained at pre-defined depths by replacing the solid-stem auger with a hollow-stem auger fitted with a split-spoon sampling device over short depth intervals. These samples are suitable for describing cryogenic structure, evaluating visible ice volume, and soil testing; but information from several samples cannot be extrapolated to the whole section. To obtain reliable geotechnical information, we strongly recommend drilling boreholes using continuous-coring methods in at least some part of a study area. A detailed description of boreholes helps clarify permafrost structure and origin, and furthers the study of frozen soils properties with undisturbed samples.

Without a good-quality core, it is impossible to distinguish the nature of ground ice. For example, massive ice bodies encountered by augering at different depths can be interpreted either as layers of tabular massive ice (Figure 8a) or as syngenetic ice wedges (Figure 8b). This problem can be solved only by studying undisturbed samples of ice obtained by a SIPRE corer, moderately disturbed samples of ice obtained by split spoons via hollow-stem augering, or direct-push Geoprobe drilling. Typical wedge ice has a foliated structure and numerous air bubbles (Figure 9). Vertical foliation of ice is formed by particles of silt and organic matter that penetrate the ice body, with water coming through the frost (contraction) cracks in springtime. Wedge ice usually has a gray to yellow color, depending on the color of the soil particles.

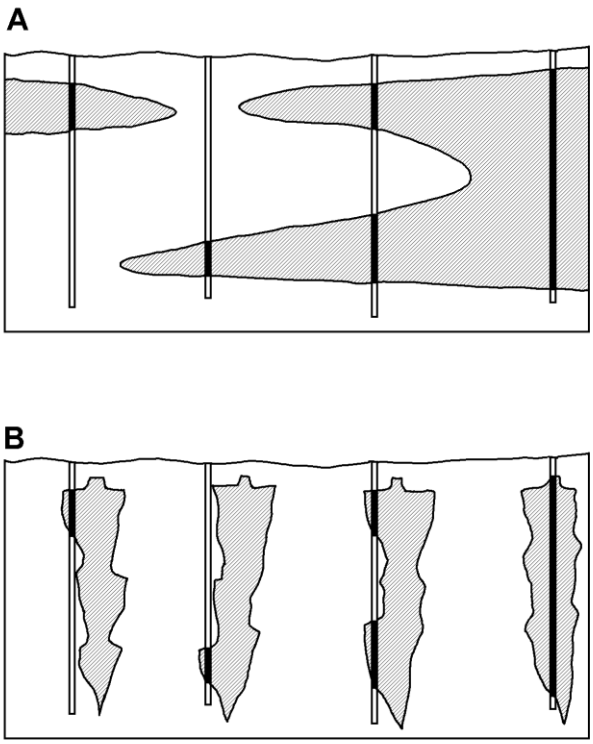


Figure 8. Alternative interpretations of massive ice bodies based on drilling results
a) tabular massive ice; b) syngenetic ice wedges

Figure 9. Appearance of wedge ice, sample obtained by SIPRE corer
(9-Mile Hill area, Dalton Highway, Alaska)

**Soil Testing**

Grain-size analyses of sediments are performed with sieves and hydrometers (ASTM D422, 1998). The ice content of frozen soil is evaluated by oven-drying (90°C, 72 h) samples. Gravimetric moisture content is calculated on a dry-weight basis. Volumetric moisture content is calculated as the ratio of the volume of ice (mass of the ice in a sample = 0.9 g/cm$^3$) to the volume of the whole sample (van Everdingen, 1998). For volumetric moisture content, samples of frozen core with a cylindrical shape should be prepared for the most precise volume calculations. For ice-rich soils, thaw strain analysis can be performed. Thaw strain (the amount that frozen ground compresses thawing) is equal to thaw settlement divided by the original thickness of the frozen ground before thawing (van Everdingen, 1998).

## OVERVIEW OF PERMAFROST CHARACTERISTICS

For geotechnical investigations in areas of ice-rich permafrost, specific methods of permafrost field studies have been successfully applied. We used the cryofacies method (Katasonov, 1969, 1978), a method based on the close relationship between shape, size, and spatial pattern of ice inclusions in soils (i.e., cryostructures) and specific terrain units, which reveal the nature of permafrost formation. Study of cryostructures allows for the identification of the nature of permafrost and the estimation of ice distribution within it. The cryofacies method has been especially useful in the study of syngenetic permafrost (Katasonov, 1969, 1978; Shur and Jorgenson, 1998; Kanevskiy et al., 2008, 2011a). For description of soil cryogenic structure, we used a classification of cryostructures (patterns formed by ice inclusions in the frozen soil) that has been adapted from several Russian and North American classifications (Gasanov, 1963; Katasonov, 1969; Kudryavtsev, 1978; Zhestkova, 1982; Shur and Jorgenson, 1998; French and Shur, 2010). A simplified classification of the cryostructures of mineral soils is shown in Figure 10.

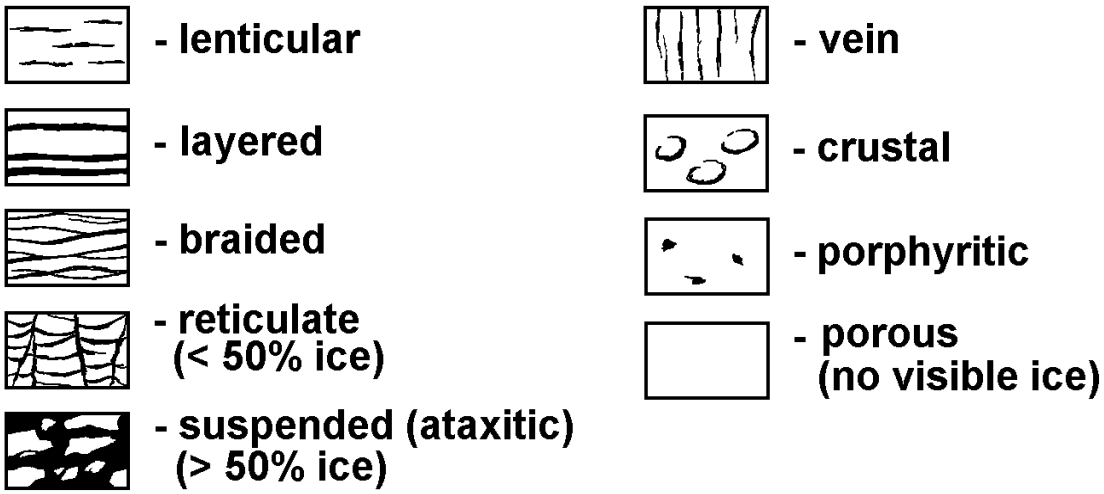


Figure 10. Simplified classification of the cryostructures of mineral soils (ice is black)

Different types of permafrost have different cryogenic structures. There are two main types of permafrost: epigenetic and syngenetic (Figure 11). These permafrost types are characterized by

differing mechanisms of formation, structure, and properties. Permafrost usually can be distinguished by its cryogenic structure, which is formed within perennially frozen soils by inclusions of pore, segregated, and massive ice.

*Epigenetic permafrost* forms through lowering of the permafrost base in previously deposited sediment or other earth material (van Everdingen, 1998). Aggradation of epigenetic permafrost proceeds downward. Epigenetic freezing of unconsolidated saturated soils results in accumulation of ice mostly in the upper part of the section (Figure 11a). Ice distribution relates to the rate of freezing, which slows with depth. Generally, when no additional sources of water are available, the ice content of the epigenetically frozen soil decreases with depth, and the density of the ice increases.

*Syngenetic permafrost* forms through rising of the permafrost table during the deposition of additional sediment or other earth material on the ground surface (van Everdingen, 1998). Syngenetic permafrost formation is a complex process related to sedimentation in cold conditions, when the base of the active layer rises following accumulation of new sediment on the soil surface. The mechanism of syngenetic permafrost formation is illustrated in Figure 11b, based on the scheme suggested by Popov (1967). According to this scheme, syngenetic permafrost formation is connected to the consequential addition of bottom portions of the frozen active layer to permafrost, which occurs with new sediment accumulation on the soil surface.

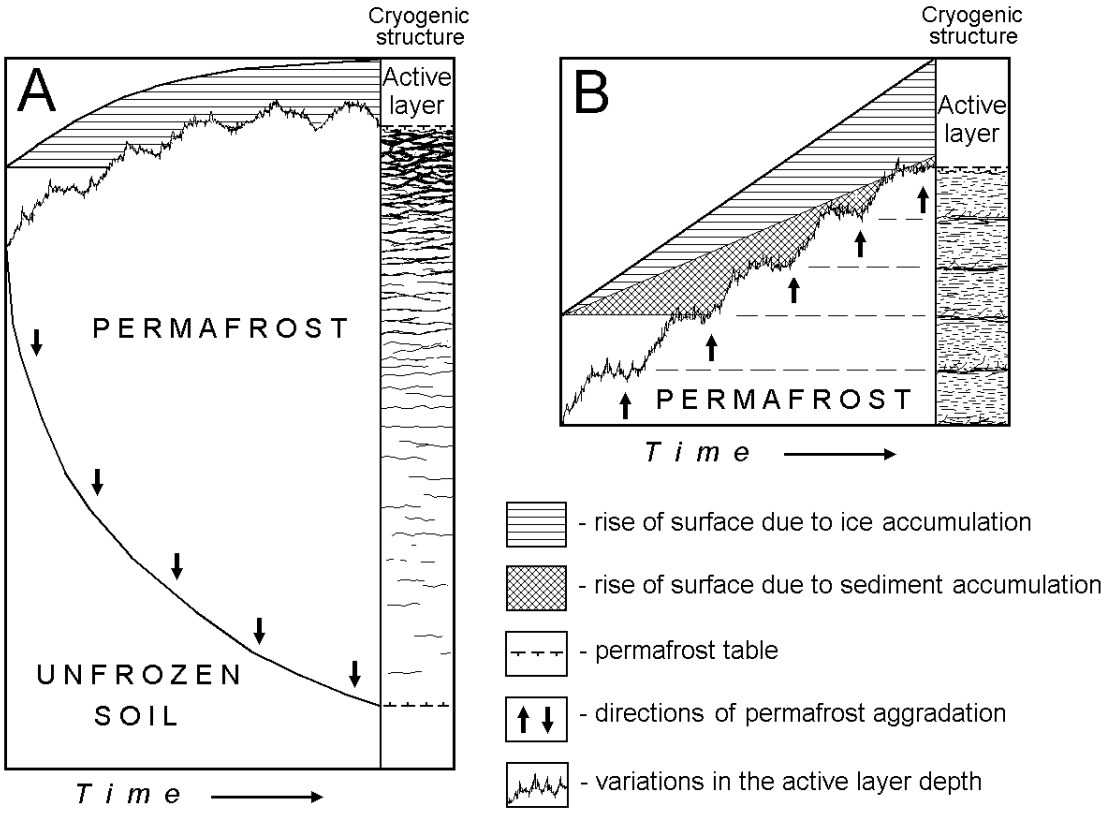


Figure 11. Mechanisms of formation of epigenetic (a) and syngenetic (b) permafrost

Syngenetic permafrost forms in response to sedimentation (alluvial, slope, aeolian, lacustrine, etc.) that causes the base of the active layer to aggrade upwards. Transformation of a part of the active layer into a perennially frozen state occurs virtually simultaneously with sedimentation. Typically, syngenetically frozen sediments are silty or loess-like (70–80% silt fraction) and ice-rich (the soil gravimetric moisture content may exceed 100–200%). Syngenetically frozen sediments contain significant amounts of organic matter and buried peat horizons, and have rhythmically organized, generally layered cryogenic structures. The occurrence of almost undecomposed rootlets indicates a relatively small gap in time between sedimentation and freezing of sediments.

Syngenetic permafrost is usually extremely ice-rich and contains ice wedges throughout its entire thickness. Several systems of ice wedges, which can be found at different depths, are also common. Formation of ice wedges is triggered by repeated contraction cracking of the soil (Leffingwell, 1915; Lachenbruch, 1962; Popov, 1967; Romanovskii, 1993). During abrupt temperature drops during winter, the frozen soil contracts and forms a crack up to 2 cm wide. The following spring, surface water flows into the crack and freezes. Because ice is weaker than the surrounding frozen soil, a crack forms in the same place the following winter, and the process repeats itself. Thickening of ice wedges causes deformation of previously accumulated sediments and development of inclined and even vertically oriented cryostructures.

In contrast to epigenetic permafrost, in which ice wedges rarely exceed 10–15 ft (4–5 m) in depth, ice wedges in syngenetic permafrost may extend through the entire strata, reaching 30–140 ft (10–50 m) in depth and 6–17 ft (2–6 m) in width. This varying width and depth reflect different rates of sedimentation and climate conditions. In syngenetic permafrost, wedge ice can occupy 20–50% (and even more in some cases) of the total section.

The main cryostructure of syngenetic permafrost is micro-lenticular (Shur et al., 2004; Kanevskiy, 1991, 2003; Kanevskiy et al., 2008, 2011a). The term *lenticular* is used in several existing classifications of cryostructure (e.g., Zhestkova, 1982; Popov et al., 1985; Murton and French, 1994; Melnikov and Spesivtsev, 2000; French, 2007). *Micro-lenticular* generally means the occurrence of very small subhorizontal (sometimes wavy), relatively short ice lenses. The thickness of uniformly distributed ice lenses (and spacing between them as well) usually does not exceed 0.5 mm. Inexperienced observers often do not pay enough attention to recognition of numerous but tiny ice inclusions, describing soil with such a cryostructure as without visible ice.

Our studies in Russia and Alaska show several varieties of cryostructure similar to micro-lenticular, which often appear similar (because of the small size of the ice lenses), but after thorough examination, reveal significant differences. We term these varieties *micro-cryostructures* (Kanevskiy et al., 2011a). Frequently, instead of seeing short, separate lenses, we observe rather long, wavy intercrossing ice layers with lens-like thickenings (i.e., such cryostructure has a braided appearance). Sometimes we notice tiny elongated mineral blocks suspended in the ice. Thus, we can distinguish the following sequence of closely related cryostructures (ranked approximately in the order of the ice content increase): latent micro-lenticular, micro-porphyritic (porous visible), micro-lenticular, micro-layered lenticular, micro-layered, micro-braided lenticular, micro-braided, and micro-ataxitic (suspended). In many sections, these micro-cryostructures easily transform into each other.

Figure 12 shows generalized images of these micro-cryostructure varieties. Minute ice inclusions, especially for latent micro-lenticular and micro-porphyritic cryostructures, make it difficult to distinguish the occurrence of ice lenses. Ice lenses often reveal themselves in the core only when it is partly melted, which explains why such cryostructures are often distinguished as porous invisible (or structureless, according to Murton and French, 1994).

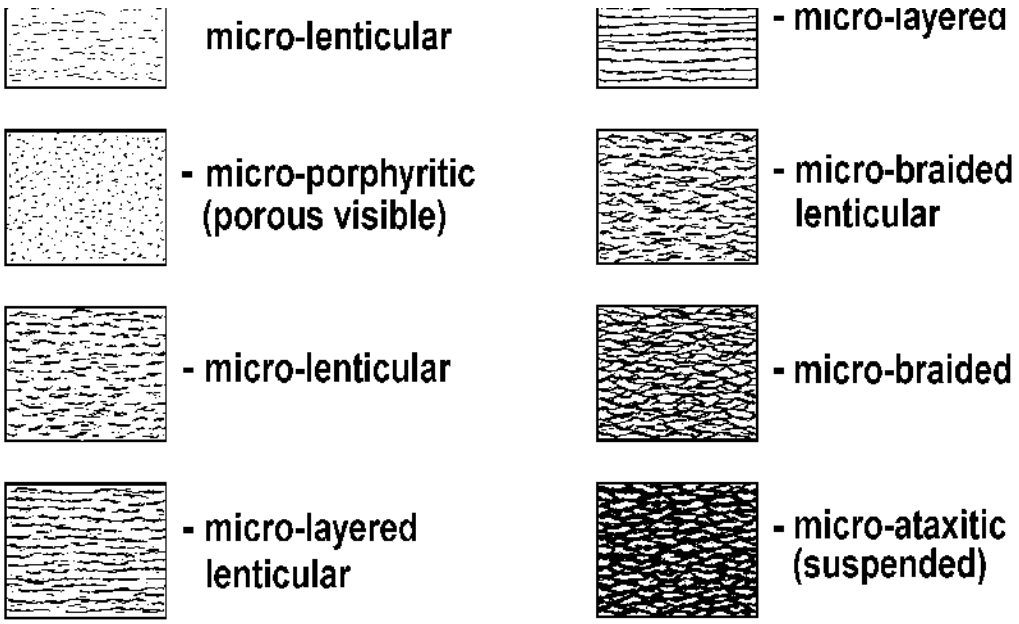


Figure 12. Micro-cryostructures typical of syngenetic permafrost (ice is black) (from Kanevskiy et al., 2011a)

Micro-cryostructures are most typical for syngenetic permafrost and usually form not less than 60% of the entire thickness of such sections (Kanevskiy, 1991, 2003). The ice content of sediments with a micro-lenticular cryostructure can be very high, despite the small size of the ice lenses. Gravimetric moisture content for such sediments varies from 35–50% (for latent micro-lenticular and micro-porphyritic cryostructures) up to 200% and even more (for micro-ataxitic cryostructure). The other feature typical of syngenetic permafrost is the occurrence of distinct layers of ice from several millimeters to several centimeters thick (referred to as ice belts in the Russian permafrost literature). Belts usually divide layers of micro-cryostructures that are more or less uniform (Figure 12).

**Yedoma in Alaska**

Extremely ice-rich late Pleistocene syngenetic permafrost, known in permafrost literature as yedoma, is abundant in various parts of Alaska. Soils of yedoma typically contain about 70% silt, and buried organic-rich horizons are common. Formation of yedoma occurred with the accumulation of a high volume of segregated ice that formed a specific set of cryostructures. Large ice wedges penetrate the entire section of yedoma. The width of ice wedges in syngenetic permafrost can reach 3 to 6 m and even more. At some locations, the thickness of syngenetic permafrost with huge ice wedges can reach 30–40 m. The volume of wedge ice frequently exceeds 50–60%, over half the proportion of sediment. The most impressive section of yedoma

in Alaska was studied in the 34 m high exposure along the Itkillik River (Kanevskiy et al., 2011a,b). A general view of this exposure (69°34′ N, 150°52′ W) is shown in Figure 13.

Figure 13. Overview of the Itkillik River exposure, August 2011

Our preliminary map of yedoma occurrence in Alaska (Figure 14) shows that yedoma is widespread across both arctic and boreal regions. Yedoma is abundant along the lower portion of the Arctic Foothills, in the northern part of the Seward Peninsula, and in numerous areas in Interior Alaska. Data for the map combine our field observations in different parts of Alaska, an analysis of satellite and aerial imagery, and an analysis of published sources.

**Near-Surface Permafrost**

Properties of the upper part of permafrost are especially important because permafrost behavior (and first of all the development of thermokarst, thermal erosion, and other hazardous processes) strongly depends on properties of the near-surface permafrost. The concept of a transition zone (Shur et al., 2005) helps to describe the interactions between the active layer and the permafrost. The upper part of the transition zone is known as the transient layer that is typically a part of the uppermost permafrost but which, under certain conditions, occasionally joins the active layer (Yanovsky, 1933). During most warm years, the transient layer protects the underlying ice-rich soils from thawing. The relative thickness of the transient layer varies widely

depending on climate and soil, and in some cases can exceed 30% of the active layer thickness (Shur et al., 2005).

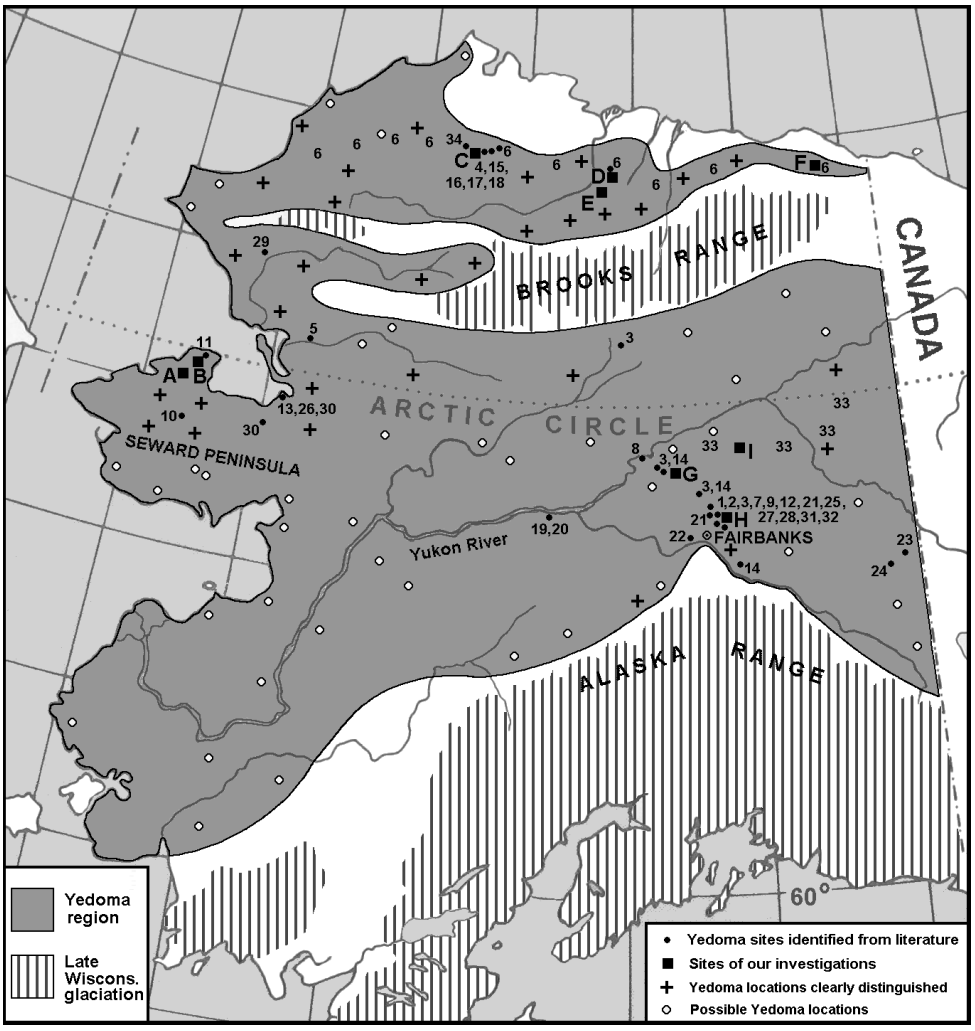


Figure 14. Preliminary map of yedoma distribution in Alaska (from Kanevskiy et al., 2011a) Yedoma sites identified from the literature sources: 1. Black 1978; 2. Bray et al. 2006; 3. Brown and Kreig 1983; 4. Brewer et al. 1993; 5. Cantwell 1887; 6. Carter 1988; 7. Fortier et al. 2008; 8. Hamilton 1979; 9. Hamilton et al. 1988; 10. Hopkins 1963; 11. Hopkins and Kidd 1988; 12. Kanevskiy et al. 2008; 13. Kotzebue 1821; 14. Kreig and Reger 1982; 15. Lawson 1982; 16. Lawson 1983; 17. Lawson 1986; 18. Livingstone et al. 1958; 19. Maddren 1905; 20. Matheus et al. 2003; 21. Meyer et al. 2008; 22. Péwé 1975; 23. Porter 1986; 24. Porter 1988; 25. Prindle 1913; 26. Quackenbush 1909; 27. Sellmann 1967; 28. Shur et al. 2004; 29. Smith 1913; 30. Taber 1943; 31. Tuck 1940; 32. Wilkerson 1932; 33. Williams 1962; 34. Williams and Yeend 1979. Sites of our field investigations: A – Devil Mountains; B – Cape Espenberg; C – Oumalik; D – Itkillik River; E – Umiat; F – Jago River; G – Erickson Creek, Hess Creek; H – CRREL Permafrost tunnel; I – Boot Lake. Other yedoma locations are identified based on analysis of satellite and aerial imagery. Limits of late Wisconsinan glaciation are shown after Péwé 1975; Hamilton 1994.

The lower part of the transition zone is formed by the ice-rich intermediate layer (Shur, 1988a,b), the structure and properties of which have provided stability for late Pleistocene permafrost during the last 10,000 years in a climate much warmer than during its formation. The

intermediate layer forms because of a gradual decrease of the active layer thickness after termination of sedimentation (Shur, 1988a,b). A decrease in active layer thickness can be connected with a succession of vegetation, changes of surface conditions, and various local factors. As a result, a significant part of the active layer transforms into a perennially frozen state due to freezing from below. Along with this process, the surface rises gradually because of ice formation in the freezing layer. This process resembles syngenetic permafrost formation, but without continuing sedimentation on the surface.

The intermediate layer, which is extremely ice-rich, is characterized by thick, up to 0.5 ft (10–15 cm) ice belts and specific cryostructures (ataxitic and reticulate mostly) with relatively thick (1–2 cm) ice lenses. In conditions of relatively warm permafrost (including the climatic conditions of Interior Alaska), however, micro-braided and micro-ataxitic cryostructures are more typical of the intermediate layer. The intermediate layer is widespread in different permafrost regions; its thickness usually varies from 2–5 ft (0.5–1.5 m).

The intermediate layer divides the transient layer from the original permafrost and prevents massive ice from thawing. This protective role of the intermediate layer is especially important for the conservation of ice-rich syngenetic permafrost with large ice wedges (Shur, 1988a). Besides the contemporary intermediate layer, buried intermediate layers often occur at various depths in sections of syngenetic permafrost as lenses and layers of extremely ice-rich soil with a thickness of 6–10 ft (2–3 m) (Kanevskiy, 1991, 2003). These layers usually correspond to periods of termination or slowdown of sedimentation, which are often related to changes of surface conditions. In many cases such layers can be found beneath organic-rich horizons (buried soils); frequently they overlay buried ice wedges.

A general sketch of soil sequence common in ice-rich syngenetic permafrost is shown in Figure 15, which also illustrates the structure of upper permafrost (including transient and intermediate layers) and the typical distribution of wedge ice and segregated ice.

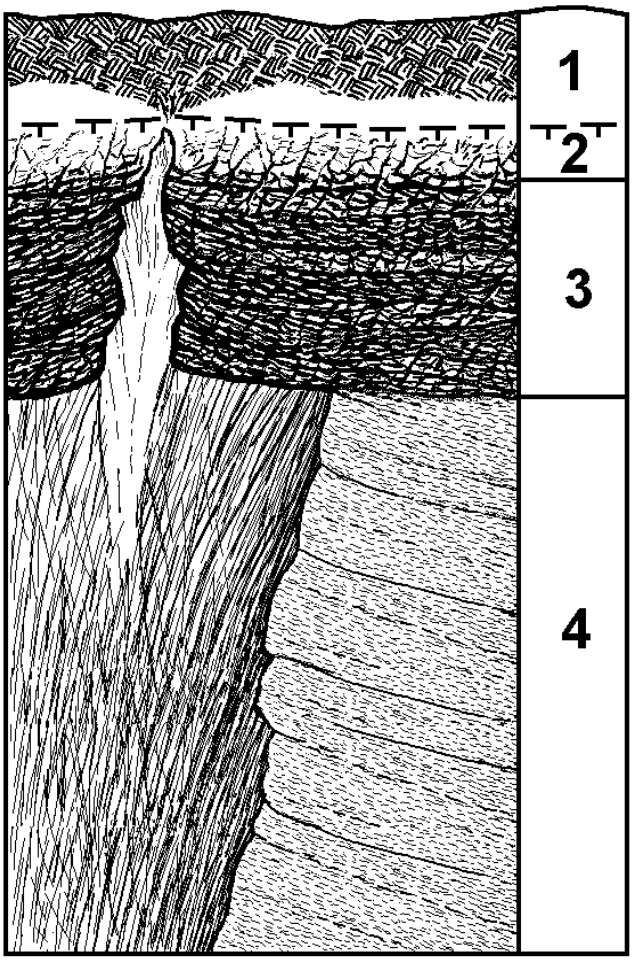


Figure 15. Typical sequence of the upper part of ice-rich syngenetic permafrost
1 – Active layer; 2 – Transient layer; 3 – Intermediate layer with thin contemporary ice wedge; prevailing cryostructures – ataxitic and reticulate; 4 – Late Pleistocene syngenetic permafrost with big buried ice wedge; prevailing cryostructure – micro-lenticular

# CHAPTER 2 – PROJECT FIELD RESULTS

## FIELD ACTIVITIES AND TIMELINE

This study was based on five field deployments throughout northern Alaska (Figure 16) conducted over approximately two years (Table 4). In most field efforts, multiple techniques were used to characterize the subsurface. The field activities, dates, and geophysical methods investigated are provided in Table 4.

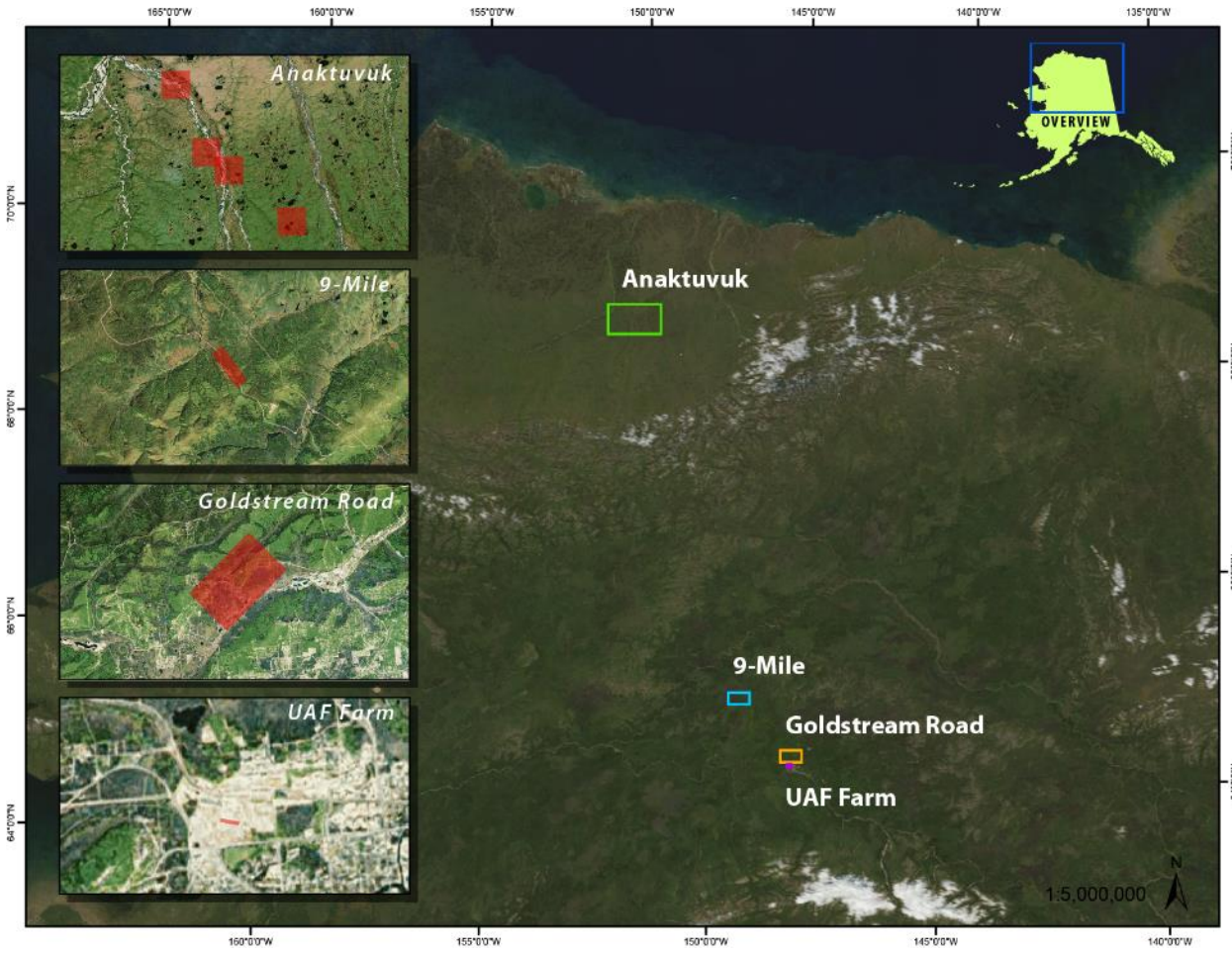


Figure 16. Locations of field sites in northern Alaska

Table 4. Summary of field activities

| Field Activity | Location Description | Date of Activity | Methods Employed* |
|---|---|---|---|
| 9-Mile Field Survey | New highway alignment at Dalton Highway, Mile 9, Alaska. Boreal forest underlain by discontinuous permafrost. | May 2010 | CCR, DCR, GPR, Borehole data |
| Anaktuvuk Field Survey | Anaktuvuk River basin near Umiat, Alaska. Tussock tundra underlain by continuous permafrost. | September 2010 | DCR, Borehole data |
| UAF Farm Survey | Cultivated farm field on UAF campus. Fairbanks, AK. | March 2011 | CCR, DCR |
| 9-Mile Revisit | New highway alignment at Dalton Highway, Mile 9, Alaska. Boreal forest underlain by permafrost. | March 2011 | CCR, Borehole data |
| Goldstream Road Survey | Paved road near Fairbanks, AK. Boreal forest underlain by discontinuous permafrost. | April 2012 | GPR, Borehole data |

* Methods include capacitive-coupled resistivity (CCR), direct-current resistivity (DCR), ground-penetrating radar (GPR), and analysis of existing or newly derived borehole data.

## GEOPHYSICAL INSTRUMENTATION EMPLOYED

The geophysical surveys performed during this study are ground-penetrating radar (GPR) profiling and two types of electrical resistivity tomography (ERT). The two types of ERT are (1) direct-current resistivity using galvanic contact through steel electrodes driven into the ground (the standard method, DCR-ERT), and (2) capacitive-coupled resistivity (CCR-ERT; Timofeev et al., 1994; Kuras et al., 2006) measurements. A Sensors & Software pulseEKKO Pro with antennas of 100 MHz was used in the geophysical investigation to perform two types of GPR survey: (1) fixed-offset reflection profile for stratigraphic mapping, and (2) common midpoint (CMP) sounding for assessing the velocity of the radar signal in the ground. The DCR-ERT and CCR-ERT surveys were achieved with an Earth Resistivity/IP Meter SUPER STING R1 IP from AGI Advanced Geosciences, Inc., owned by UAA, and an OhmMapper TR5 system with one transmitter and five receivers operating at a frequency of about 16.5 kHz made by Geometrics and owned by CRREL. These geophysical tools used along the same survey line are complementary methods (De Pascale et al., 2008; Fortier et al., 2011; Fortier and Savard, 2010).

## DRILLING METHODS/DATA EMPLOYED

Different methods of geotechnical investigations were used in the different case studies (9-Mile, Anaktuvuk, UAF Farm, Goldstream Road). For the 9-Mile study, we obtained drilling data in cooperation with ADOT&PF. In the Anaktuvuk area, we drilled shallow boreholes with the SIPRE corer. For the Goldstream Road study, we used drilling data obtained by ADOT&PF.

**9-Mile Survey**

At the 9-Mile study site, hollow-stem drilling was conducted by ADOT&PF with a drill rig equipped with a modified CME sampler (2 in. inside diameter) (Figure 17). Eight AUTC boreholes from 24.5 ft (7.5 m) to 70.5 ft (21.5 m) deep were cored by an ADOT&PF crew (drillers Tom Johnson and Jason Cline) and logged by UAF researchers. The total length of obtained core in these boreholes reached 358.7 ft (109.4 m). All frozen cores were delivered to UAF for detailed permafrost descriptions and photography. Wedge ice occurrence and its distribution with depth were evaluated based on data obtained from 8 AUTC hollow-stem boreholes and 54 ADOT&PF solid-stem boreholes, which were drilled and logged by ADOT&PF. Grain-size analyses of the sediments were performed on 25 samples obtained from 6 AUTC boreholes (AUTC08-2–AUTC08-7). Gradistat software was used for the analysis of grain-size distributions (Bloot and Pye, 2001). Gravimetric moisture content (on a dry-weight basis) was calculated for 189 soil samples. For volumetric moisture content, 99 samples with a cylindrical shape were selected. The thaw strain of ice-rich soil from the study site was evaluated for 2 conditions. Forty-four samples obtained from 7 AUTC boreholes (AUTC08-3–AUTC08-9) were thawed without external load. A consolidation test of thawed soils was performed on 5 samples. The results of geotechnical investigations at this site were summarized in a report prepared for the ADOT&PF (Shur et al., 2010).

Figure 17. Drill rig at the Dalton Highway Innovation Project field site, May 2008

**Anaktuvuk Field Survey**

At the Anaktuvuk geophysical investigation sites, drilling was performed by UAF researchers with a SIPRE corer (7.5 cm inner diameter) that had been equipped with a small (1.89 cu. in., 1.3 h.p.) two-stroke Tanaka TIA-340 engine (Figure 18). Fourteen boreholes were

drilled to depths that ranged from 1.5 to 3.9 m. Gravimetric moisture content (on a dry-weight basis) was calculated for 58 samples of frozen soil.

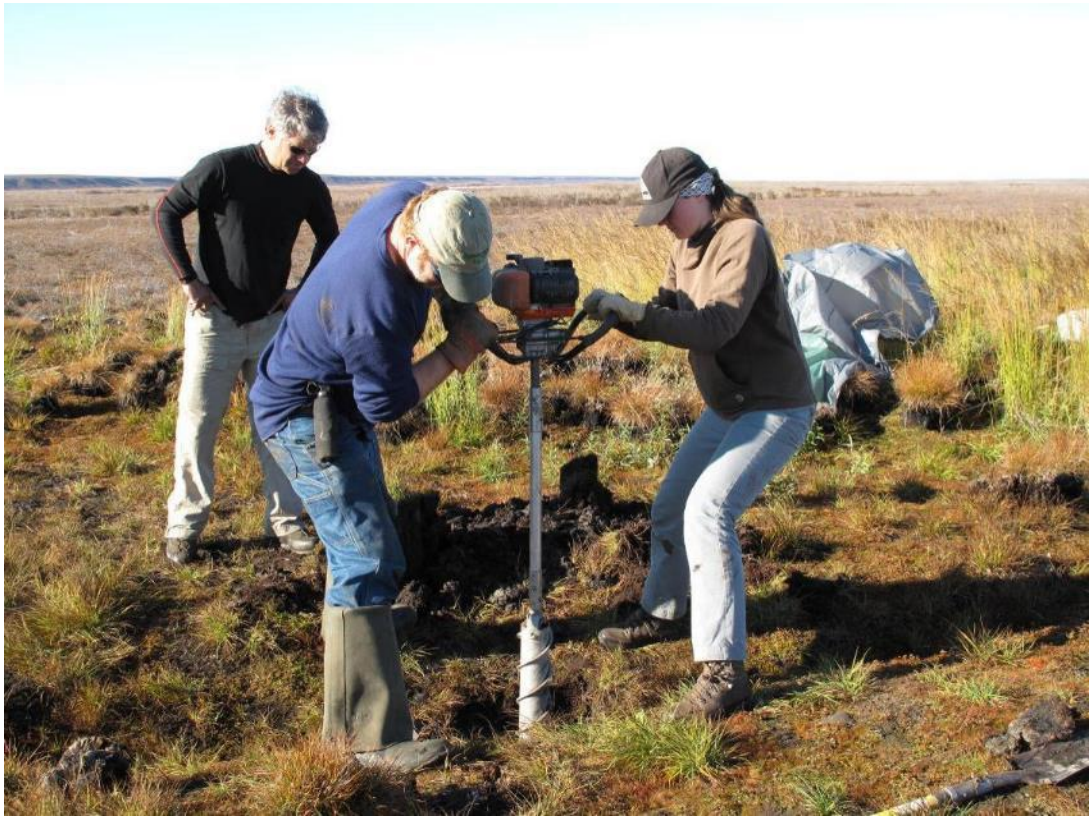

Figure 18. Drilling with the SIPRE corer, field site AR-6 (Bridge), Anaktuvuk area, September 2010

### Goldstream Road Survey

Drilling and logging data for the Goldstream Road survey were provided courtesy of ADOT&PF, based on boreholes obtained from Miles 1 through 7 between September 2011 and January 2012. Borehole results from this investigation are provided in Table 8.

## 9-MILE FIELD SURVEY RESULTS

### Site Description and Field Timeline

The 9-Mile study site is located along a proposed realignment of the Dalton Highway at 9-Mile Hill near Livengood. The ADOT&PF was investigating the reconstruction of approximately four miles of highway between Miles 8 and 12 to upgrade the road to current design standards and provide safer alignments and grades and a new asphalt surface. The principal goal of our study was to assess the spatial distribution of permafrost conditions along the realignment based on the interpretation of geophysical surveys and information from boreholes.

The study area is located approximately 20 km northwest of Livengood and about 100 km north of Fairbanks (Figure 19); the Trans-Alaska Pipeline is about 2 km east of the Dalton

Highway. The area is drained by the Yukon River and belongs to the Yukon-Tanana Upland, which is formed by generally rolling low mountains (Wahrhaftig, 1965). The 4.5 km long alignment slopes gently to the northwest 320–470 m above sea level.

According to Péwé (1975) and Jorgenson et al. (2008), the study area is in the discontinuous permafrost zone. The bedrock is formed of highly deformed and weathered sedimentary rocks, overlain by colluvial and fluvial gravelly soils and silt (loess). The permafrost here, which was formed syngenetically during the late Pleistocene, is ice-rich with a high occurrence of ice wedges. The vegetation is primarily black spruce, with alternating areas of birch close to riparian areas. The black spruce varies from burned toward the top of the ridge to unburned toward the road Figure 20. The last forest fire in the area—the Erickson Creek fire—occurred in 2003.

Permafrost temperatures at the site vary from -1.5°C to -0.5°C (Rowland, 2010). Active layer thickness generally reaches 0.5 to 1 m. Contemporary growth of ice wedges is not found in this area. Wedge-ice development in Interior Alaska can only be expected in organic soils, usually at a flat surface with limited drainage, mostly in peat bogs (Hamilton et al., 1983). Recent forest fire activity (the Erickson Creek fire) was documented to increase the active layer thickness. Despite the forest fire, the near surface remains relatively resilient to thaw settlement, as it does not exceed 0.5 to 1 m and thermokarst features in the project area are limited to shallow, irregular thermokarst scars. Distinct thermokarst troughs above melting ice wedges were not observed in the examination of high-resolution aerial photographs or in our surface observations. Numerous old gullies in the study area have not shown any evidence of recent rejuvenation.

Over the last 20 years, the Northern Region Materials Section (NRMS) has conducted four separate geotechnical investigations of the project area, which included the drilling of several boreholes (Schlichting et al., 2006). In 2008, eight boreholes were drilled for permafrost sampling to allow for detailed description of the cryostructure (Shur and Kanevskiy, 2010). Ground truthing from these boreholes offers a unique opportunity for verifying the capabilities of geophysical methods used in permafrost investigation along linear infrastructures with well-documented borehole data.

The geophysical investigations occurred as two separate campaigns during May 2010 and March 2011 (Table 5). Timing and methods allowed for comparison of both the accuracy and precision of different geophysical techniques in identifying subsurface and permafrost characteristics. The second campaign took place during early spring, when adequate snow cover permitted the use of snowmachines and tracked all-terrain vehicles (ATVs). Snow-covered ground also allowed the evaluation of various transportation methods during collection periods.

The surveys were carried out from about Mile 10 to Mile 11 along two sections with different ice content—the ice-rich Section 1 and the ice-poor Section 2—according to the synthesis of borehole logs made by Shur and Kanevskiy (2010).

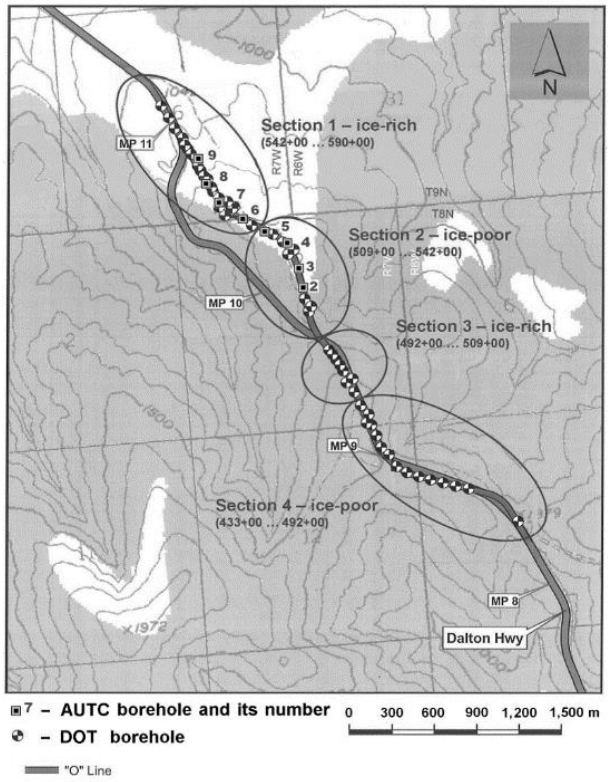


Figure 19. Location of the proposed realignment of the Dalton Highway and positions of boreholes drilled in 2008

Figure 20. Burned black spruce surrounding transect during the CCR-ERT survey at 9-Mile Hill, March 2011

## Borehole Results and Soils Analysis

Based on Shur et al. (2010) and Kanevskiy et al. (2012a), 8 hollow-stem boreholes (referred to as AUTC boreholes further in the text) from 24.5 ft (7.5 m) to 70.5 ft (21.5 m) deep were cored by the ADOT&PF crew (drillers Tom Johnson and Jason Cline) and logged by UAF researchers. The total length of obtained core in these boreholes reached 358.7 ft (109.4 m). Additionally, 54 solid-stem boreholes (referred to as DOT boreholes further in the text) were drilled and logged by ADOT&PF.

Table 5: CCR results from 9-Mile Hill, March 2011

| Name | Description | Electrodes | Electrode Spacing (m) | Maximum Resolution Depth (m) |
|---|---|---|---|---|
| 9-Mile #1 | CCR-ERT May 2010 (4 runs combined into 1 transect) | 4 | 5–65 | 20 |
| 9-Mile #2 | DCR-ERT May 2010 | 84 | 2 | 30 |
| 9-Mile #3 | GPR May 2010 | | | |
| 9-Mile #4 | CCR-ERT March 2011 (4 runs combined into 1 transect) | 4 | 5–65 | 20 |

## Soil Characteristics

The surficial deposit is frozen silt (loess). Particle-size distribution analysis of the sediments from 6 boreholes (AUTC08-2 to AUTC08-7) performed on 25 samples showed that the content of silt particles comprised 70% to 80% of bulk soils. The percentage of sand did not exceed 15%, and clay content varied between 10% and 20%. According to loss-on-ignition measurements by ADOT&PF (Rowland, 2010), organic matter content varied from 2% to 20%, with an average value of 6.7%. In most AUTC boreholes, horizons of organic-rich silt and peat were encountered at different depths. The thickness of silt varied from 0.5 m to more than 26 m. The radiocarbon age of sediments varied from 22,600 to 43,100 yr BP (8 samples were obtained from the AUTC boreholes). Radiocarbon ages of similar sediments from 18,000 to 27,000 yr BP were reported for the adjacent area (O'Donnell et al., 2011). Silt deposits are underlain by colluvial and fluvial gravelly soils up to 3 m thick or by weathered bedrock. Bedrock in the study area is represented mostly by highly deformed weathered sedimentary rocks. Neither AUTC nor DOT boreholes (the deepest hole was about 26 m) located at the base of the slope at elevations from 320 to 380 m reached the base of silt deposits.

## Cryogenic Structure and Ice Content

The ground-ice distribution and moisture content of soils for eight hollow-stem boreholes (AUTC08-2 to AUTC08-9) are shown in Figure 21–Figure 28. Study of the cryogenic structure of cores obtained from these eight AUTC boreholes showed the prevalence of micro-cryostructures typical of syngenetic permafrost (Kanevskiy et al., 2011a). Most of the AUTC boreholes revealed a similar structure in the upper permafrost. Five of eight boreholes showed a well-developed ice-rich intermediate layer (Shur, 1988a,b) from 0.7 m to 1.0 m thick (Figure 21–

Figure 23, Figure 26 and Figure 27). A rudimentary intermediate layer up to 0.3 m thick was encountered in two more boreholes. We related the formation of these poorly developed layers to recovery of the upper permafrost after the forest fire, which triggered an increase in the active layer thickness and degradation of the original intermediate layer.

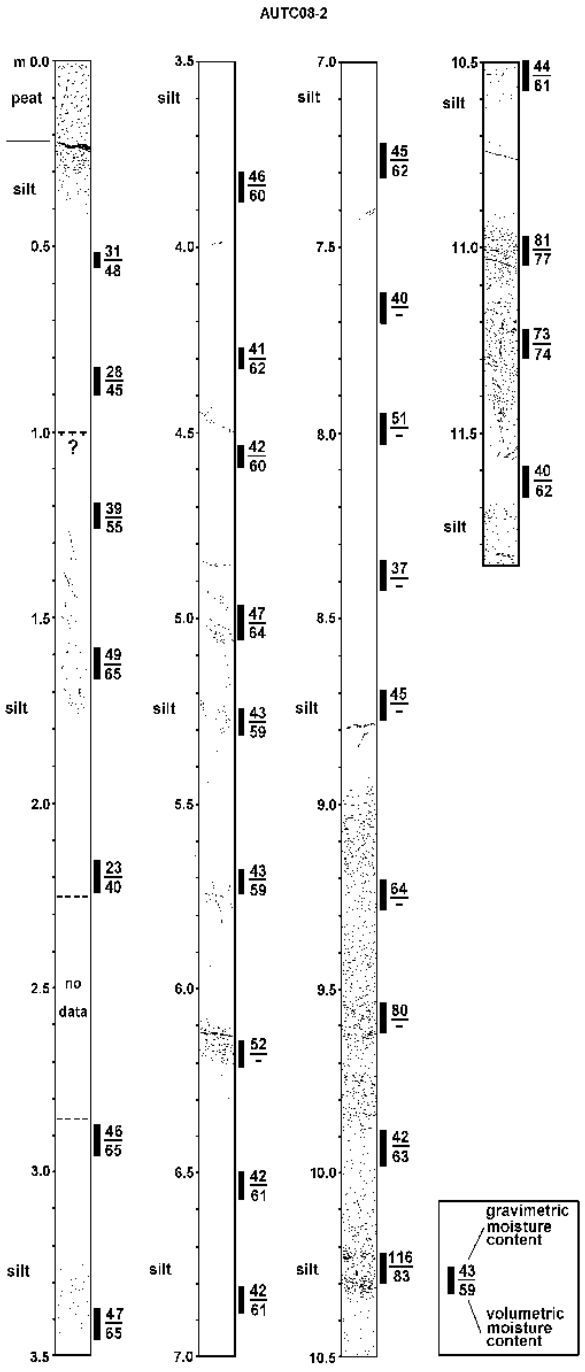


Figure 21. Cryogenic structure (ice is black) and ice content of frozen soil,
Dalton Highway Innovation Project, borehole AUTC08-2
Up to 9 m – thawed and refrozen sediments; from 9 m – syngenetic permafrost

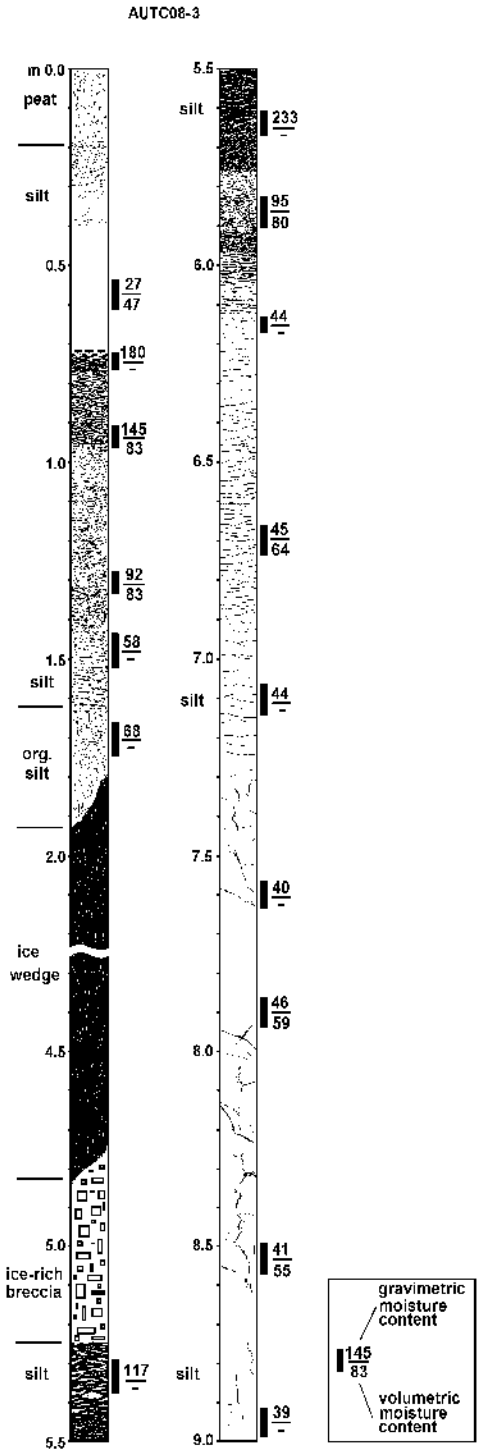


Figure 22. Cryogenic structure (ice is black) and ice content of frozen soil, Dalton Highway Innovation Project, borehole AUTC08-3

From 0.7 to 1.6 m – intermediate layer; from 1.6 to 1.8 m – thawed and refrozen sediments; from 1.8 to 6.1 m – syngenetic permafrost. Wedge ice: 1.8–4.8 m. From 6.1 m – epigenetic permafrost

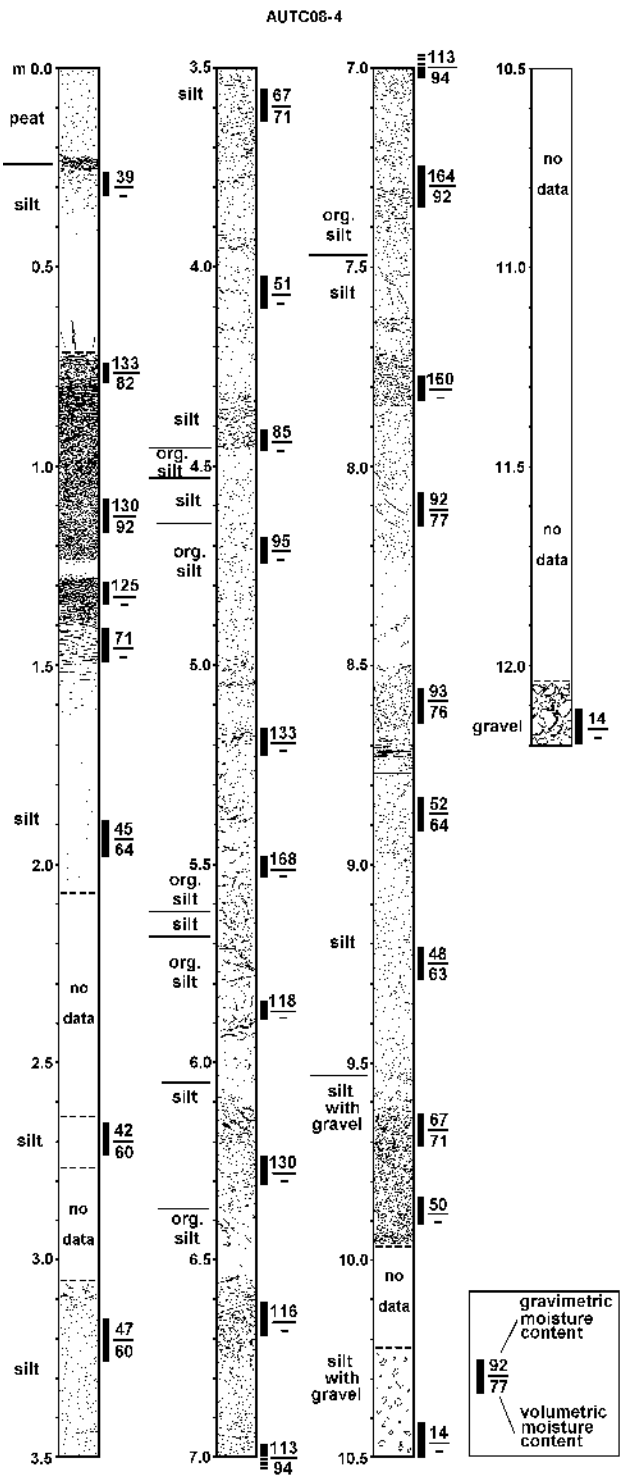


Figure 23. Cryogenic structure (ice is black) and ice content of frozen soil,
Dalton Highway Innovation Project, borehole AUTC08-4
From 0.7 to 1.5 m – intermediate layer; from 1.5 to 3 m – thawed and refrozen sediments;
from 3 to 10.2 m – syngenetic permafrost. From 10.2 m – epigenetic permafrost (gravel)

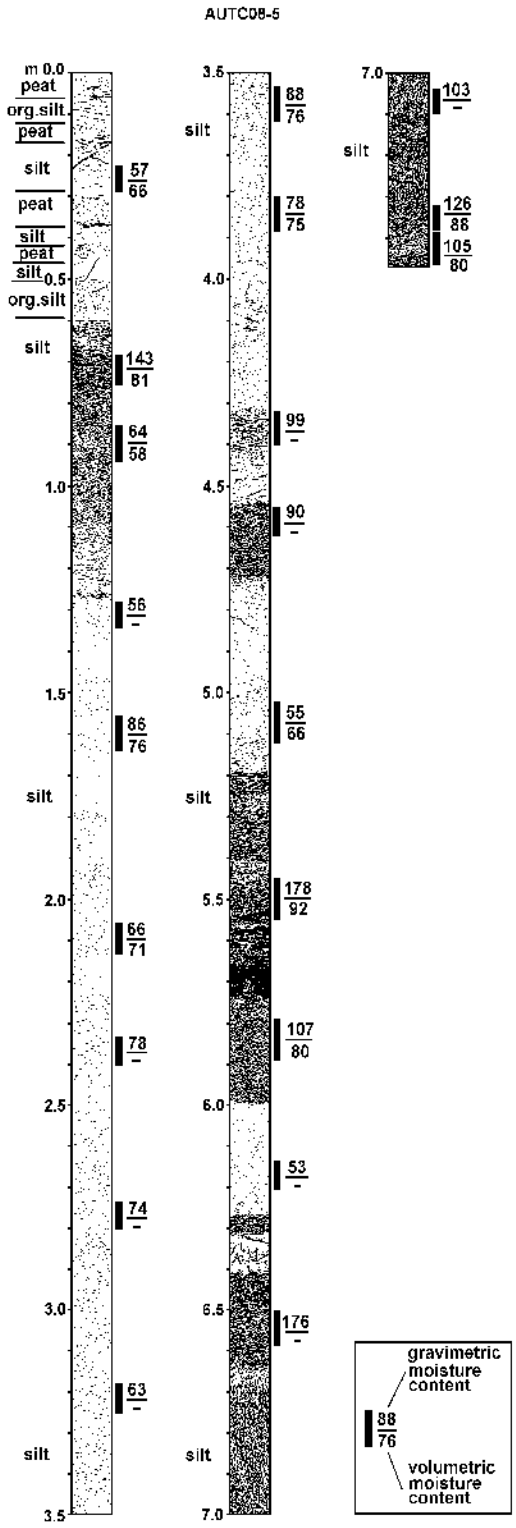


Figure 24. Cryogenic structure (ice is black) and ice content of frozen soil,
Dalton Highway Innovation Project, borehole AUTC08-5
From 0.6 to 1.25 m – intermediate layer; from 1.25 m – syngenetic permafrost

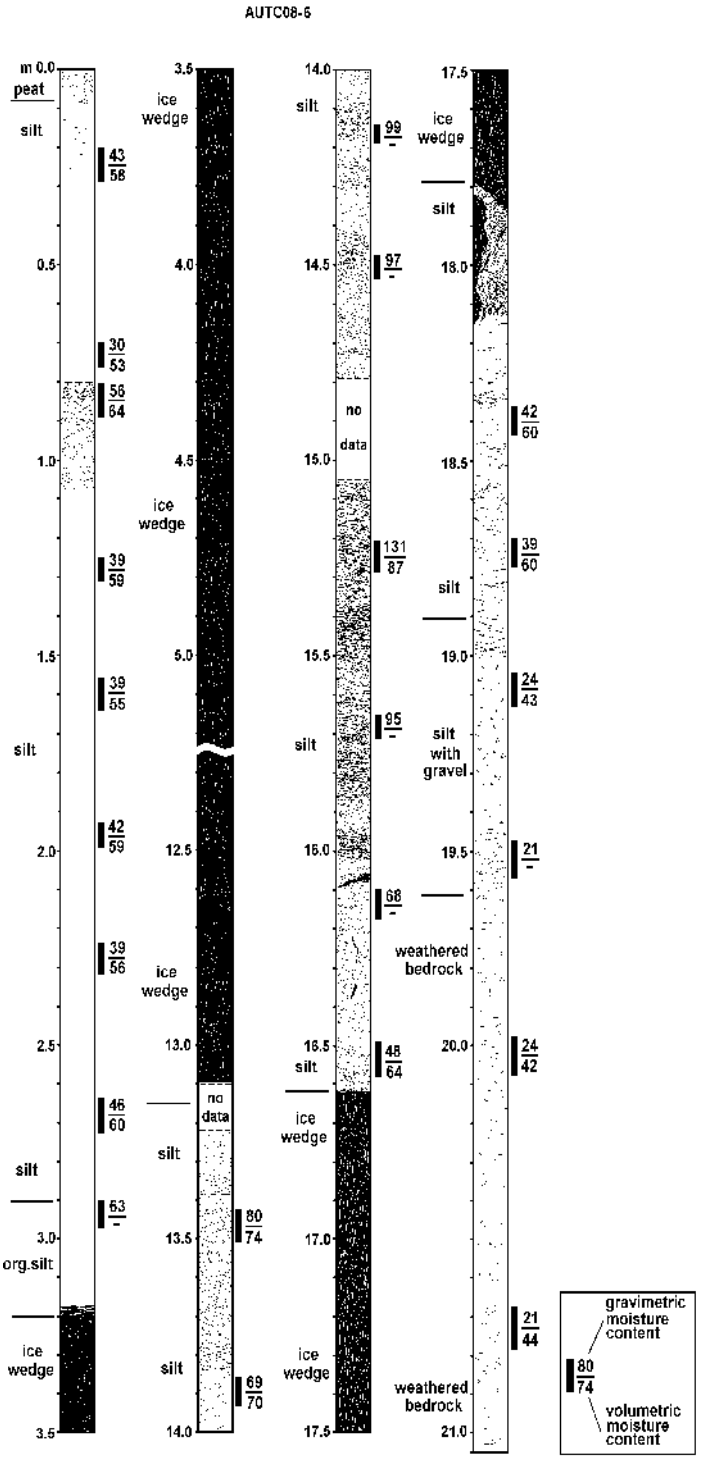


Figure 25. Cryogenic structure (ice is black) and ice content of frozen soil, Dalton Highway Innovation Project, borehole AUTC08-6

From 1.1 to 3.2 m – thawed and refrozen sediments; from 3.2 to 18.1 m – syngenetic permafrost. Wedge ice: 3.2–13.1; 16.6–18.1 m. From 18.6 m – epigenetic permafrost (gravel from 19 m)

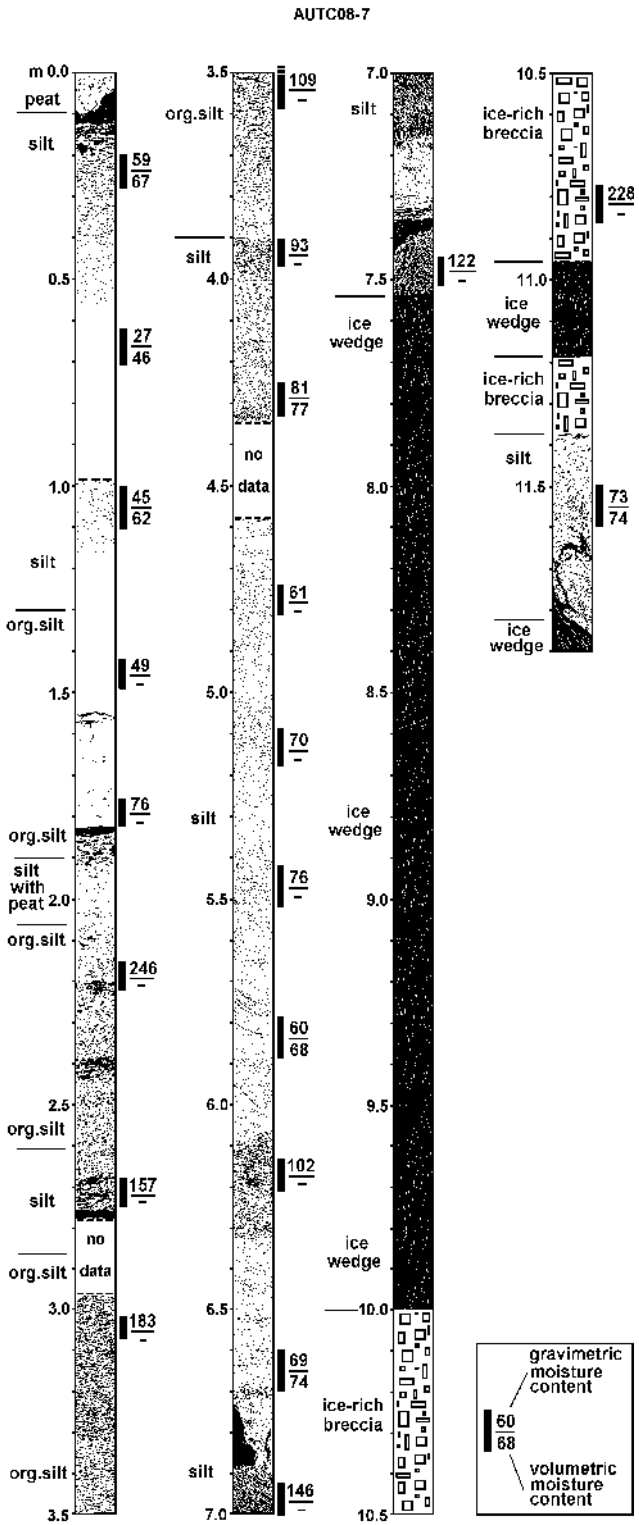


Figure 26. Cryogenic structure (ice is black) and ice content of frozen soil,
Dalton Highway Innovation Project, borehole AUTC08-7
From 1.15 to 1.8 m – thawed and refrozen sediments; from 1.8 m – syngenetic permafrost.
Wedge ice: 7.5–10; 11–11.2; 11.8–11.9 m

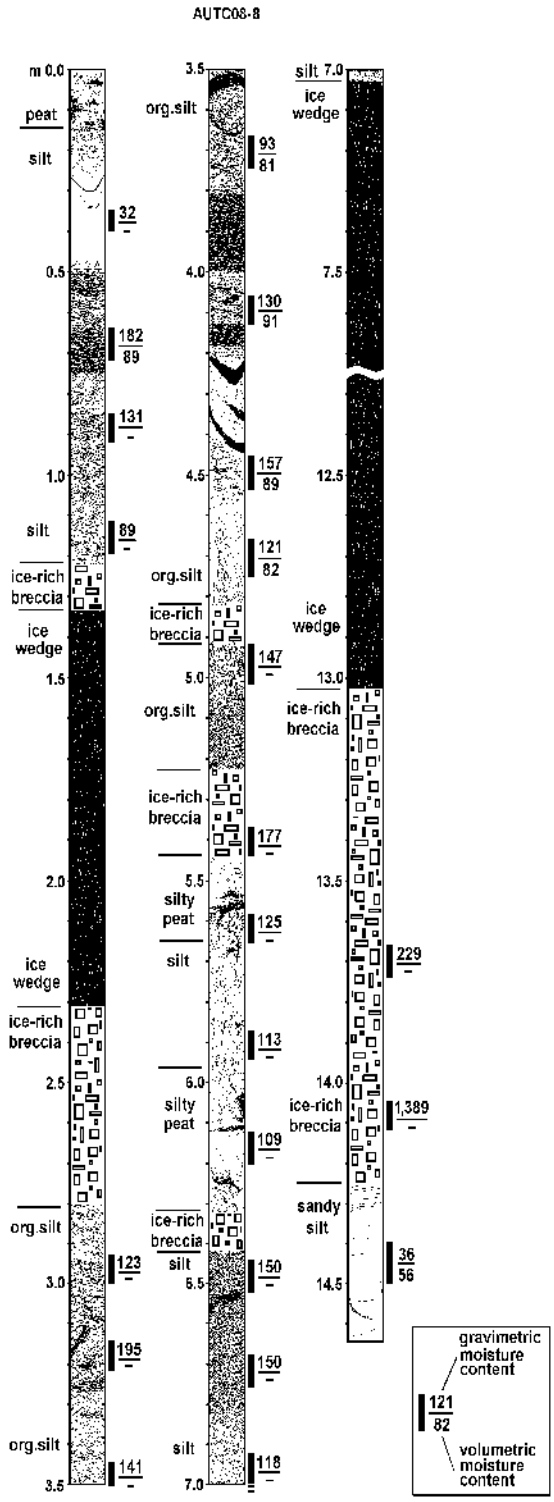


Figure 27. Cryogenic structure (ice is black) and ice content of frozen soil,
Dalton Highway Innovation Project, borehole AUTC08-8
From 0.5 to 1.3 m – intermediate layer; from 1.3 to 14.3 m – syngenetic permafrost. Wedge ice: 1.3–2.3; 7–13 m. From 14.3 m – thawed and refrozen sediments

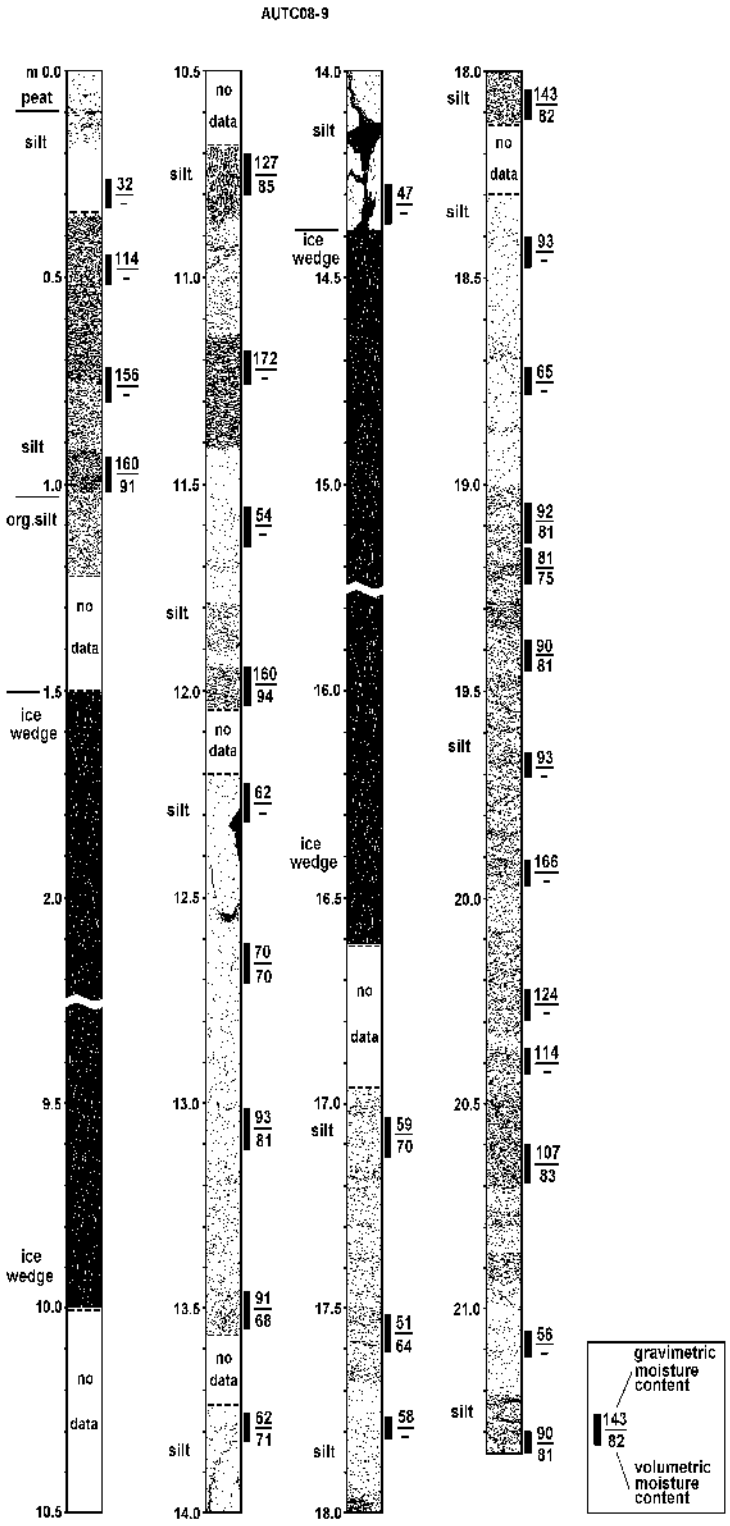


Figure 28. Cryogenic structure (ice is black) and ice content of frozen soil,
Dalton Highway Innovation Project, borehole AUTC08-9
From 0.35 to 1.2 m – intermediate layer; from 1.2 (?) m – syngenetic permafrost. Wedge ice: 1.5–10; 14.4–16.6 m

In five boreholes, an ice-poor layer of thawed and refrozen sediments (ranging from 0.3 to 8.0 m thick) was encountered below the intermediate layer. The wide occurrence of thawed and refrozen sediments in Interior Alaska was documented by Péwé (1975). Wedge ice was encountered at various depths in all boreholes except AUTC08-2, AUTC08-4, and AUTC08-5. In boreholes AUTC08-8 and AUTC08-9, ice wedges started just below the ice-rich intermediate layer, at depths of 1.2 m and 1.5 m, respectively. Soils between ice wedges are mostly ice-rich. The wide range (from ~40% to 200% and more) and high values (85.5% average) of gravimetric moisture content, which do not change significantly with depth, are typical of syngenetic permafrost.

**Origin of Permafrost**

Our study of soils and ground ice shows that frozen silt in the study area is mostly ice-rich syngenetic permafrost formed in the late Pleistocene (yedoma). Evidence for this finding includes the thick deposits of homogeneous silt with poorly decomposed organic matter, age of sediments (22,600 to 43,100 yr BP), very high ice content, prevalence of micro-cryostructures, and occurrence of large foliated ice wedges penetrating through the entire silt sequence. Yedoma deposits were formed by simultaneous accumulation of windblown silt partly reworked by slope and fluvial processes (Péwé, 1975) and upward permafrost aggradation. Ice-rich syngenetic Pleistocene permafrost widely occurs in Interior Alaska, on the Seward Peninsula, and in the Arctic Foothills of the Brooks Range; it can be encountered in other areas that remained unglaciated during the late Pleistocene (Kanevskiy et al., 2011a). Until recently, this type of permafrost has been understudied in Alaska, and investigations for engineering projects usually do not provide sufficient information for its characterization. In Interior Alaska, the cryogenic structure of these sediments has been studied extensively in the well-known CRREL permafrost tunnel at Fox, near Fairbanks (Sellmann, 1967; Hamilton et al., 1988; Shur et al., 2004; Bray et al., 2006; Fortier et al., 2008; Kanevskiy et al., 2008). A comparison of ice-rich soils in the study area with those of the CRREL permafrost tunnel shows that the soils are of similar age, cryogenic structure, and ice content.

**Thaw Strain**

Evaluation of thaw strain of frozen soils was based on 44 tests of thawing without external load (free thawing) and 5 consolidation tests. Average thaw strain was 0.23. Average thaw strain values for mineral and organic soils were 0.26 (35 samples) and 0.13 (9 samples), respectively. Figure 29 shows the correlation between thaw strain and gravimetric moisture content for 35 samples of mineral soils. We found that organic soils behaved differently from mineral soils and that their thaw strain in free thawing was much lower. In consolidation tests, the part of the thaw strain of organic soils related to the impact of a load was greater than that of mineral soils, and the total thaw strain of organic-rich silt was comparable to the thaw strain of mineral soils.

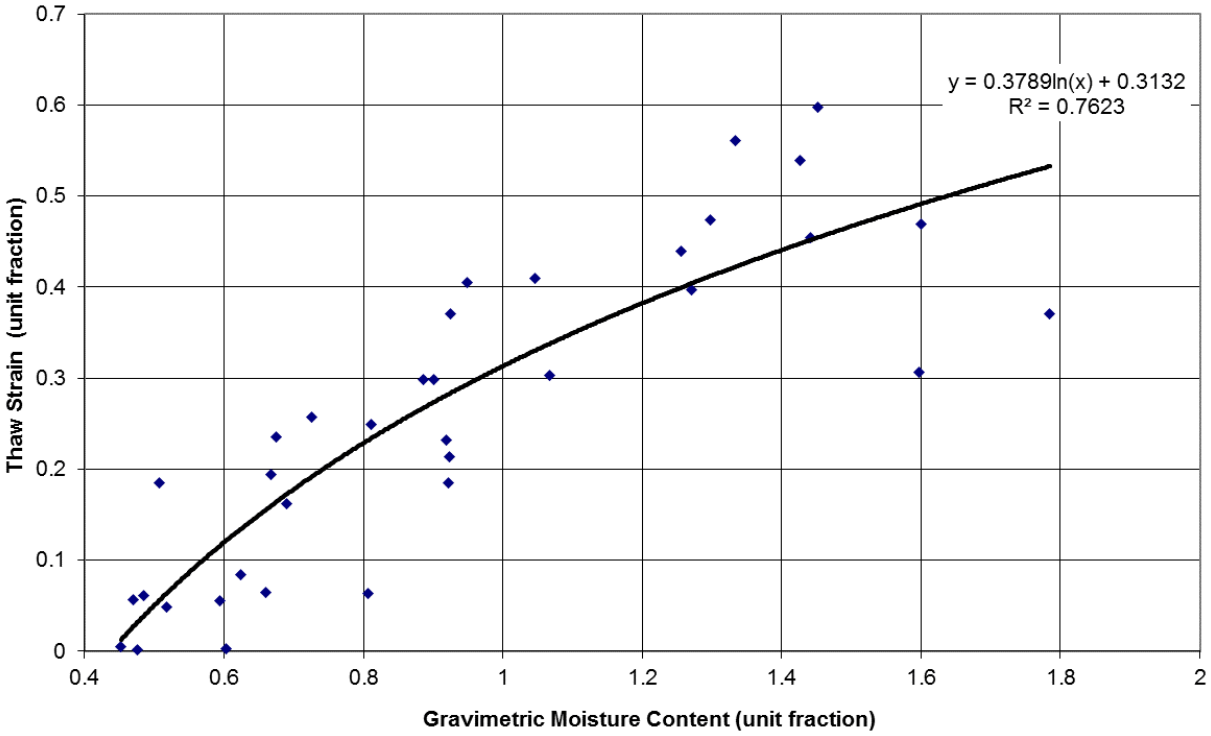


Figure 29. Relationship between thaw strain of mineral soil (without external load) and gravimetric moisture content (based on the data for 35 samples from AUTC boreholes)

**Wedge-Ice Volume and Description of Alignment Sections**

Wedge ice is the main type of ground ice in syngenetic permafrost and the only type identified in boreholes in the study area. Gray- and brown-colored wedge ice with distinct vertical foliation due to mineral and organic inclusions was encountered at various depths in both AUTC and DOT boreholes. Our experience with drilling in areas of ice-rich syngenetic permafrost (yedoma) shows that wedge ice can be found at different depths. The occurrence of ice wedges buried at different depths is related to the irregular boundaries of ice wedges, variability of the wedge thickness with depth, and the inclination of wedges. The penetration of wedges through the entire silt stratum is typical of yedoma**.**

Wedge ice was found in most of the AUTC and DOT boreholes, but its occurrence varied along the alignment. Based on wedge-ice occurrence, we identified 4 sections: 2 (Sections 1 and 3) defined as rich in massive ice and 2 (Sections 2 and 4) defined as poor in massive ice (Figure 19 and Figure 30). In further discussion, these sections are defined as ice-rich and ice-poor sections. Wedge-ice occurrence was estimated for different sections based on data from all boreholes (both AUTC and DOT). General characteristics of these sections are shown in Table 6. For ice-rich Section 1, wedge ice was observed in 24 of 26 boreholes, and for Section 3, wedge ice was observed in 8 of 9 boreholes. In Section 2, wedge-ice was found in 1 borehole of 12. In Section 4, wedge ice was found in 1 borehole of 15. Wedge ice occurs especially often in Section 3, where it occupies 47% of the combined length of all boreholes.

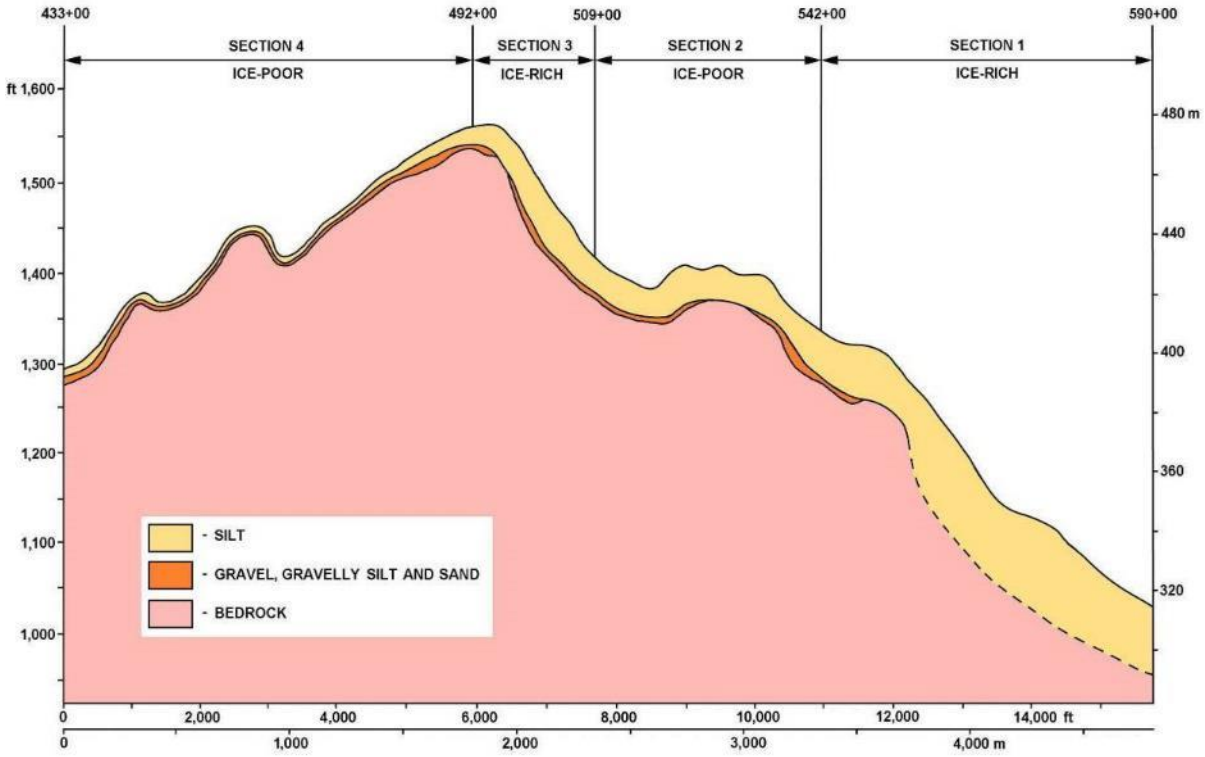


Figure 30. Division of 9-Mile alignment in ice-rich and relatively ice-poor sections (profile)

Table 6. General characteristics of ice-rich and relatively ice-poor sections, based on AUTC and DOT 9-Mile drilling logs

| | Sections | | | |
|---|---|---|---|---|
| | 1 (ice-rich) | 2 | 3 (ice-rich) | 4 |
| Number of AUTC boreholes | 4 | 4 | - | - |
| Number of DOT boreholes | 22 | 8 | 9 | 15 |
| Total number of boreholes | 26 | 12 | 9 | 15 |
| Number of boreholes with wedge ice | 24 | 1 | 8 | 1 |
| Wedge-ice occurrence, % | 34.7 | 2.4 | 47.0 | 3.1 |
| Thickness of silt, ft (m) | **52…>85** (16…>26) | **31…39** (9.5…12) | **30…46** (9…14) | **2…13** (0.6…4) |
| Thickness of gravel over bedrock, ft (m) | **0…11** (0…3.4) | **0…16** (0…5) | **0…5** (0…1.6) | **1…7** (0.4…2.1) |

Figure 31 shows wedge-ice occurrence with depth, estimated for ice-rich Sections 1 and 3. Wedge-ice occurrence significantly increases at a depth of 3–4 m, which means that a significant part of ice wedges is covered by a layer of thawed and refrozen sediments (this layer

was distinguished in several AUTC boreholes). The absence of ice wedges in the upper 1 m of a sequence can be explained by the occurrence of an intermediate layer beneath the active layer.

Based on data from AUTC and DOT boreholes, we developed a cryostratigraphic profile for Sections 1 and 2 of the study site (Figure 32**).** Expected wedge-ice distribution in all four sections of the proposed alignment is shown in Figure 33. The maximum thickness of syngenetic ice-rich permafrost in the area varies along the slope, but can be more than 25 m (at the base of the slope). The width of an ice wedge in its upper part can reach 3–5 m, and the distance between ice wedges usually varies from 5–15 m. It is common in such sediments for an ice wedge to penetrate slightly deeper than the layer of soil in which it is developing.

Section 1 was characterized by the sequence of ice-rich syngenetically frozen silt from 12 m thick to more than 26 m thick. Wedge ice was observed at various depths in 24 of 26 boreholes. Average wedge-ice occurrence in this section reached 35%, but the wedge-ice volume was not distributed evenly with depth. Absence of ice wedges in the upper meter of the sequence can be explained by the occurrence of an intermediate layer beneath the active layer. Where wedge-ice volume is relatively small (less than 15%) at depth intervals from 1 to 2 m, the occurrence is described as an ice-poor layer of thawed and refrozen soils. The highest values of moisture content (more than 40%) were at depth intervals from 6 to 10 m and 17 to 20 m. The average gravimetric moisture content of silt between ice wedges was 102% (based on measurements of 85 samples from 4 AUTC boreholes). The lowest values of moisture content were obtained mostly at depth intervals from 0 to 3 m (they correspond to the active layer and the layer of thawed and refrozen sediments). The estimation of average thaw strain due to segregated ice was 0.32, so the total thaw strain (due to wedge ice and segregated ice) was 0.56. This thaw strain estimation was not conservative, because it reflected only the settlement on thawing without load.

In ice-poor Section 2, wedge ice was found only in 1 of 12 boreholes at depths ranging from 1.8 to 4.8 m; wedge-ice occurrence in this section was about 2%. Syngenetic permafrost was identified in every AUTC borehole in Section 2, although it can be overlain by a layer of thawed and refrozen sediments up to 9 m thick. The thickness of silt in this section varied from 10 m to 12 m. The ice content of soil in this section was 79% (based on measurements of 88 samples from 4 AUTC boreholes), which is lower than in Section 1. The lowest values corresponded to the active layer and the layer of thawed and refrozen sediments. The average thaw strain due to segregated ice was 0.23, and the total thaw strain estimation was 0.25.

In ice-rich Section 3, wedge ice was found in 8 of 9 boreholes and occupied 47% of the combined length of all boreholes. Wedge ice was not observed from 0 to 2 m, and from 2 to 4 m its volume did not exceed 17%. We relate this condition to the occurrence of an ice-poor layer of thawed and refrozen soils. Wedge-ice volume of more than 50% was observed from 6 to 14 m, and at 8 to 14 m, the volume reached more than 80%. The thickness of silt in this section varied from 9 to 14 m. The average gravimetric moisture content of silt was 81% (based on measurements of 38 samples from 9 DOT boreholes). The lowest values of moisture content of soils were obtained mostly at depth intervals of 0 to 4 m (they correspond to the active layer and the layer of thawed and refrozen sediments) and 12 to 17 m (gravelly soil and bedrock). The average thaw strain due to segregated ice was 0.23, and the total thaw strain was 0.59.

In ice-poor Section 4, wedge ice was found in 1 of 15 boreholes. Wedge-ice occurrence is very small (about 3%), but the gravimetric moisture content of perennially frozen silt is relatively high (63% average, based on measurements of 21 samples obtained from 15 DOT boreholes). This section was characterized by a 0.5 to 4 m thick sequence of silt overlaying gravel and weathered bedrock. The average thaw strain due to segregated ice was 0.13, and total thaw strain was 0.16.

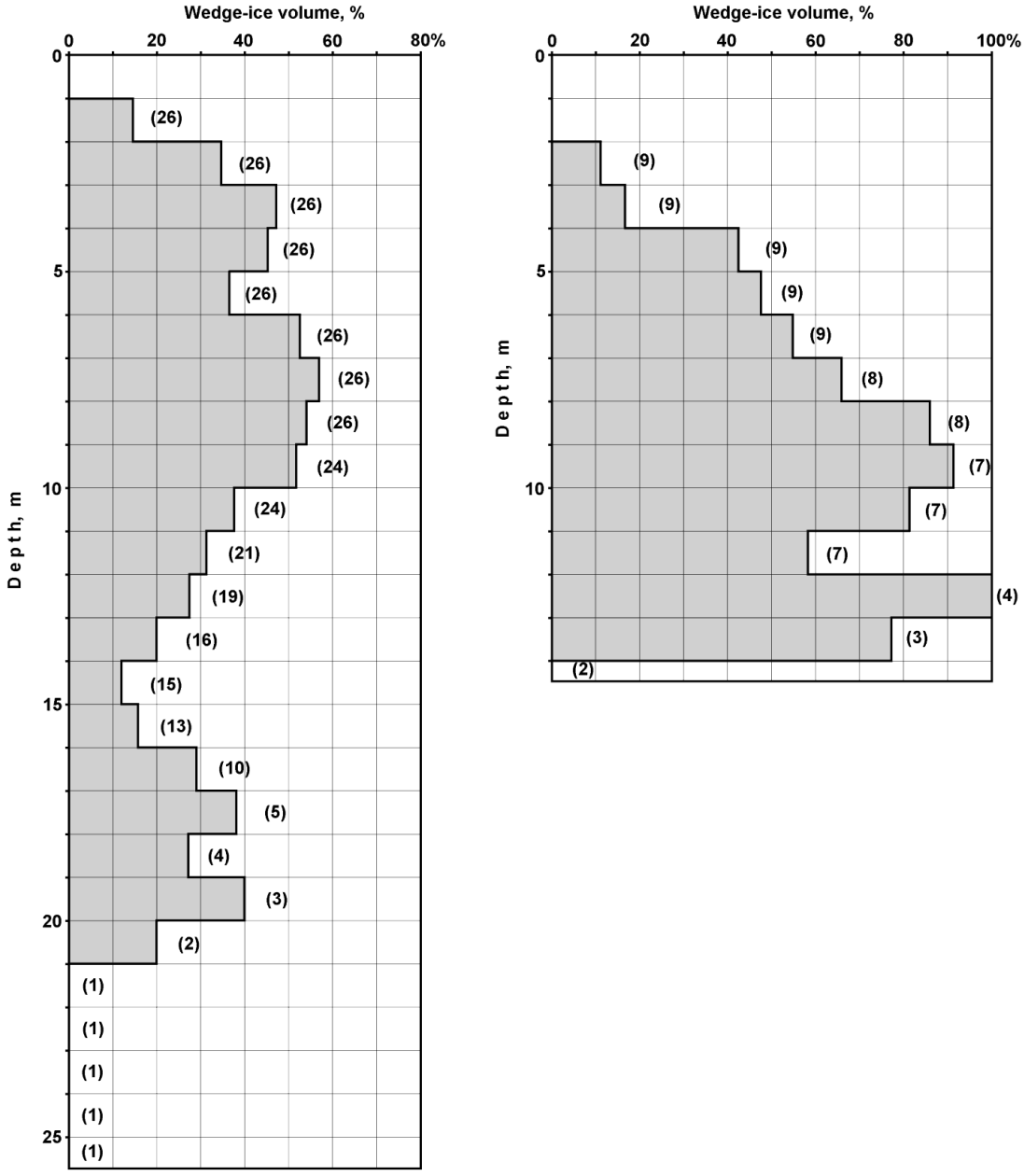


Figure 31. Wedge-ice occurrence with depth
Sections 1 (left) and Section 3 (right). Numbers in parentheses show number of boreholes (both AUTC and DOT) that reached this depth interval. For locations of Sections 1 and 3, see Figure 19

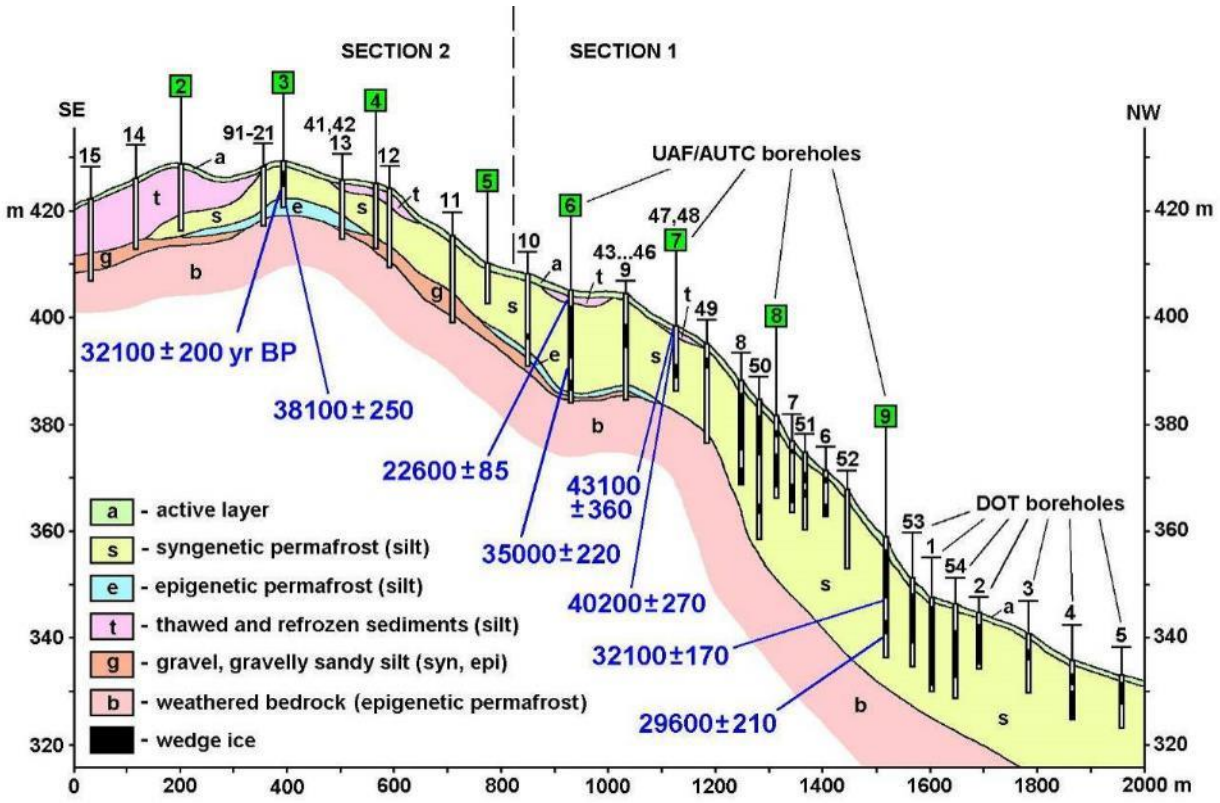


Figure 32. Cryostratigraphic profile and radiocarbon age of sediments (C14 years BP). AUTC boreholes are marked by squares; the rest are DOT boreholes

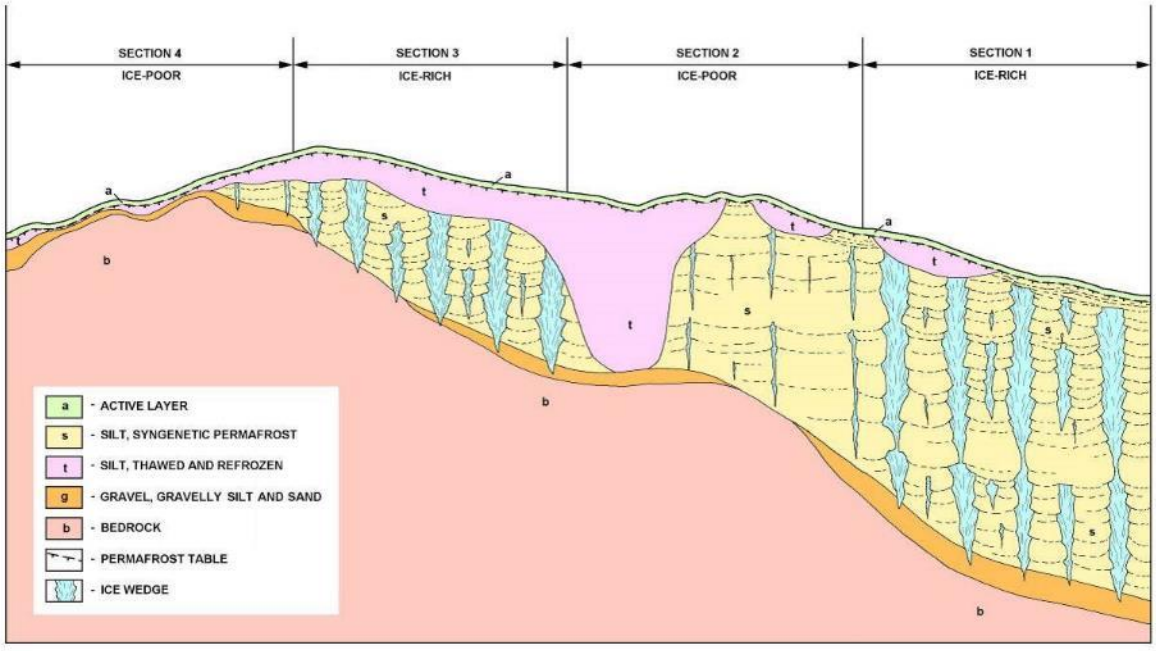


Figure 33. Expected wedge-ice distribution in different sections of the proposed 9-Mile alignment (not to scale)

**Geophysical Results**

The geophysical data from the 9-Mile site can be interpreted with respect to the technique as well as to the variation between collection dates.

The combined results of GPR, DCR-ERT, CCR-ERT, and borehole analysis obtained during the May 2010 campaign at 9-Mile Hill are presented in Figure 34. The data files of the four OhmMapper runs along the survey line were merged before the data analysis (inversion). Topographic variations along the survey line (Figure 32) have been integrated into the GPR, DCR-ERT, and CCR-ERT data files for topography correction. The pseudo-sections of apparent electrical resistivity measured during DCR-ERT and CCR-ERT were inverted using the software RES2DINV (Loke and Barker, 1995). Models of electrical resistivity were produced from the inversion of the pseudo-sections. In Figure 35, the resistivity results for 2010 are presented along with the additional CCR-ERT cross section obtained during March 2011 under the snow cover.

As illustrated in Figure 34, useful data obtained via GPR were limited to approximately the top meter of depth. While not visible in the figure due to the vertical scale, GPR data did reveal the transition between thawed soil and the top of permafrost. Additional GPR results are discussed in subsequent sections describing the Goldstream Road survey

Both models of electrical resistivity show not only a striking resemblance but also major differences (Figure 34 and Figure 35). The downhill section of the survey line is more resistive than the uphill section. The downhill section, defined as Section 1 by Shur and Kanevskiy (2010) according to the borehole logs, is ice-rich, while the uphill part corresponds to the ice-poor Section 2. The values of electrical resistivity in the model found from inversion of the DCR-ERT pseudo-section are much higher, by as much as one order of magnitude, than the values of the CCR-ERT model. The apparent electrical resistivity measured during DCR-ERT is through direct-current flow in the ground, while the apparent electrical resistivity measured during CCR-ERT is through capacitive-coupled contact between the OhmMapper cables and the ground, inducing an alternative current flow at a frequency of about 16.5 kHz. The frequency effect of this capacitive-coupled contact explains the lowering of the apparent electrical resistivity measured with this method. Both models suggest vertical contacts between bodies of different electrical resistivity; however, the CCR-ERT model has higher sensitivity to lateral variations than the DCR-ERT model does. Differences in the two inversions are primarily the result of the respective electrode array, which we discuss further in our interpretation.

The DCR-ERT model shows large areas of high resistivity downhill and low resistivity uphill, but the CCR-ERT model shows much smaller but more numerous areas of high and low resistivity. The resolution of the CCR-ERT method for detecting small areas of variable electrical resistivity is higher than the resolution of DCR-ERT. As much as 2022 apparent electrical resistivity measurements per 100 m were taken during the CCR-ERT survey in comparison with only 857 measurements per 100 m for DCR-ERT. The small areas of high values of electrical resistivity in excess of 15,000 ohm-m in the CCR-ERT model suggest the presence of numerous ice wedges. Some of these ice wedges were sampled during the drilling campaigns (Shur and Kanevskiy, 2010). More ice wedges are downhill than uphill. Their vertical extent can be as deep as 15 m. An example of an ice wedge observed in a road cut along the Dalton Highway is given in Figure 9.

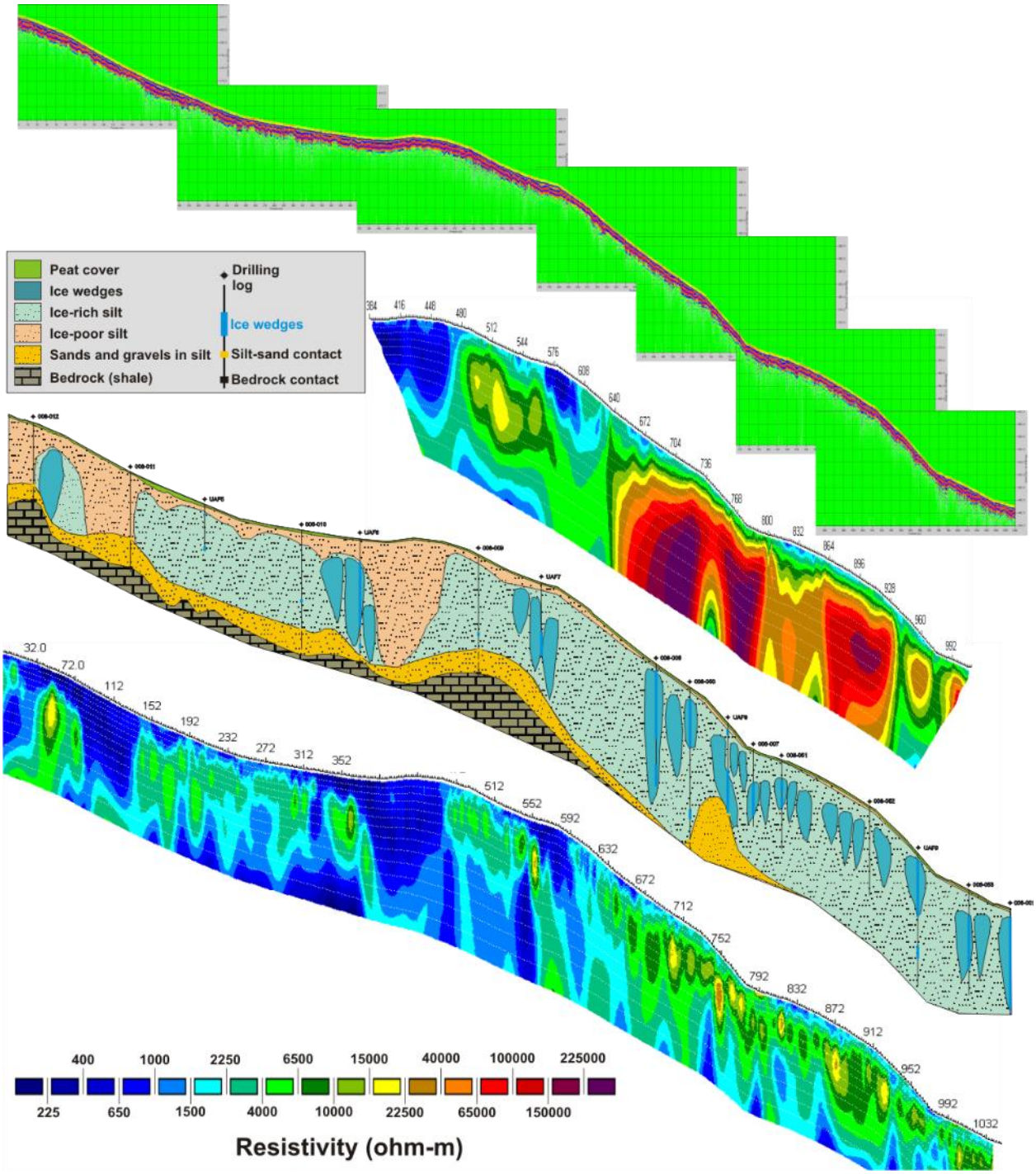


Figure 34. Geophysical results at 9-Mile Hill
From top to bottom: GPR profile, DCR-ERT model of electrical resistivity, cross section of ground and permafrost conditions including borehole logs, and CCR-ERT model of electrical resistivity along the survey line at 9-Mile Hill, May 2010

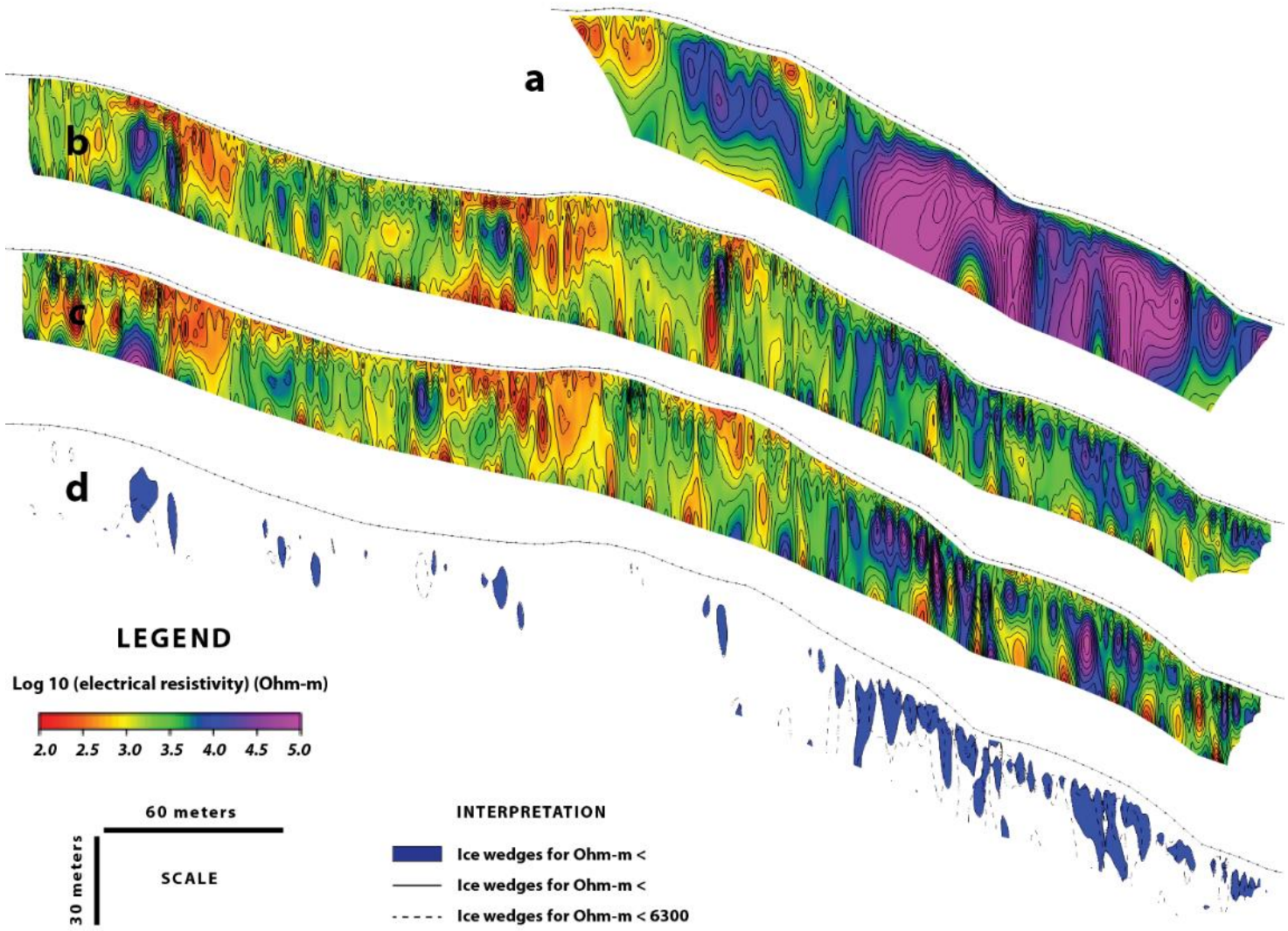


Figure 35. Resistivity transects at 9-Mile Hill
a) DCR-ERT transect from May 2010; b) CCR-ERT transect from May 2010; c) CCR-ERT transect from March 2011; d) Interpreted location of ice wedges based on electrical resistivity for 9-Mile Hill

**Interpretation of Geophysics with Respect to Soils Analysis**

The 9-Mile site was an important component of the study because it allowed the research team to compare three geophysical methods (DCR-ERT, CCR-ERT, and GPR) along a transect that had been well characterized with a dense array of boreholes. Thus, the relative strengths and weaknesses between the methods could be more clearly evaluated due to the availability of observed borehole data. The following is a comparison of the methods, based largely on our experiences at 9-Mile Hill.

While limited to a dipole-dipole array configuration, the CCR-ERT method has several important advantages over DCR-ERT. Namely, the method does not require direct contact with the ground and, hence, eliminates the need to insert electrodes. In frozen ground, electrode placement can be difficult and time-consuming using DCR-ERT. Additionally, the conductivity in frozen ground can be insufficient to obtain data using DCR-ERT, which does not pose a problem for CCR-ERT. The transect illustrated in Figure 35c, for example, was collected via CCR-ERT through not only a layer of frozen surface soil, but also a relatively thick snowpack. Advantages of DCR-ERT include greater flexibility with respect to the array configuration. Examples would include the Wenner array, the pole-dipole, and the Schlumber array, in addition to the dipole-dipole array employed by CCR-ERT.

The Wenner array is commonly employed to image horizontal layers in the subsurface, while the dipole-dipole array is more sensitive to horizontal variations and thus is useful for imaging vertical subsurface features. With respect to the 9-Mile site, we were particularly interested in delineating two highly resistive anomalies—namely ice wedges from frozen ground. This is evident in Figure 34 and Figure 35, which illustrate the effectiveness of the CCR-ERT system in resolving vertical variations in resistivity, particularly when compared with DCR-ERT, which employed a Wenner array. A comparison of CCR-ERT-derived cross sections obtained during May 2010 and March 2011 show strong similarities, giving some indication of the robustness of the OhmMapper system.

Ground-penetrating radar (GPR) represents a complementary, rather than a competing method to ERT, and can provide valuable information with respect to the near surface. Using high-frequency electromagnetic waves (approximately 10 MHz–1 GHz), GPR delineates variations in electrical permittivity and conductivity in the near subsurface. Shown to scale, the GPR data obtained on 9-Mile Hill show one limitation of the method, specifically the depth of penetration, which in this case is limited to about 1 m. The GPR data were obtained using a Sensors & Software system that employs a 100 MHz bi-static antenna system.

Penetration depths are limited by several variables, including ground conductivity and spherical spreading losses in the transmitted and received wave fields. Increased penetration depths can be obtained by using a lower-frequency antenna system, with the tradeoff being lower resolution and a physically larger antenna. Finally, since conductivity decreases in frozen soils, improvements in penetration can also be achieved by taking GPR measurements over a frozen surface.

## ANAKTUVUK FIELD SURVEY RESULTS

### Site Description and Field Timeline

The Anaktuvuk field survey site delineates permafrost characteristics in the proposed Foothills West Transportation Access project, a plan to construct a new all-season road that connects the Dalton Highway to Umiat. The road corridor crosses an area of continuous permafrost and the Toolik, Itkillik, Anaktuvuk, Chandler, and Colville Rivers between the northwestern foothills of the Brooks Range and within the National Petroleum Reserve-Alaska. The goals in this area involved using a combination of techniques including shallow boreholes and electrical resistivity tomography (ERT) to characterize the presence or absence of ground ice and variations in two dimensions over transects, and to determine the depth to groundwater if present.

The study area is primarily located in the North Slope physiographic province of the Arctic Foothills. At Umiat (69°22′ N, 152°08′ W, 81 m above sea level), mean annual air temperature is -11.8°C, and mean annual precipitation and snow depth are 136 mm and 229 mm based on National Climate Data Center records from 1971 to 2000. Depth of permafrost in this region can range from 200 m toward the foothills to 600 m at Prudhoe Bay on the coast (Osterkamp and Payne, 1981). Estimated ground-ice distribution (Jorgenson et al., 2008) shows that finer-grained soils tend to be more ice-rich; however, features such as ice-wedge polygons and relict glacial ice occur in a variety of environments depending on the climate of an area. Yedoma or silt-dominated deposits with ice wedges up to 50 m thick have been documented in exposures along the Itkillik River and date from over 40,000 years (Kanevskiy et al., 2011a,b). Current and future permafrost temperatures in the area have been numerically simulated using the GIPL 1.3 model (Sazonova and Romanovsky, 2003), where estimates for the mean annual soil temperature at 1 m depth in the year 2100 will be between -2.5 and 0°C (Jafarov et al., 2012) in the proposed road corridor. The major ecosystems consist of upland low birch-willow shrub tundra and upland shrubby tussock tundra (Jorgenson and Heiner, 2008), where *Betula nana* and *Salix pulchra* are present as canopy cover and overlapping understory species include *Vaccinium uliginosum, Vaccinium vitis-idaea, Epetrum nigrum, Equisetum arvense,* and *Sphagnum* spp. On alluvial plains the ecosystem changes to riverine low willow shrub tundra, where *Salix alaxensis, S. arbusculoides,* and *S. glauca* are the main tall shrubs in frequently flooded areas, whereas *Salix lanata richardsonii* and *S. pulchra* dominate inactive areas.

Figure 36. Stream meandering between high-center ice-wedge polygons near the Colville River

Fieldwork was completed in the first week of September 2010 in four major areas known as ANTRAN, AL4TRAN, AL2TRAN, and BRIDGETRAN (Figure 37 and Figure 38). Site selection was based on potential bridge alignment sites and characterization of ice-rich tundra with ice-wedge polygons. Inclusion of sites that encompassed the area of the 2008 Anaktuvuk tundra fire (Jones et al., 2009) was a secondary consideration. These sites represent a range of conditions including gravel bars, alluvial plains, tussock tundra (in both unburned and burned conditions), high- and low-centered ice-wedge polygons, and an active thermokarst feature. DCR-ERT transects were completed in conjunction with the drilling of shallow and deep boreholes in the study area. The spacing of electrodes and the total length of the survey (detailed in Table 7) varied by transect. Both of these characteristics determined the depth that could be effectively resolved using the DCR-ERT methodology. A Wenner array was employed to measure variations in subsurface resistivity, which maximized discriminating features with variability lateral to the ground surface.

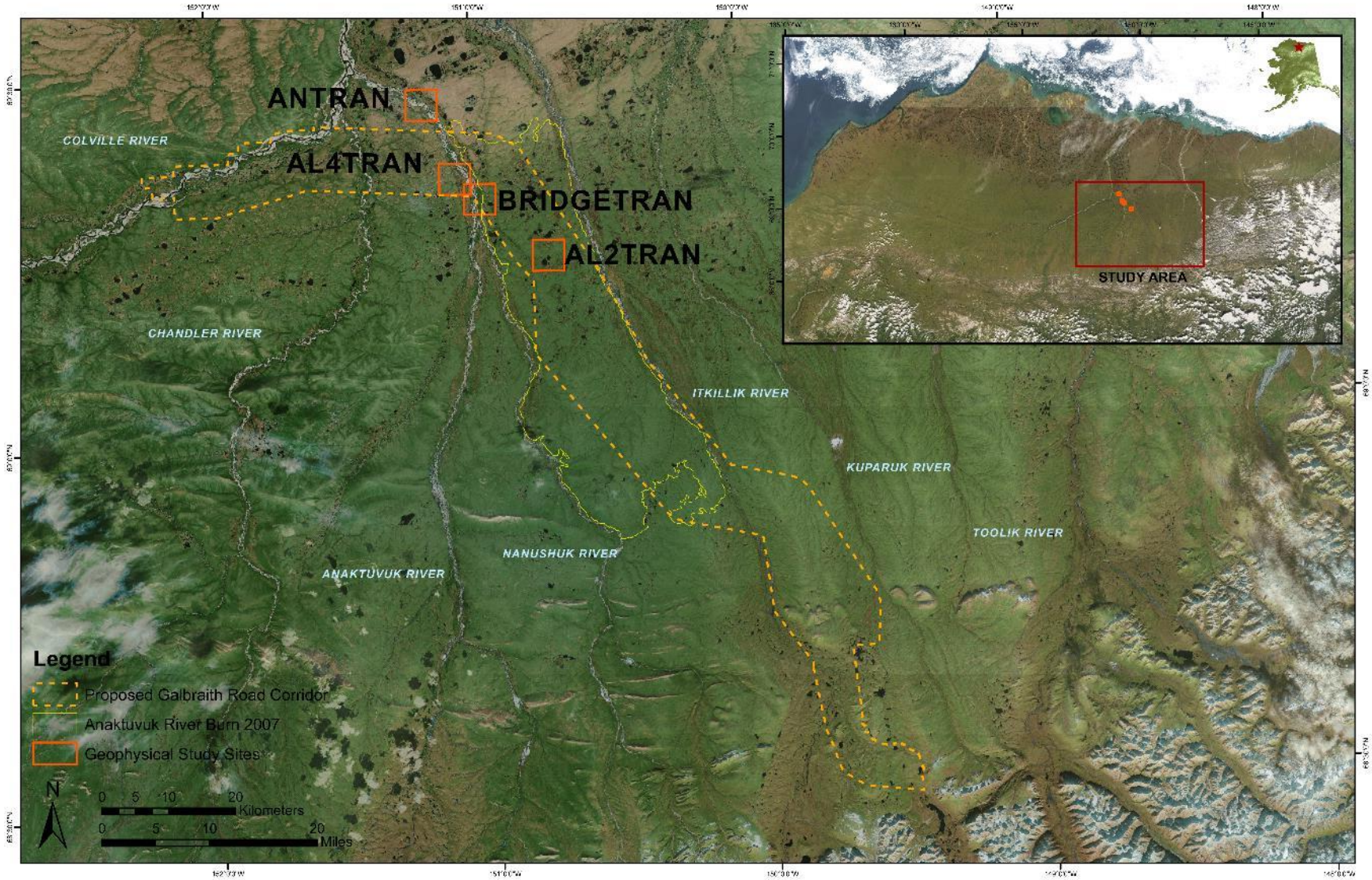

Figure 37. Overview of study area including proposed Galbraith Road Corridor and 2007 Anaktuvuk River burn

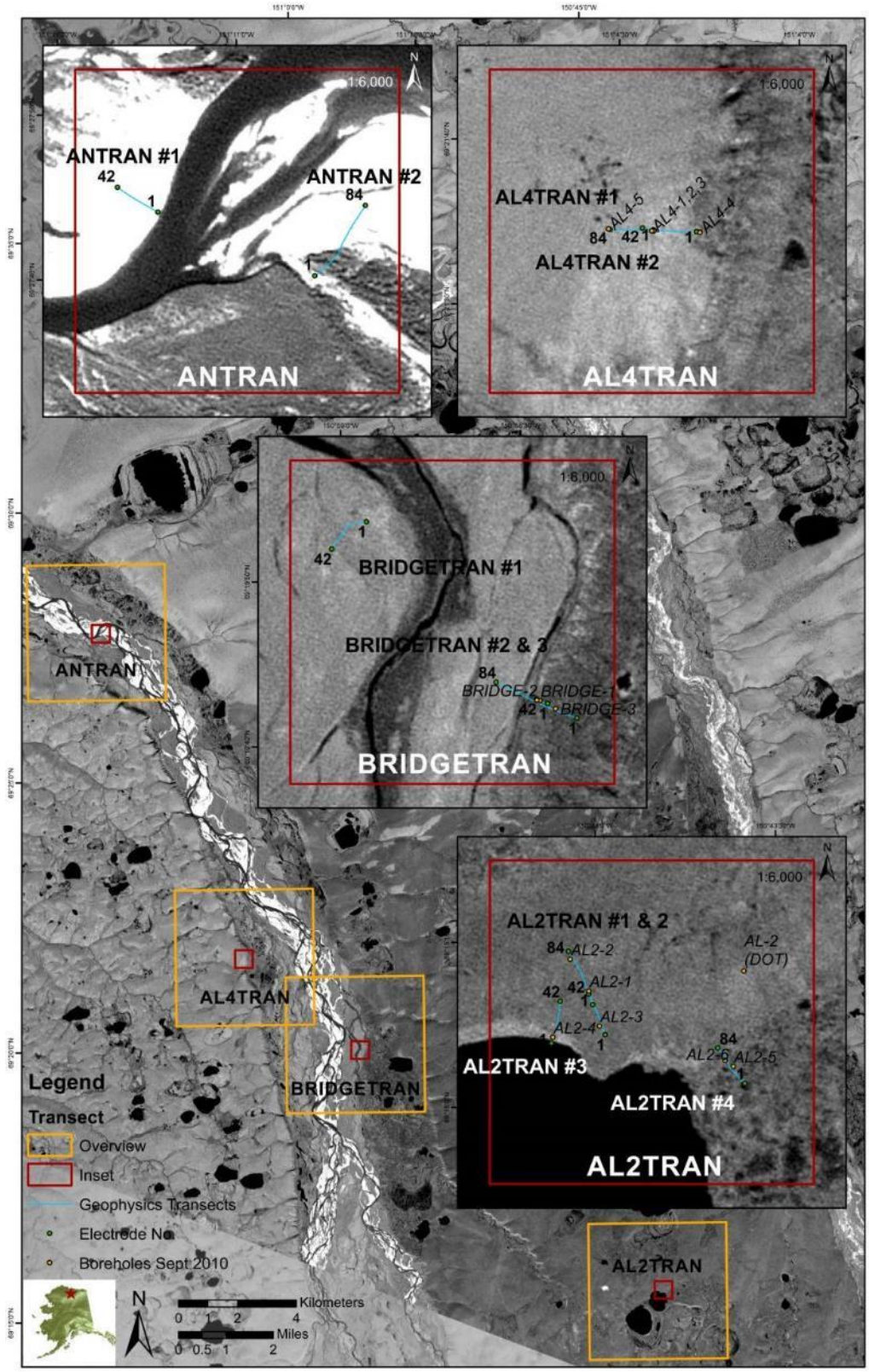


Figure 38. Locations of DCR-ERT transects with electrodes and boreholes indicated with SPOT 2.5 m panchromatic image in the background

Table 7. DCR transect summaries for the Anaktuvuk-area study sites

| Site | Description | Electrodes | Electrode Spacing (m) | Maximum Resolution Depth (m) | Resistivity (Ω m) | | Permafrost (P) / Groundwater (GW) Present | Average Active Layer Depth (cm) | Depth to Wedge Ice (cm) |
|---|---|---|---|---|---|---|---|---|---|
| | | | | | Min. | Max. | | | |
| ANTRAN #1 | Anaktuvuk River Gravel Bar | 42 | 2 | | | | | | |
| ANTRAN#2 | Anaktuvuk River Gravel Bar & Side Channel | 84 | 2 | 25 | 9.64 | 1819 | GW | -- | -- |
| AL4TRAN#1 | Alignment Hole #4 Tussock Tundra and Hillslope | 84 | 2 | 25 | 320 | 29775 | P | 49 | 43 |
| AL4TRAN#2 | Alignment Hole #4 Tussock Tundra | 42 | 0.5 | 3.25 | 56.6 | 7506 | P | 51 | 43 |
| BRIDGETRAN#1 | Anaktuvuk River Alluvial Plain | 42 | 2 | 13 | 305 | 8833 | *?* | -- | -- |
| BRIDGETRAN#2 | Burned Tussock Tundra to Flood Plain | 84 | 2 | 25 | 265 | 20960 | P | 54 | 30 |
| BRIDGETRAN#3 | Burned Tussock Tundra and Degrading High Centered Polygons | 42 | 0.5 | 3.5 | 117 | 9703 | P | 48 | 30 |
| AL2TRAN#1 | Alignment Hole #2 Burned Tussock Tundra on Gentle Slope | 84 | 2 | 25 | 296 | 19370 | P | 55 | 92 |
| AL2TRAN#2 | Alignment Hole #2 Burned Tussock Tundra | 42 | 0.5 | 3.25 | 84.5 | 4582 | P | 58 | -- |
| AL2TRAN#3 | Alignment Hole #2 Burned Tussock Tundra and Thermokarst | 42 | 2 | 14.5 | 62.4 | 12262 | P | 62 | -- |
| AL2TRAN#4 | Alignment Hole #2 Low & High Centered Polygons | 84 | 1 | 13.5 | 121 | 10034 | P | 50 | 47 |

**Borehole Results and Soils Analysis**

Permafrost properties were studied at the AL2, AL4, and AR6 (Bridge) sites located within the physiographic province of the Arctic Foothills (Wahrhaftig, 1965), which is in the continuous permafrost zone (Péwé, 1975; Jorgenson et al., 2008). This area is dominated by syngenetic permafrost, including ice-rich late Pleistocene silty deposits known as yedoma (Kanevskiy et al., 2011a,b).

Yedoma deposits are widespread in the study area. In the low foothills of the Brooks Range, Carter (1988) described continuous areas of silt with tall ice wedges formed in the late Pleistocene, locally more than 30 m thick. According to Carter, these areas form a belt from 5 to 70 km wide at the boundary between the Arctic Coastal Plain and the Arctic Foothills. In our estimation, the area of ice-rich silt cover is larger than described by Carter (1988), and isolated yedoma sequences of a smaller scale can be found outside the silt belt area as well (Figure 39).

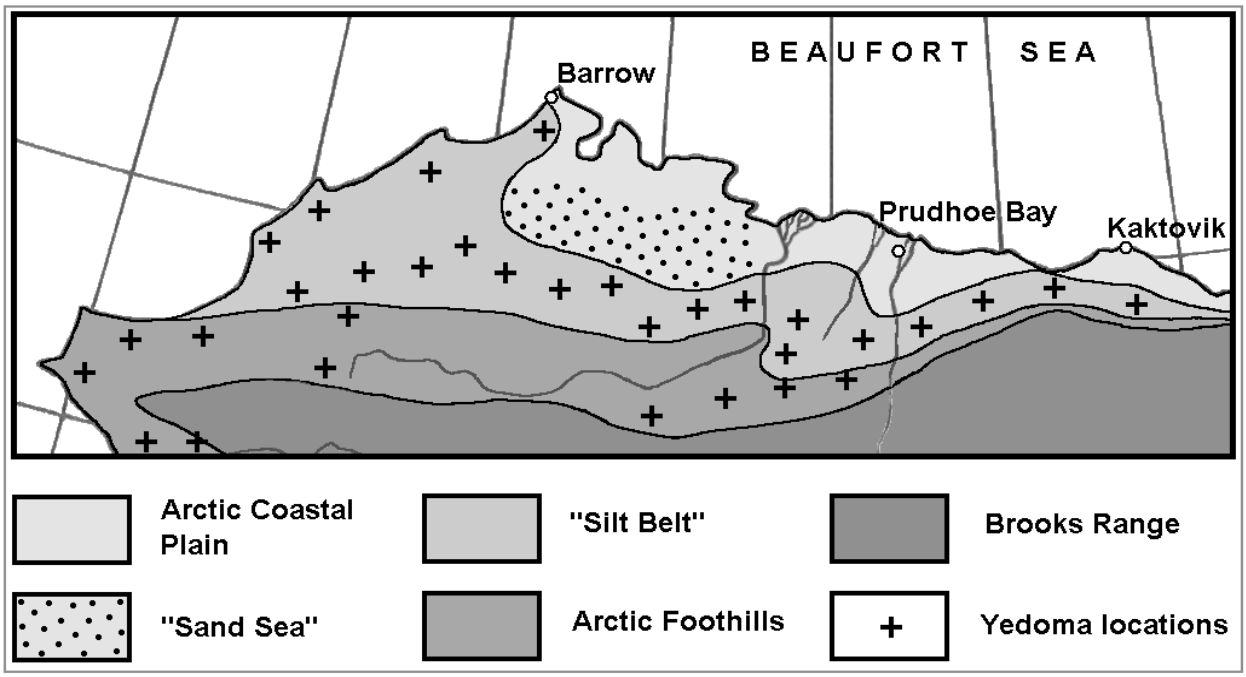


Figure 39. Permafrost regions of northern Alaska (from Kanevskiy et al. 2011b)

The silt belt is composed of thick sequences of ice-rich syngenetic permafrost (yedoma). This permafrost formed during the last glaciation by the accumulation of eolian, slope, and fluvial sediments that froze almost simultaneously with deposition. Mineral soils of yedoma typically contain about 70% silt, and buried organic-rich horizons are common. Formation of yedoma occurred with the accumulation of a high volume of segregated ice that formed a specific set of cryostructures. Large ice wedges penetrate the entire section of yedoma. Ice wedges are usually 3–6 m wide and sometimes wider. At some locations, the thickness of syngenetic permafrost with huge ice wedges can reach 30–40 m. The volume of wedge ice in such sediments frequently exceeds 60%. Permafrost within the silt belt has been described by Lawson (1982, 1983), Carter (1988), Brewer et al. (1993), and Kanevskiy et al. (2011a,b). Similar sediments have been studied extensively in Interior Alaska in the well-known CRREL

permafrost tunnel near Fairbanks (Sellmann, 1967; Hamilton et al., 1988; Shur et al., 2004, 2010; Bray et al., 2006; Kanevskiy et al., 2008, 2012). Thawing of yedoma deposits in the study area, which started at the end of the Pleistocene, has resulted in the formation of large thaw-lake basins 20–30 m deep (Livingstone et al., 1958; Williams and Yeend, 1979; Carter, 1988).

The most impressive section of yedoma in northern Alaska was studied in 2006–2007 in the 33 m high exposure of the right bank of the Itkillik River (Kanevskiy et al., 2011a,b). This site is located 27 km to the north of our site AR6 (Bridge). A general view of the yedoma exposure (69°34′ N, 150°52′ W) is shown in Figure 40.

Figure 40. Site overview of the Itkillik River exposure

The exposed permafrost sequence comprises seven cryostratigraphic units (Figure 41), including:

| | |
|---|---|
| 0.0–0.6 m | Unit 1 – Active layer (organic-rich brown-gray silt with fine sand). |
| 0.6–1.5 | Unit 2 – Contemporary intermediate layer (organic-rich yellow-gray silt; ice-rich; radiocarbon age from 5300 to 8600 $^{14}$C yr BP) with modern ice wedges. |
| 1.5–13.0 | Unit 3 – Yedoma with relatively thin ice wedges (yellow-gray and gray silt with rare small inclusions of organic matter; radiocarbon age from 14,300 to 29,600 $^{14}$C yr BP). |
| 13.0–27.0 | Unit 4 – Yedoma with thick ice wedges (yellow-gray and gray silt with rare small inclusions of organic matter; radiocarbon age from 23,900 to 41,700 $^{14}$C yr BP). |
| 27.0–29.0 | Unit 5 – Buried peat layer (dark-brown peat grading with depth into ice-rich organic silt). |
| 29.0–30.0 | Unit 6 – Buried intermediate layer (organic silt, ice-rich; radiocarbon age >48,000 $^{14}$C yr BP). |
| 30.0–33.0… | Unit 7 – silt with small, buried ice wedges. |

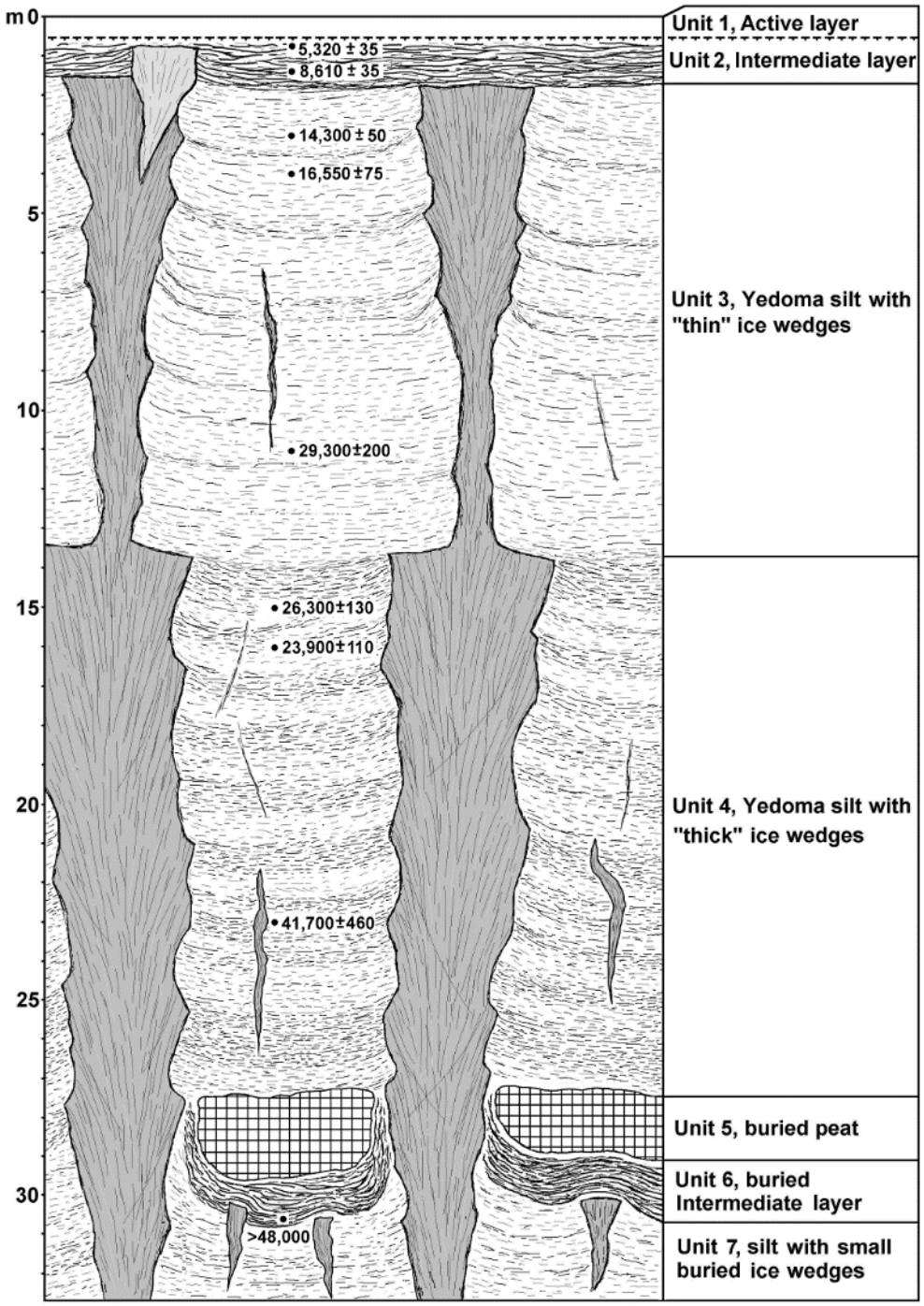


Figure 41. Cryostratigraphic units of the Itkillik yedoma (ice wedges width not to scale) and radiocarbon age of deposits, $^{14}$C yr BP (from Kanevskiy et al., 2011a)

The organic carbon content of yedoma varies from 0.01–1.7% (average 0.4%), which is low in comparison with many other yedoma sequences. The Itkillik yedoma has a very high content of wedge ice (Figure 42), in contrast to the relatively low water content due to pore and segregated ice in the silt. There are four generations of wedge ice, which we attribute to four periods of formation. Relatively thin and short Holocene ice wedges occur within the

intermediate layer (Unit 2). These wedges are 1−2 m wide and 3−4 m tall, triangular, and still active. Ice wedges in Unit 3 are relatively wide at the top (3−4 m), and their width decreases gradually with depth. In the lower part of the unit (at depths from 6−7 m to 13−14 m), the width of ice wedges rarely exceeds 1−2 m. The space between ice wedges varies from 7–10 m. Ice wedges in Unit 4 are 5−7 m wide, and their width remains fairly constant with depth. The total vertical size of ice wedges at this location cannot be determined because most of them continue below the Itkillik River water level. Ice wedges in Unit 7, located at the bottom of the exposure beneath the peat layer, are less than 0.7 m in width and 2.5−3 m in height. The space between ice wedges varies from 3–8 m.

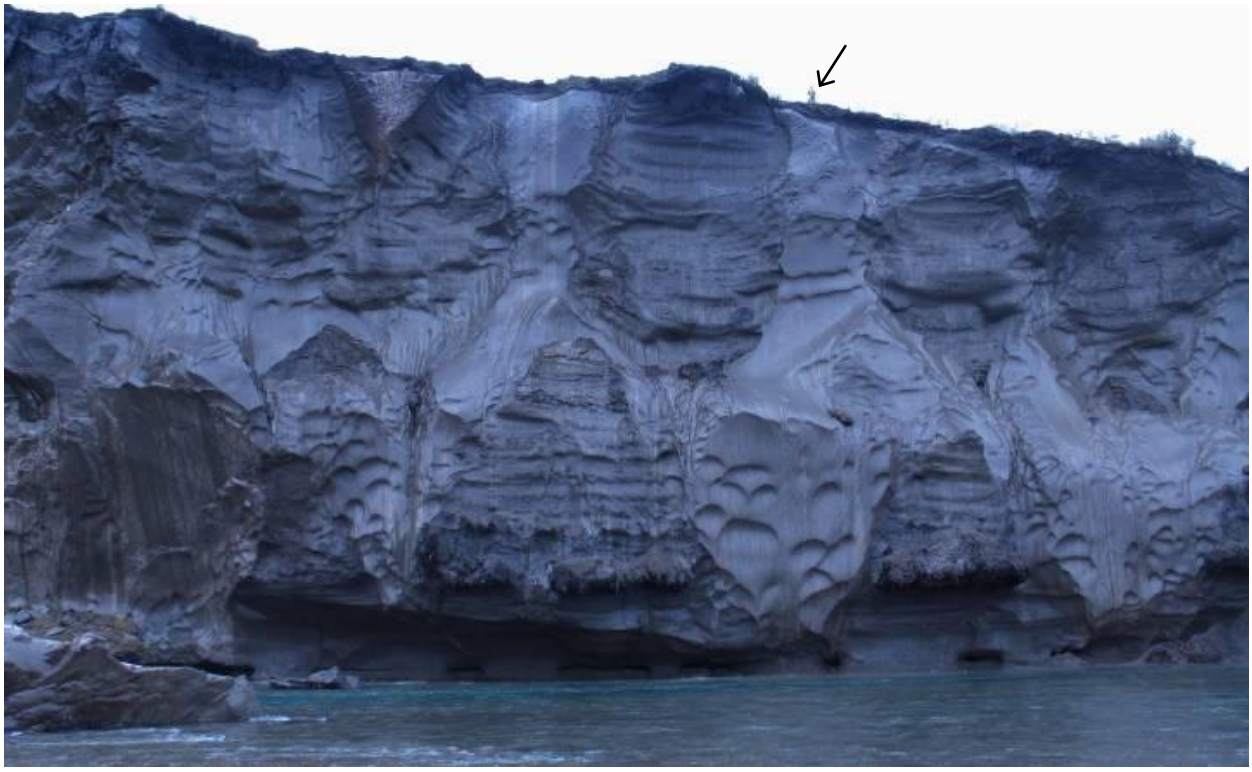

Figure 42. Large ice wedges in the Itkillik River exposure, August 2007
A person stands above the bluff for scale (from Kanevskiy et al., 2011b)

To estimate the wedge-ice volume, a composite of black and white images from numerous photographs of ice wedges taken in August 2006 and August 2007 was created (Figure 43). Based on measurements of the areas occupied by wedge ice in these images, wedge-ice volume varies from 40–52% in cryostratigraphic Units 2–3, and is about 78% in Units 4–7 (calculations were performed for the 240 m central section of the exposure). On average, wedge ice occupies 57% of the entire exposed bluff.

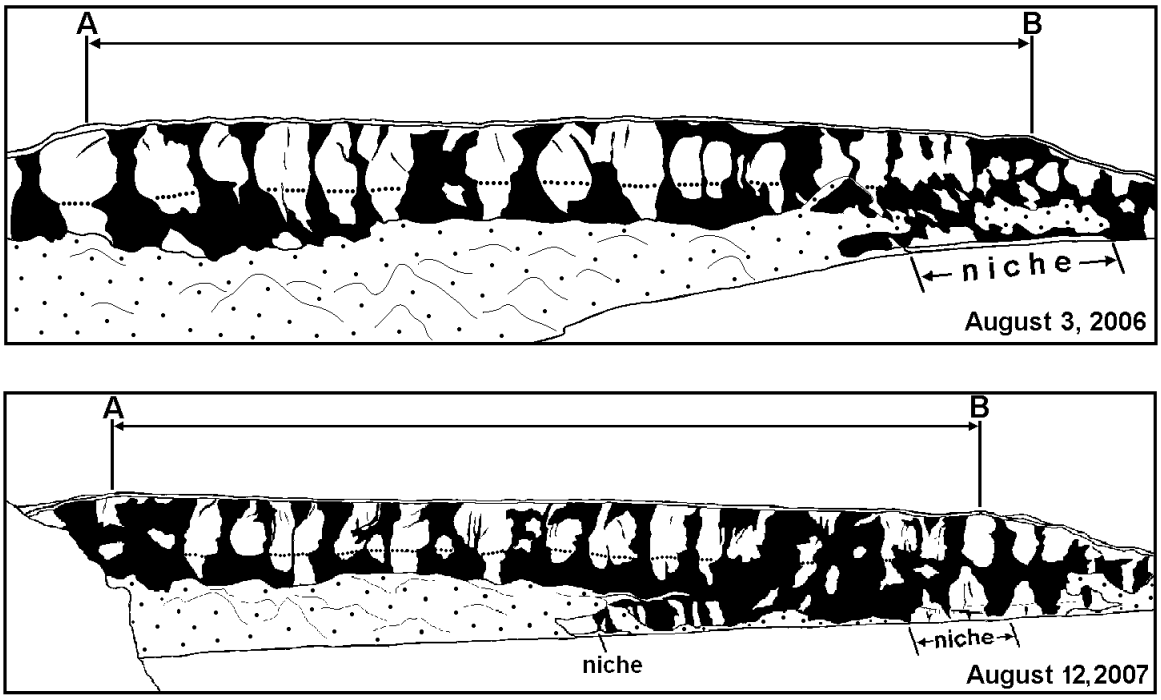


Figure 43. Appearance of wedge-ice (black) in the Itkillik River exposure on August 3, 2006, and August 12, 2007
AB – central part of the bluff with flat yedoma surface, the length is 240 m.
Dotted line shows the boundary between Units 3 and 4 (Kanevskiy et al., 2011b)

The total volume of ground ice including wedge ice, pore ice, and segregated ice between ice wedges is 90% in Unit 4 and 83% for the entire bluff (Figure 44). Thawing of this extremely ice-rich material can cause a dramatic decrease in elevation of the ground surface. The total thaw settlement of the Itkillik yedoma can reach at least 20 m, which corresponds to observed depths of thaw-lake basins in the study area.

In August 2011, 21 boreholes were drilled on the main yedoma surface at the Itkillik River site along the 200 m long transect (the distance between boreholes was 10 m). Fifteen boreholes (71%) encountered wedge ice at depths from 0.58 to 2.43 m. We could distinguish 2 different generations of ice wedges: active Holocene ice wedges (clean ice with very thin vertical air bubbles) and buried (inactive) late Pleistocene ice wedges (sediment-rich ice with bigger air bubbles). Holocene ice wedges were encountered in 7 boreholes at depths from 0.58 to 0.94 cm (0.73 m average), while Pleistocene ice wedges were encountered in 8 boreholes at depths from 1.42 to 2.43 cm (1.87 m average). According to these data, the volume of Holocene wedge ice within the intermediate layer is estimated at 33%, and the total volume of wedge ice in the upper permafrost at 71%. Such estimation gives us slightly greater values than the volume of wedge ice calculated for the black and white images of ice wedges in the exposure (Figure 43). For the upper 4 m of the exposure, this value was about 57% (Figure 44).

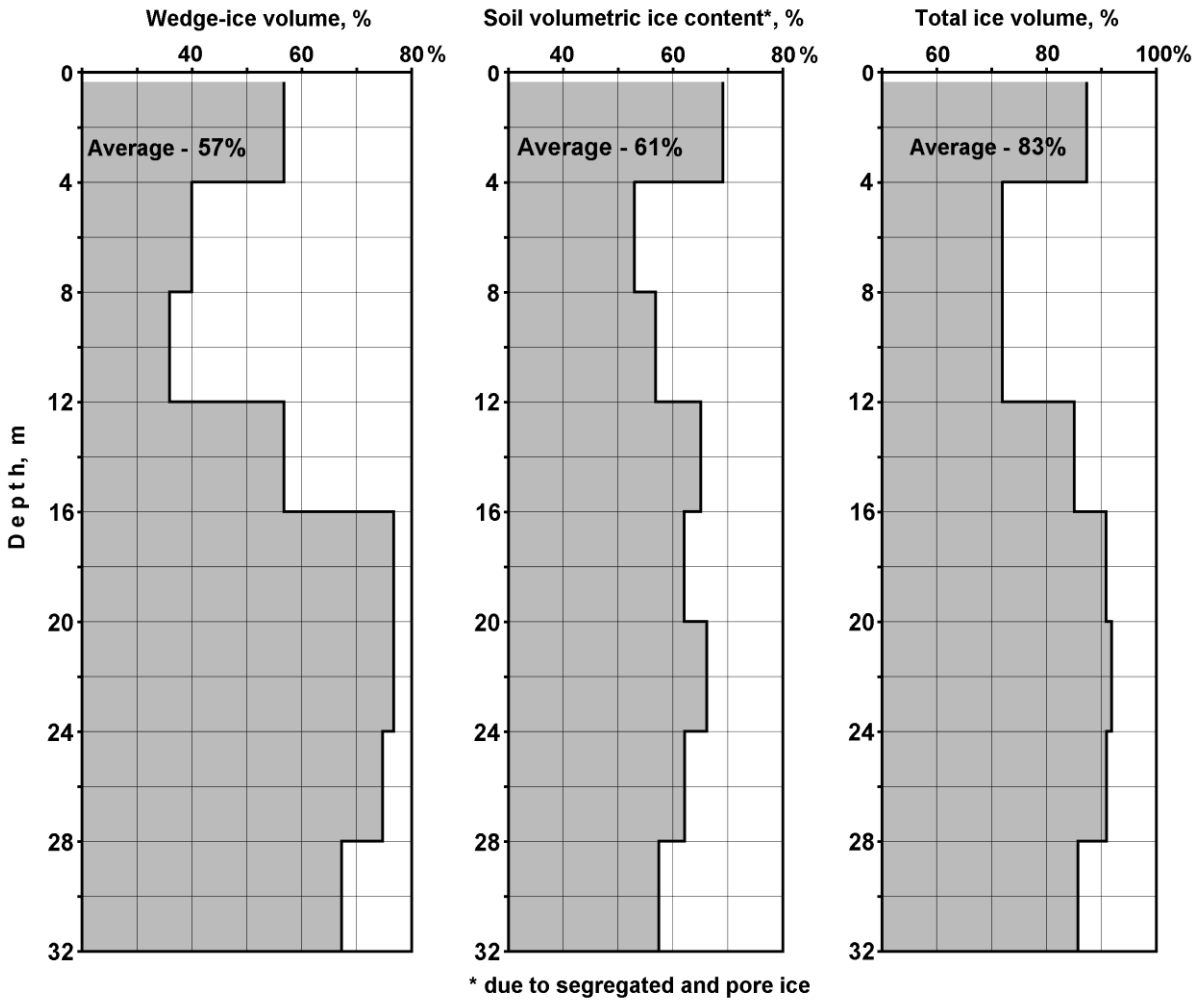


Figure 44. Percent volume of wedge, segregated, and pore ice with depth in the Itkillik River exposure (from Kanevskiy et al., 2011a)

Our study sites of 2010 were located within an area of widespread yedoma deposits. During fieldwork, 14 boreholes up to 4 m deep were drilled in permafrost with the SIPRE corer at 3 study sites: AL2, AL4, and AR6 (Bridge) (Figure 37 and Figure 38).

**Alignment Hole #2 – AL2**

The AL2 study site is located in an area of burned tussock tundra (the 2007 Anaktuvuk River burn) between the Itkillik and Anaktuvuk Rivers (Figure 37). This area comprises two major terrain units: low hills with gentle slopes formed by ice-rich yedoma deposits and flat thaw-lake basins connected by erosional patterns (Figure 45 and Figure 46). Deposits of thaw-lake basins consist of ice-rich peat and organic-rich silt, with modern ice wedges underlain by relatively ice-poor lacustrine and taberal (thawed and refrozen) silt.

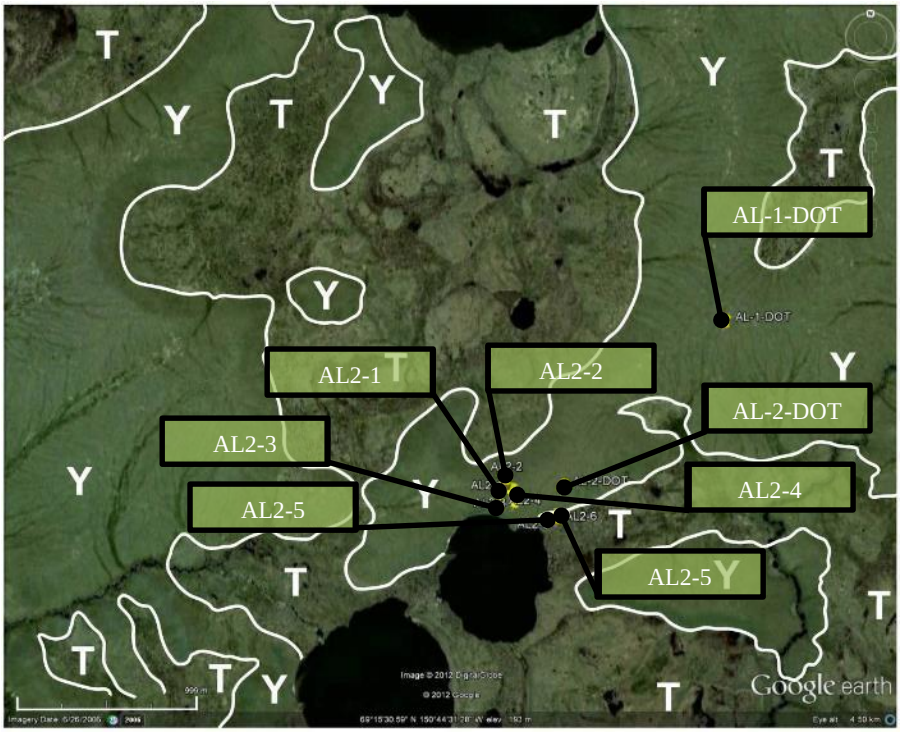


Figure 45. Surficial geology map of the area of AL2 study site
Y – yedoma deposits (ice-rich silt with large ice wedges); T – deposits of thaw-lake basins (ice-rich peat with modern ice wedges underlain by lacustrine and taberal silt)

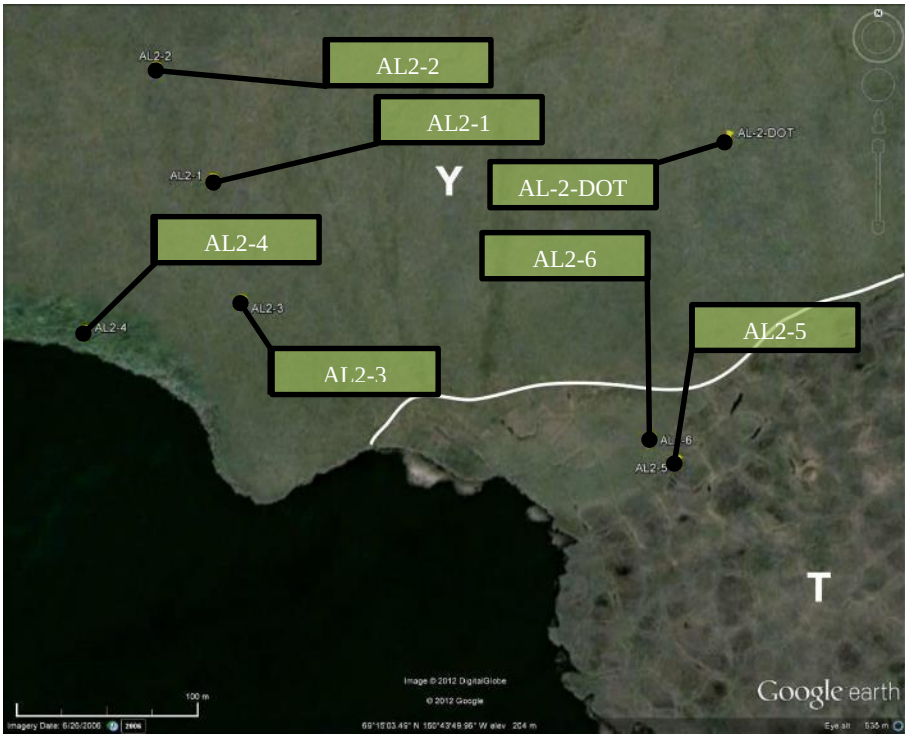


Figure 46. Location of boreholes at AL2 study site
Y – yedoma deposits (boreholes AL2-DOT, AL2-1, AL2-2, AL2-3, AL2-4);
T – deposits of thaw-lake basins (boreholes AL2-5, AL2-6)

The sections of boreholes AL1-DOT (TH10-632), AL2-DOT (TH10-631), AL2-1, AL2-2, AL2-3, AL2-4, AL2-5, and AL2-6 (Figure 45 and Figure 46**)** are briefly described below. The cryogenic structure and gravimetric water content of soils from the boreholes (study site AL2) are summarized in Figure 47.

**AL1-DOT (TH10-632)**

9/1/2010, N69.26022 W150.70390, yedoma deposits

| | |
|---|---|
| 0-39 cm | Active layer |
| 39-73 | Gray silt, very ice-rich |
| 73-79 | Peat |
| 79-145 | Gray silt, very ice-rich from 120 cm |
| 145-400… | Wedge ice |

**AL2-DOT (TH10-631), elevation approximately 199 m**

9/1/2010, N69.25206 W150.72679, yedoma deposits

| | |
|---|---|
| 0-57 cm | Active layer |
| 57-97 | Gray silt, very ice-rich |
| 97-600… | Wedge ice |

**AL2-1, elevation 197.8 m**

9/8/2010, N69.25185 W150.73398, yedoma deposits

| | |
|---|---|
| 0-42 cm | Active layer (0-12 cm – org.) |
| 42-92 | Gray silt, mostly ice-rich |
| 92-150… | Wedge ice |

**AL2-2, elevation 198.7**

9/8/2010, N69.25240 W150.73477, yedoma deposits

| | |
|---|---|
| 0-43 cm | Active layer (0-18 cm – org.) |
| 43-60 | Peat/silt vertical structure |
| 60-100 | Gray to brown-gray silt with vertical peat “veins”, ice-rich |
| 100-217 | Gray to yellow-gray silt, mostly ice-rich |
| 217-250… | Wedge ice |

**AL2-3, elevation 194.8 m**

9/8/2010, N69.25125 W150.73357, yedoma deposits

| | |
|---|---|
| 0-49 cm | Active layer (0-15 cm – org.) |
| 49-100 | Gray silt with organics, mostly ice-rich |
| 100-163 | Gray silt, ice-rich/relatively ice poor (interbedding), |
| 163-200… | Wedge ice |

**AL2-4, elevation 192.7 m**,
yedoma deposits, top of baidzharakh (thermokarst mound)

9/9/2010, N69.25110 W150.73575
0-150 cm Active layer (yellow-gray silt)
150-277… Yellow-gray silt, relatively ice-poor

**AL2-5, elevation 189.5 m**

9/9/2010, N69.25046 W150.72749, thaw-lake basin
0-48 cm Active layer (peat mostly)
48-137 Peat, silty peat, mostly ice-rich
137-255 Gray silt with peat layers/inclusions, ice-rich
255-389… Gray silt, mostly ice-poor

**AL2-6, elevation 189.7 m**

9/9/2010, N69.25057 W150.72786, thaw-lake basin
0-47 cm Active layer (peat)
47-110… Wedge ice

Figure 48 and Figure 49 show major cryostratigraphic units and expected massive ground ice distribution in yedoma deposits at the AL2 study site. We do not have sufficient data to estimate the thickness of yedoma deposits, but taking into account the elevation of the yedoma hill above the lake (Figure 49), we presume that it exceeds 12 m. The content of wedge ice in yedoma deposits is presumably very high: four of five SIPRE-corer boreholes encountered ice wedges at depths from 0.9 m to 2.2 m (Figure 47). Ice wedges were also encountered by two DOT boreholes (TH10-631 and TH10-632). No distinct ice-wedge polygons were visible on the yedoma surface. At some places, shallow troughs above degrading ice wedges could be observed. While choosing locations for the boreholes, we tried to avoid the surfaces affected by ice-wedge thermokarst (troughs above thawing ice wedges). The gravimetric moisture content (GMC) of the intermediate layer (above the ice wedges) varied from 56–223% (average 112%, $n$ = 14). A single borehole without wedge ice (AL2-4) was drilled from the top of a baidzharakh (thermokarst mound), which formed due to thawing of the surrounding ice wedges (Figure 49). The GMC of yedoma silt in this borehole varied from 59–82% (average 71%, $n$ = 5).

Thaw-lake basin deposits were studied in borehole AL2-5 (Figure 47). The deposits consist of ice-rich peat almost 1.5 m thick and gray lacustrine silt more than 1 m thick, which contains layers and inclusions of peat. The GMC of the peat varied from 180% to more than 300%, and the GMC of the silt varied from 80–170%. These layers, which belong to syngenetic permafrost, contain active ice wedges. In borehole AL2-6, wedge ice was encountered right below the active layer at a depth of less than 0.5 m. In borehole AL2-5, ice-poor deep-water lacustrine and taberal (thawed and refrozen) silt with peat layers was detected from 2.55–3.89 m. The GMC of silt varied from 33–61%. Though the peat layer contained almost no visible ice, its GMC was 234%.

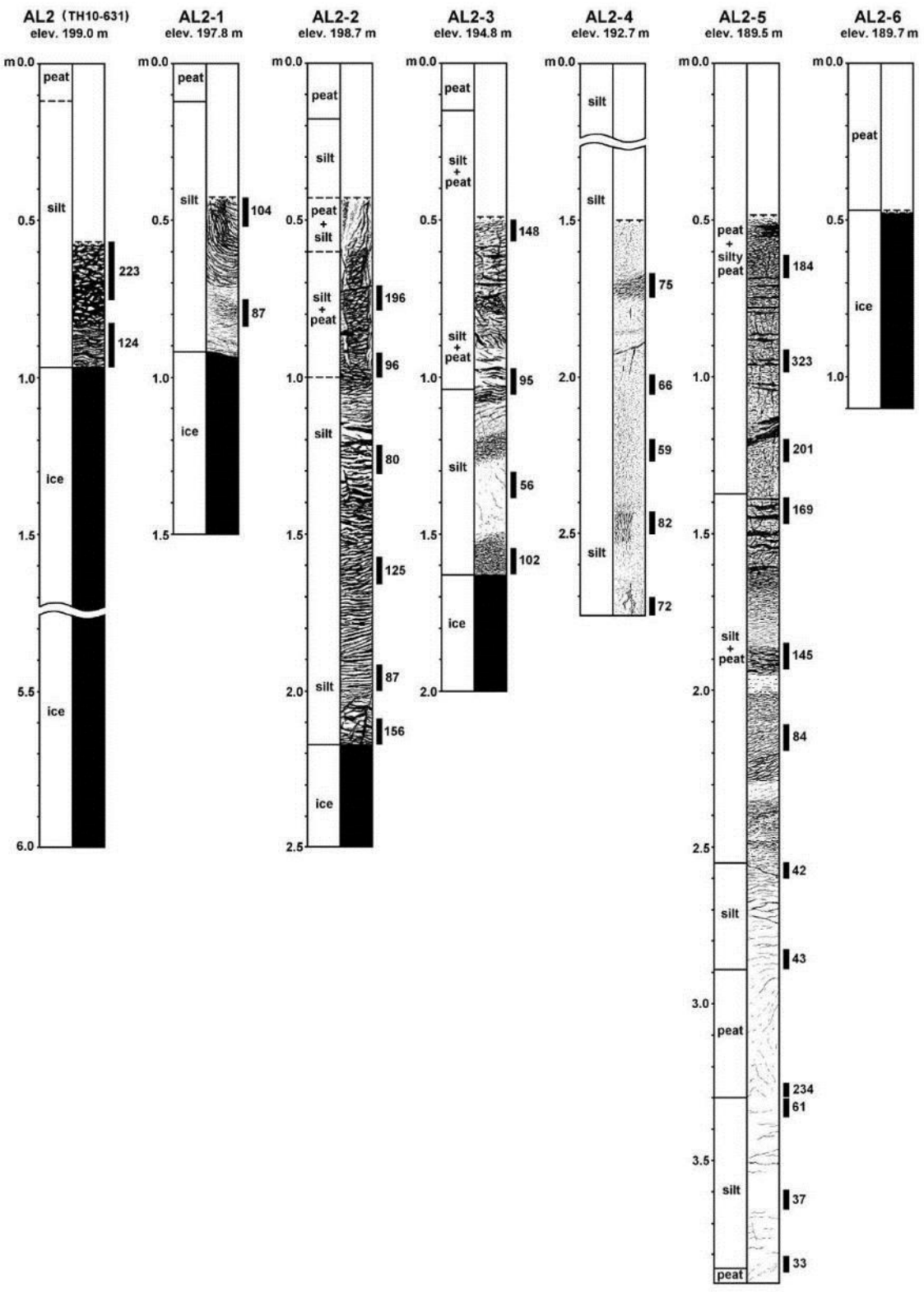


Figure 47. Cryogenic structure and gravimetric water content (%) of frozen soils, site AL2 (ice is black)

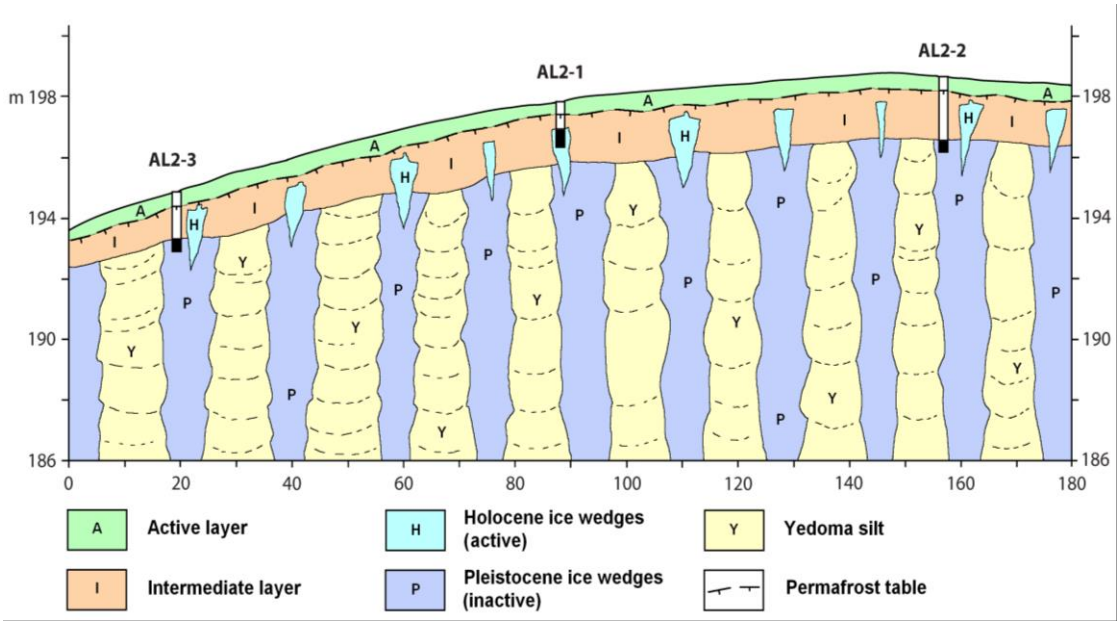


Figure 48. Cryostratigraphic profile, boreholes AL2-1, AL2-2, and AL2-3

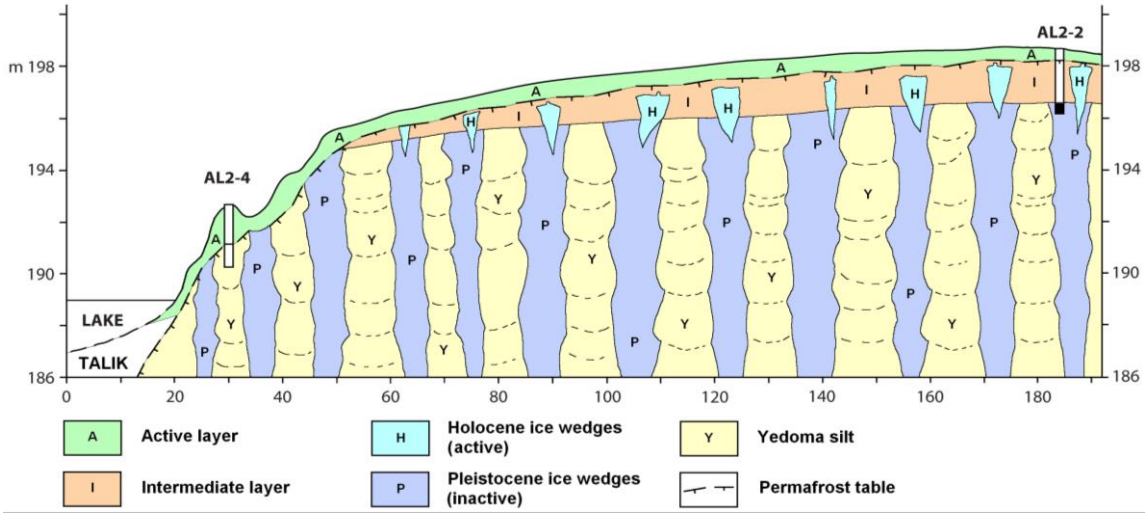


Figure 49. Cryostratigraphic profile, boreholes AL2-2 and AL2-4

**Alignment Hole #4 – AL4**

The AL4 study site is located at the left bank of the Anaktuvuk River (Figure 37). This area is comprised of four major terrain units: (1) low hills with gentle slopes formed by ice-rich yedoma deposits, (2) flat thaw-lake basins and shallow thermokarst depressions connected by erosional patterns, (3) slopes of river valleys formed by alluvial gravel, and (4) modern floodplains (Figure 50 and Figure 51). The height of the yedoma hills is 30–50 m above the surface of the Anaktuvuk River floodplain.

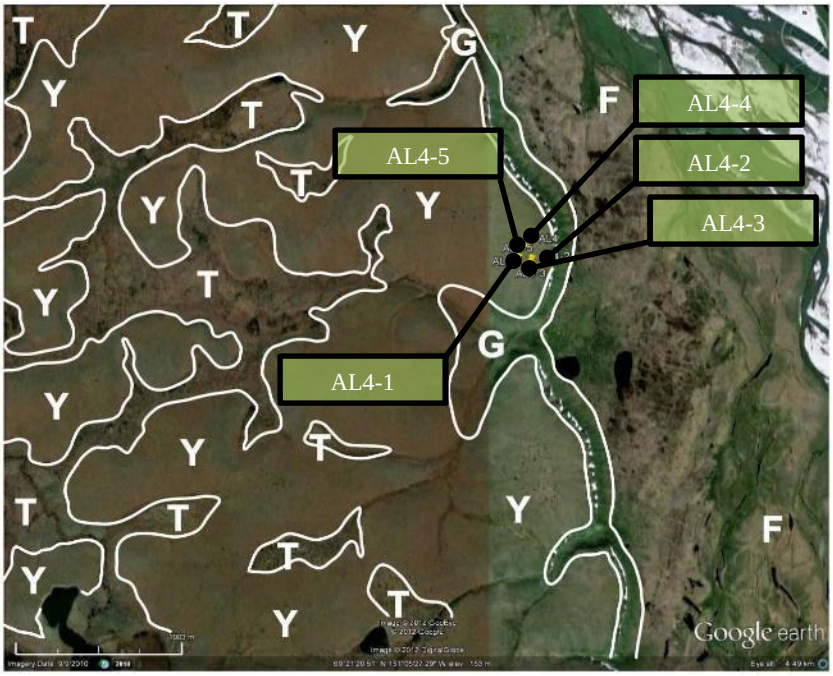


Figure 50. Surficial geology map of the area of the AL4 study site
Y – yedoma deposits (ice-rich silt with large ice wedges); T – deposits of thaw-lake basins (ice-rich peat with modern ice wedges underlain by lacustrine and taberal silt) and shallow thermokarst depressions; G – ice-poor gravel deposits exposed in slopes of river valleys; F – floodplain deposits (gravel, sand, and silt; frozen and unfrozen)

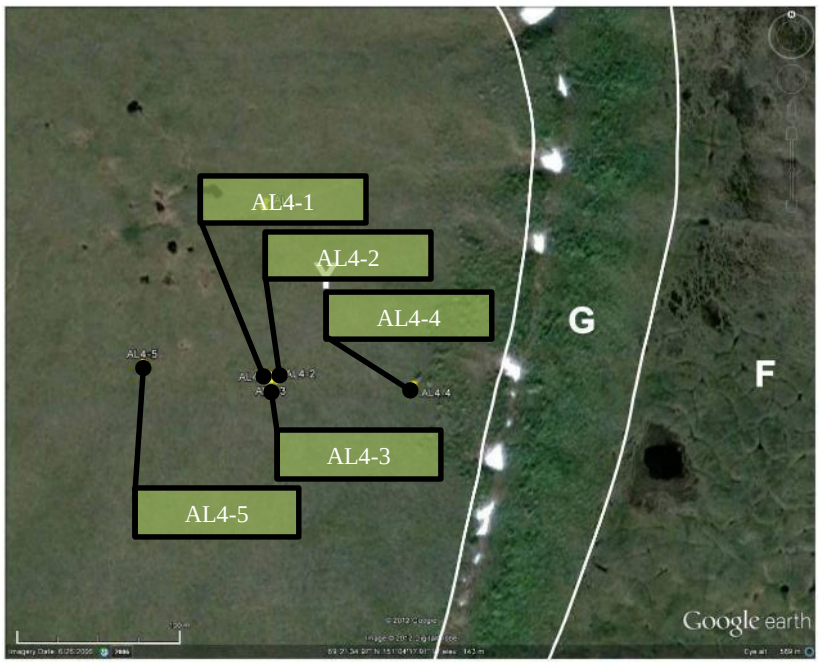


Figure 51. Location of boreholes at AL4 study site
Y – yedoma deposits (boreholes AL4-1, AL4-2, AL4-3, AL4-4, and AL4-5); G – gravel deposits exposed in slopes of river valleys; F – floodplain deposits. Modern ice-wedge polygons are visible on the surface of the floodplain. Small ponds on the surface of a yedoma hill are related to troughs developed above thawing ice wedges

The sections of boreholes AL4-1, AL4-2, AL4-3, AL4-4, and AL4-5 (Figure 50 and Figure 51**)** are briefly described below. All these boreholes, drilled with the SIPRE corer, are located within the yedoma hill. A nearby borehole drilled by DOT encountered an ice wedge with a vertical extent that exceeded 8 m. The cryogenic structure and gravimetric water content of soils from the boreholes (study site AL4) are summarized in Figure 52.

**AL4-1, elevation 155.3 m**

9/7/2010, N69.35942 W151.07379, yedoma deposits

| | |
|---|---|
| 0-59 cm | Active layer (0-9 cm – org.) |
| 59-73 | Brown silt and peat, very ice-rich |
| 73-100… | Wedge-ice |

**AL4-2, elevation 155.4 m**

9/7/2010, N69.35941 W151.07382, yedoma deposits

| | |
|---|---|
| 0-39 cm | Active layer (0-17 cm – org.) |
| 39-47 | Brown silt and peat |
| 47-73… | Wedge-ice |

**AL4-3, elevation 155.5 m**

9/7/2010, N69.35941 W151.07391, yedoma deposits

| | |
|---|---|
| 0-34 cm | Active layer (0-22 cm – org.) |
| 34-99 | Brown silt and peat, from 49 – peat with ice-rich gray silt (subvertical structure) |
| 99-212 | Gray silt, mostly ice-rich |
| 212-270… | Wedge-ice |

**AL4-4, elevation 149.5 m**

9/7/2010, N69.35935 W151.07167, yedoma deposits

| | |
|---|---|
| 0-36 cm | Active layer (0-15 cm – org.) |
| 36-70 | Brown-gray silt and peat, mostly ice-rich |
| 70-102 | Gray silt, mostly ice-rich |
| 102-216 | Yellow silt (ice-rich/relatively ice poor - interbedding), from 153 cm - with rare small coarse inclusions |
| 216-… | Gravel (no core) |

**AL4-5, elevation 154.8 m**

9/8/2010, N69.35948 W151.07591, yedoma deposits (slope of the valley)

| | |
|---|---|
| 0-43 cm | Active layer (0-13 cm – org.) |
| 43-100 | Gray silt, organic-poor, mostly ice-rich |
| 100-130… | Wedge ice |

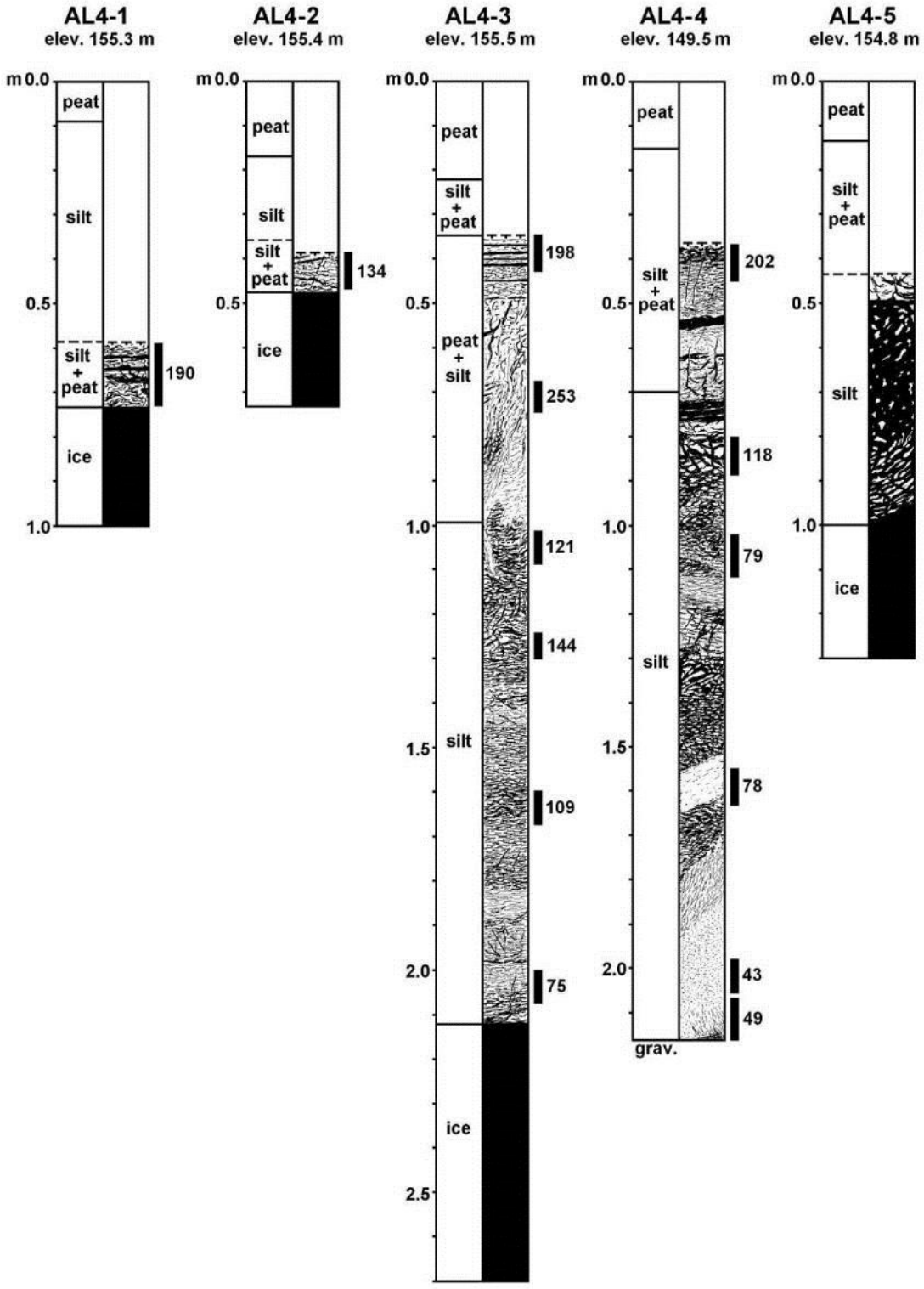


Figure 52. Cryogenic structure and gravimetric water content (%) of frozen soils, site AL4 (ice is black)

Figure 53 shows the major cryostratigraphic units and expected massive ground ice distribution in yedoma deposits at the AL4 study site. The yedoma deposits are at least 8 m thick. The wedge ice content of the yedoma deposits is presumably very high; four of five SIPRE-corer boreholes encountered ice wedges at depths of 0.5 m to 2.1 m (Figure 52). An ice wedge with a vertical extent that exceeded 8 m was also encountered in a DOT borehole located nearby on the main yedoma surface. There were no distinct ice-wedge polygons on the yedoma surface. Small ponds on the surface of a yedoma hill (Figure 51) are related to troughs developed above the thawing ice wedges. While choosing locations for the boreholes, we tried to avoid the surface affected by ice-wedge thermokarst (troughs above degrading ice wedges). The single borehole without wedge ice (AL4-4) was drilled on the slope of the river valley, approximately 2 m above the boundary between yedoma deposits and alluvial gravel (Figure 53). The GMC of the intermediate layer varied from 75–252% (average 148%, $n$ = 11). The GMC of the yedoma silt in borehole AL4-4 varied from 43–78% (average 57%, $n$ = 3).

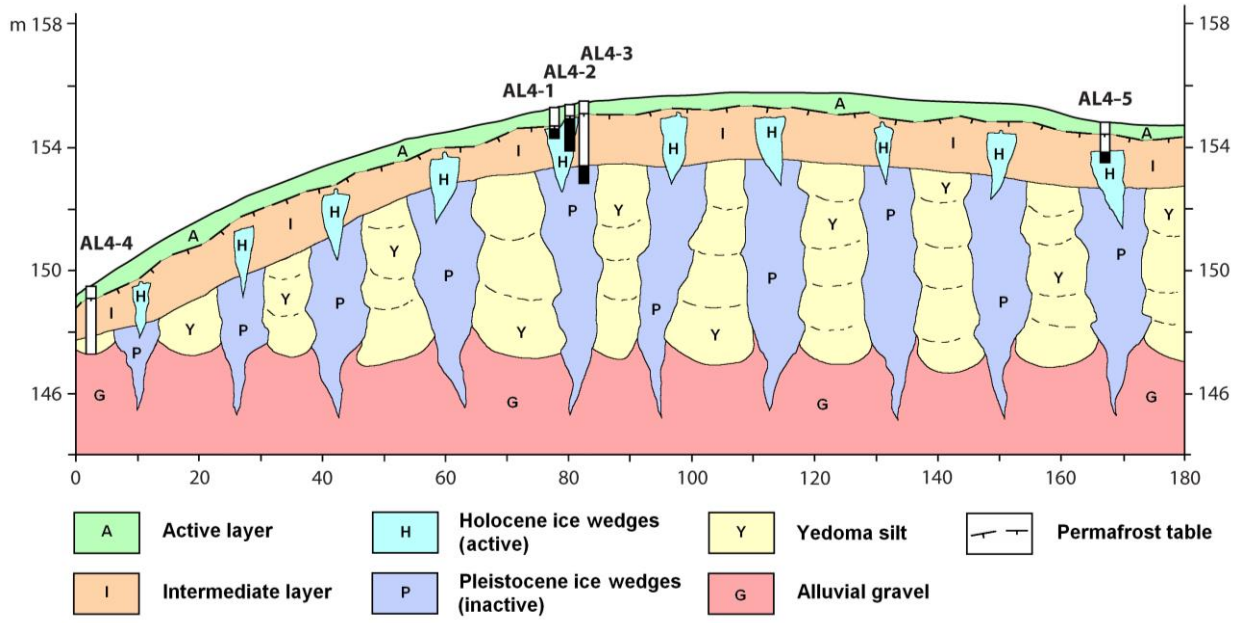


Figure 53. Cryostratigraphic profile, boreholes AL4-1, AL4-2, AL4-3, AL4-4, and AL4-5

**Anaktuvuk River Bridge Crossing (AR6) – BRIDGE**

The AR6 (Bridge) study site is located in the area of burned tussock tundra (2007 Anaktuvuk River burn) on the right bank of the Anaktuvuk River (Figure 37). This area comprises four major terrain units: (1) low hills with gentle slopes formed by ice-rich yedoma deposits, (2) slopes of river valleys formed by alluvial gravel, (3) river terrace (abandoned floodplain), and (4) modern floodplains (Figure 54 and Figure 55). The height of the yedoma hills is 30–50 m, and the height of the river terrace is approximately 5 m above the surface of the Anaktuvuk River floodplain.

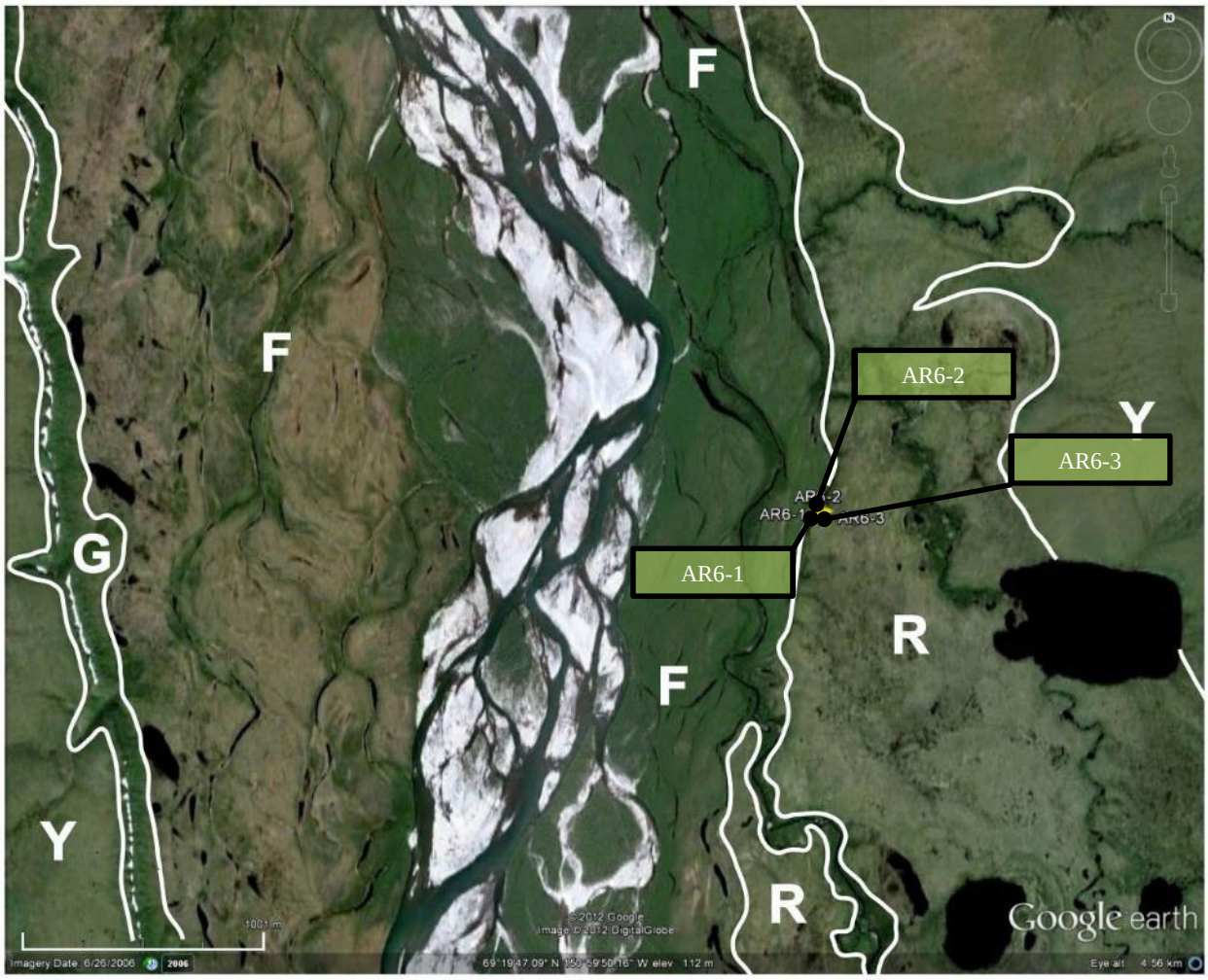


Figure 54. Surficial geology map of the area around the AR6 (Bridge) study site
Y – yedoma deposits (ice-rich silt with large ice wedges); G – ice-poor gravel deposits exposed in slopes of river valleys; F – floodplain deposits (gravel, sand, and silt; frozen and unfrozen); R – deposits of river terrace (silt, peat, sand, and gravel, ice wedges)

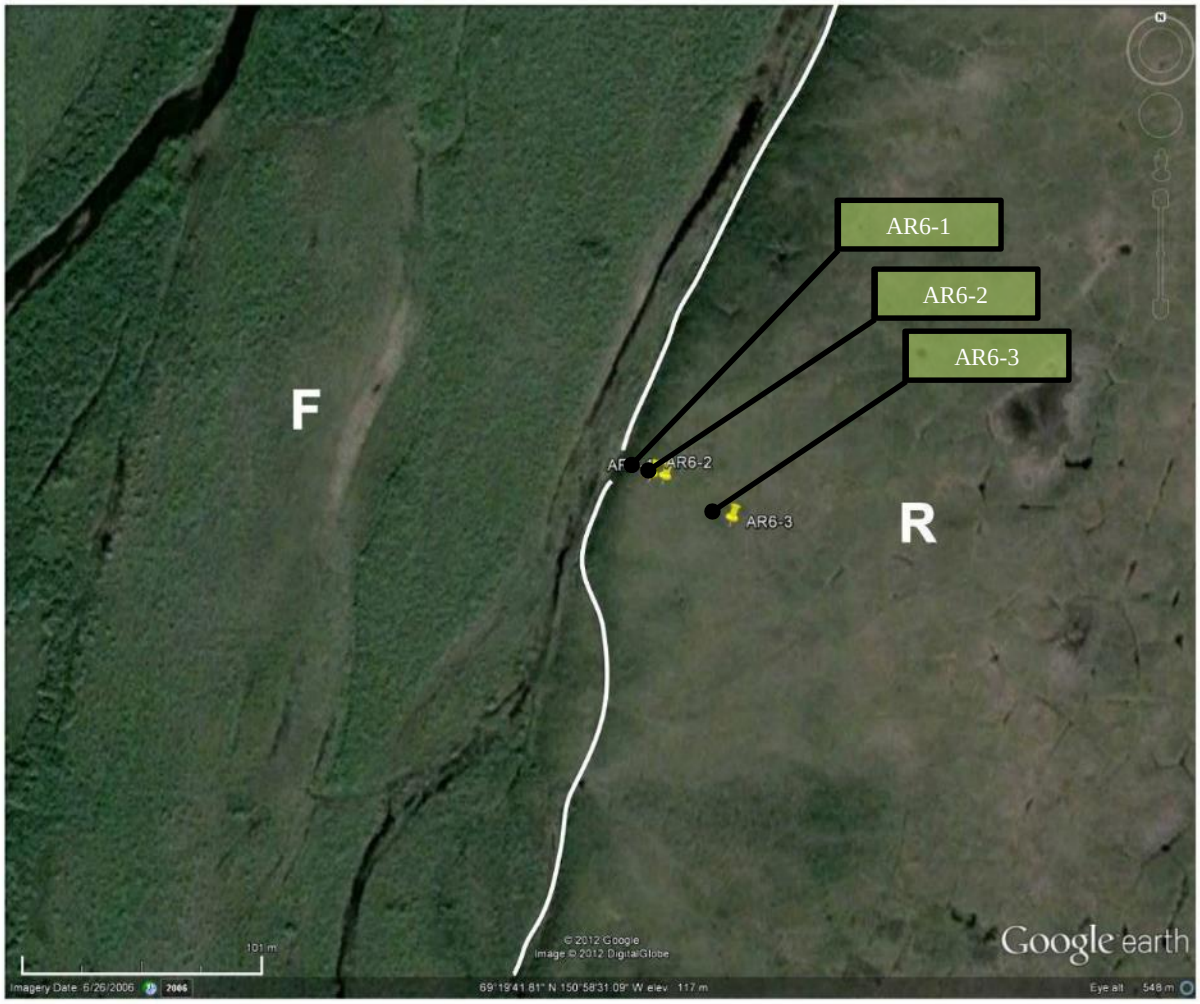


Figure 55. Location of boreholes at the AR6 (Bridge) study site
R – deposits of river terrace (boreholes AR6-1, AR6-2, and AR6-3; F – floodplain deposits (unfrozen). High-centered ice-wedge polygons are visible on the surface of river terrace

The sections of boreholes AR6-1, AR6-2, and AR6-3 (Figure 54 and Figure 55**)** are briefly described below. These boreholes, drilled with the SIPRE corer, are located within the river terrace (abandoned floodplain). All boreholes reached gravel deposits at depths of 0.9–1.9 m. The cryogenic structure and gravimetric water content of soils from the boreholes (study site AR6) are summarized in Figure 56.

**AR6-1 (Bridge-1), elevation 116.1 m**

9/10/2010, N69.32834 W150.97467, burned tussocks, center of polygon

| | |
|---|---|
| 0-46 cm | Active layer (peat mostly) |
| 46-80 | Peat, ice-rich, from 60 cm – relatively ice-poor |
| 80-90 | Gray silty sand, fine – very fine, ice-rich |
| 90-180 | Gray and yellow gray sand, fine to medium, from 173 cm – medium to coarse, mostly ice-poor |
| 180-… | Gravel (no core) |

**AR6-2 (Bridge-2), elevation 115.9 m**

9/10/2010, N69.32835 W150.97481, trough above the ice wedge

| | |
|---|---|
| 0-30 cm | Active layer (peat) |
| 30-82 | Wedge-ice |
| 82-90 | Wedge-ice/sand boundary |
| 90-… | Gravel (no core) |

**AR6-3 (Bridge-2), elevation 116.9 m**

9/10/2010, N69.32819 W150.97397, burned tussocks, center of polygon

| | |
|---|---|
| 0-45 cm | Active layer (peat, silty peat) |
| 45-153 | Peat and organic silt, extremely ice-rich, from 60 cm – relatively ice-poor |
| 153-164 | Peat and gray silty sand, fine to very fine, ice-rich |
| 164-193 | Gray sand, fine to medium, ice-rich |
| 193-… | Gravel (no core) |

Figure 57 shows the major cryostratigraphic units and expected massive ground ice distribution of the river terrace deposits at the AR6 (Bridge) study site. The upper permafrost at this location consists of ice-rich peat, silt, and silty sand deposits 0.6–1.3 m thick underlain by sand and gravel deposits. The GMC of the peat, silt, and silty sand deposits varied from 117–144% (average 293%, $n$ = 5). The GMC of the underlying sand deposits varied from 33–112% (average 64%, $n$ = 5). High-centered ice-wedge polygons are framed by troughs up to 1 m deep and 1.5 m wide, developed above thawing ice wedges. We expect that the vertical extent of ice wedges in the river terrace deposits does not exceed 3 m because gravel deposits are located close to the surface. Borehole AR6-2 (Figure 56 and Figure 57) was drilled through the small ice wedge up to 0.3 m wide (Figure 58).

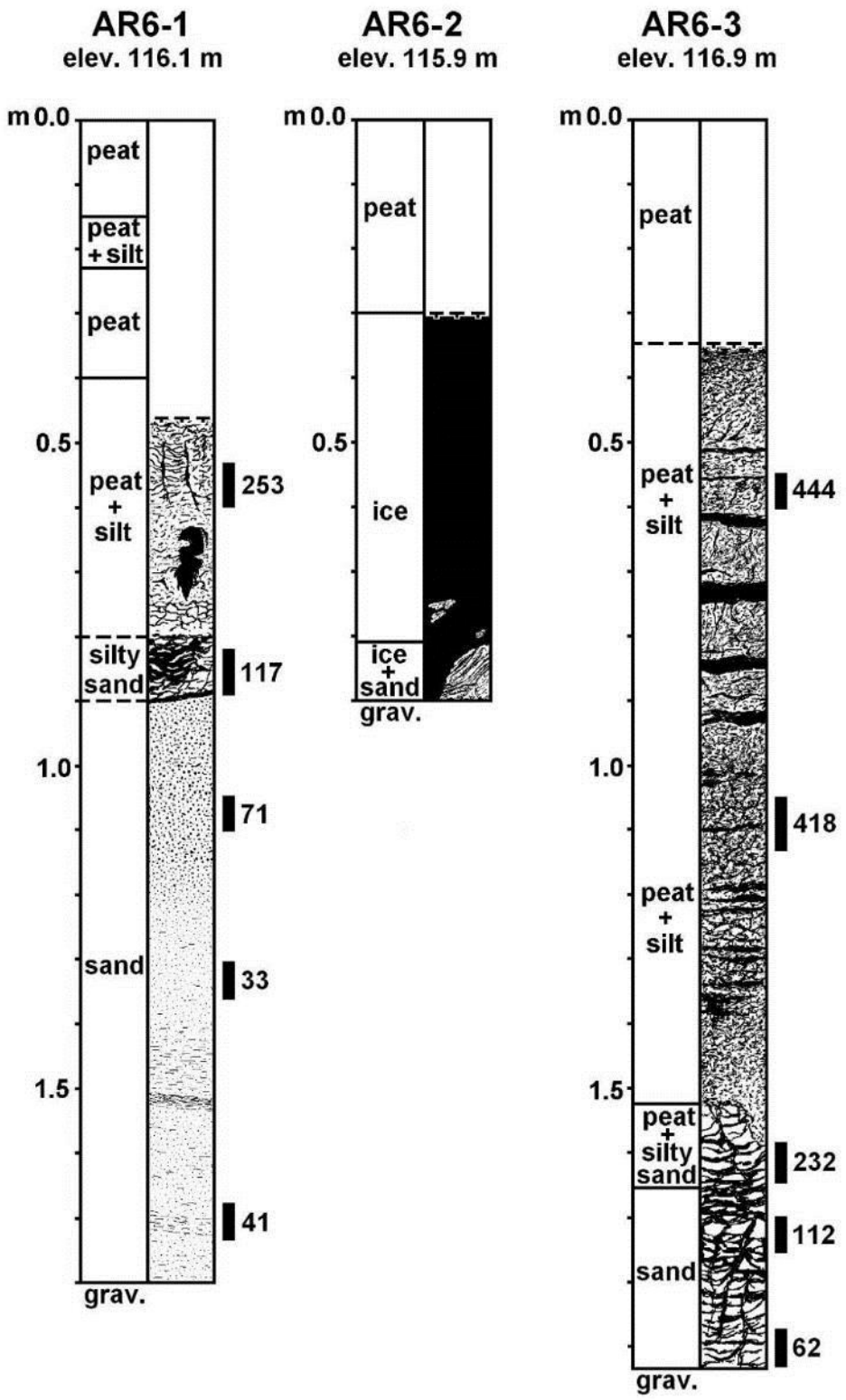


Figure 56. Cryogenic structure and gravimetric water content (%) of frozen soils, site AR6 (Bridge) (ice is black)

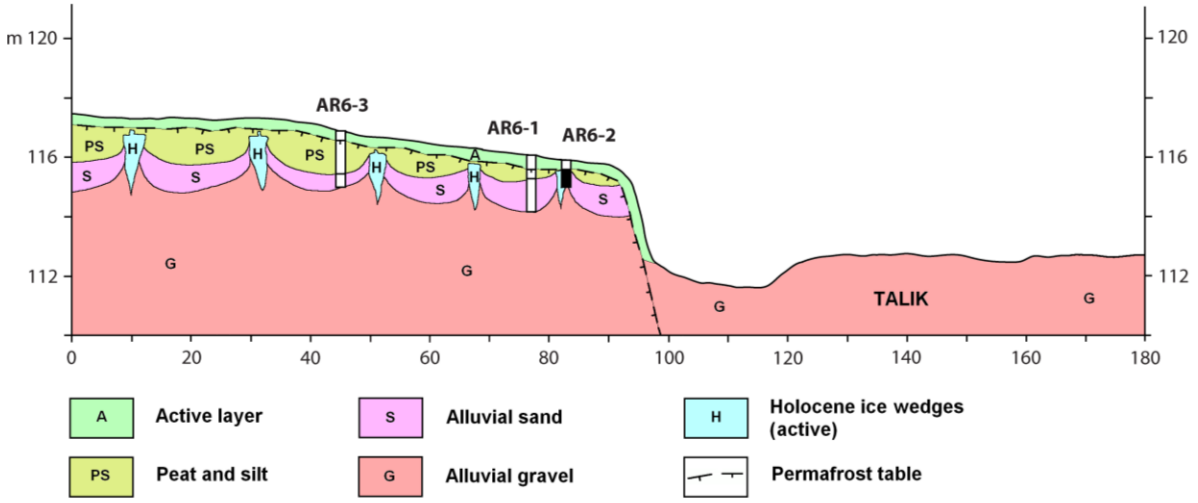


Figure 57. Cryostratigraphic profile, boreholes AR6-1, AR6-2, and AR6-3

Figure 58. Top surface of the small ice wedge, borehole AR6-2

**Terrain Units and Permafrost Properties at the Anaktuvuk Study Area**

The following summary is based on field studies at the AL2, AL4, and AR6 (Bridge) study sites and data from our study of the Itkillik River exposure (Kanevskiy et al., 2011a,b). The study area is dominated by six major terrain units: (1) low hills with gentle slopes and flat plateaus formed by ice-rich yedoma deposits, (2) flat thaw-lake basins connected by erosional patterns, (3) shallow thermokarst depressions connected by erosional patterns, (4) slopes of river valleys formed by alluvial gravel, (5) river terraces, and (6) modern floodplains.

**Low hills with gentle slopes and flat plateaus formed by yedoma deposits.** Yedoma silt deposits are characterized by extremely high ice content and include large ice wedges. The thickness of yedoma deposits varies from several meters to more than 35 m. There are two different generations of ice wedges: active Holocene ice wedges (most of them can be encountered at depths from 0.6–1.0 m) and buried (inactive) late Pleistocene ice wedges (most are encountered at depths from 1.5–2.5 m, and most penetrate through the whole yedoma stratum). The volume of Holocene wedge ice in the upper permafrost (within the intermediate layer) usually varies from 20–40%, and the volume of Pleistocene wedge ice varies from 40–70%. The GMC of the intermediate layer varies from 80% to more than 200%, while the GMC of Pleistocene yedoma deposits typically varies from 50–80%.

**Flat thaw-lake basins connected by erosional patterns.** The depth of thaw-lake basins varies from several meters to more than 20 m. Deposits of thaw-lake basins consist of ice-rich peat and organic-rich lacustrine silt (GMC varies from 80% to more than 300%) with modern active ice wedges underlain by relatively ice-poor lacustrine and taberal (thawed and refrozen) silt (GMC typically varies from 30–40%). Active ice wedges are very close to the surface and usually up to 3 m wide, with a vertical extent of up to 5 m. The thickness of peat usually varies from 1–3 m, and the thickness of ice-rich lacustrine silt typically does not exceed 2 m. The thickness of ice-poor thawed and refrozen silt depends on the initial (prior to thawing) thickness and ice content of yedoma deposits and can reach 10 m and more.

**Shallow thermokarst depressions connected by erosional patterns.** The depth of shallow thermokarst depressions does not exceed several meters. We believe these landforms are related mostly to degradation of relatively thin yedoma strata. In some cases, shallow thermokarst depressions form when thawing of yedoma under thermokarst lakes is interrupted by sudden lake drainage. Lack of drilling data prevents us from characterizing the structure and properties of deposits of shallow thermokarst depressions. Landforms transitional from thaw-lake basins to shallow thermokarst depressions can be observed.

**Slopes of river valleys formed by alluvial gravel.** Usually the slopes of river valleys formed by alluvial gravel are up to 50 m high, and at their upper parts, yedoma deposits can be detected. Gravel deposits are mostly ice-poor and do not contain large masses of ground ice.

**River terraces (abandoned floodplain).** Deposits of alluvial terraces include ice-rich peat and organic-rich silt and silty sand up to 2 m thick (GMC varies from 100% to more than 400%) with active ice wedges; the terraces are underlain by sand (up to 1 m thick; GMC decreases with depth from more than 100% to 40%) and gravel deposits, mostly ice-poor.

**Modern floodplains.** Several levels of floodplain can be detected. The younger (lower) levels are formed by unfrozen gravel (the depth of open talik is unknown). The older (higher) levels have permafrost, which is indicated by ice-wedge polygons (Figure 51). Lack of drilling data in the study area prevents us from characterizing the structure and properties of the floodplain deposits.

## Anaktuvuk Geophysical Results

### Anaktuvuk River – ANTRAN

The first transect ANTRAN#1 was located adjacent to the Anaktuvuk River on the east bank on a gravel bar and side channel that seasonally fills with water. Lack of contact between

the gravelly surface material and the electrodes (Figure 59 and Figure 60) prevented adequate data from being collected. Placed on the west bank of the Anaktuvuk River, the next transect ANTRAN#2 was perpendicular to the margin between the gravel floodplain and the vegetated alluvial plain. This transect also bisected smaller side channels that flood in peak river conditions. Active layer depths exceeded 1.5 m, and there was no indication of ice-rich permafrost. The gravelly active floodplain from 0 m to approximately 15 m had modeled resistivity values ~400 Ω m near the surface. In comparison, floodplain covered by vegetation had higher modeled resistivity values in the near surface, from 861 to over 1819 Ω m. In the field, an increase in the amount of sand further from the river was noted. The low values adjacent to the active river channel of 9 to 20 Ω m indicate a saturated condition where the presence of groundwater is highly probable. The shape of the layers indicated between 90 and 400 Ω m are indicative of channel movement over time. The phenomena are well documented in braided arctic rivers in the region.

**Alignment Hole #4 – AL4TRAN**

Two transects were located adjacent to the DOT Alignment Hole #4 borehole in moist non-acidic tussock tundra (Figure 61). The transect AL4TRAN#1 straddled the tussock tundra and hillslope leading down to the incised Anaktuvuk River valley. The average active layer depth was 49 cm with a standard deviation of 12 cm. Boreholes AL4-1, 2, and 3 indicated the presence of Holocene ice wedges on the flat-to-gently-sloping tundra. On either end of the transect, the boreholes AL-4 and 5 contained gravel at depths of 2.16 m from the surface with ice-rich silt from 0.36 m to 1.02 m and interbedded ice-rich and ice-poor sediments from 1.02 m to the top of the gravel. The AL4TRAN#1 DCR-ERT transect (Figure 62) modeled resistivities varied from 320 to 29,775 Ω m, with a maximum resolution depth of 25 m. In the section where boreholes AL4-1, 2, and 3 overlapped, the modeled resistivities were between 4269 and 8157 Ω m. There was an area of lower modeled resistivity toward electrode 1, with values around 15.5 kΩ m.

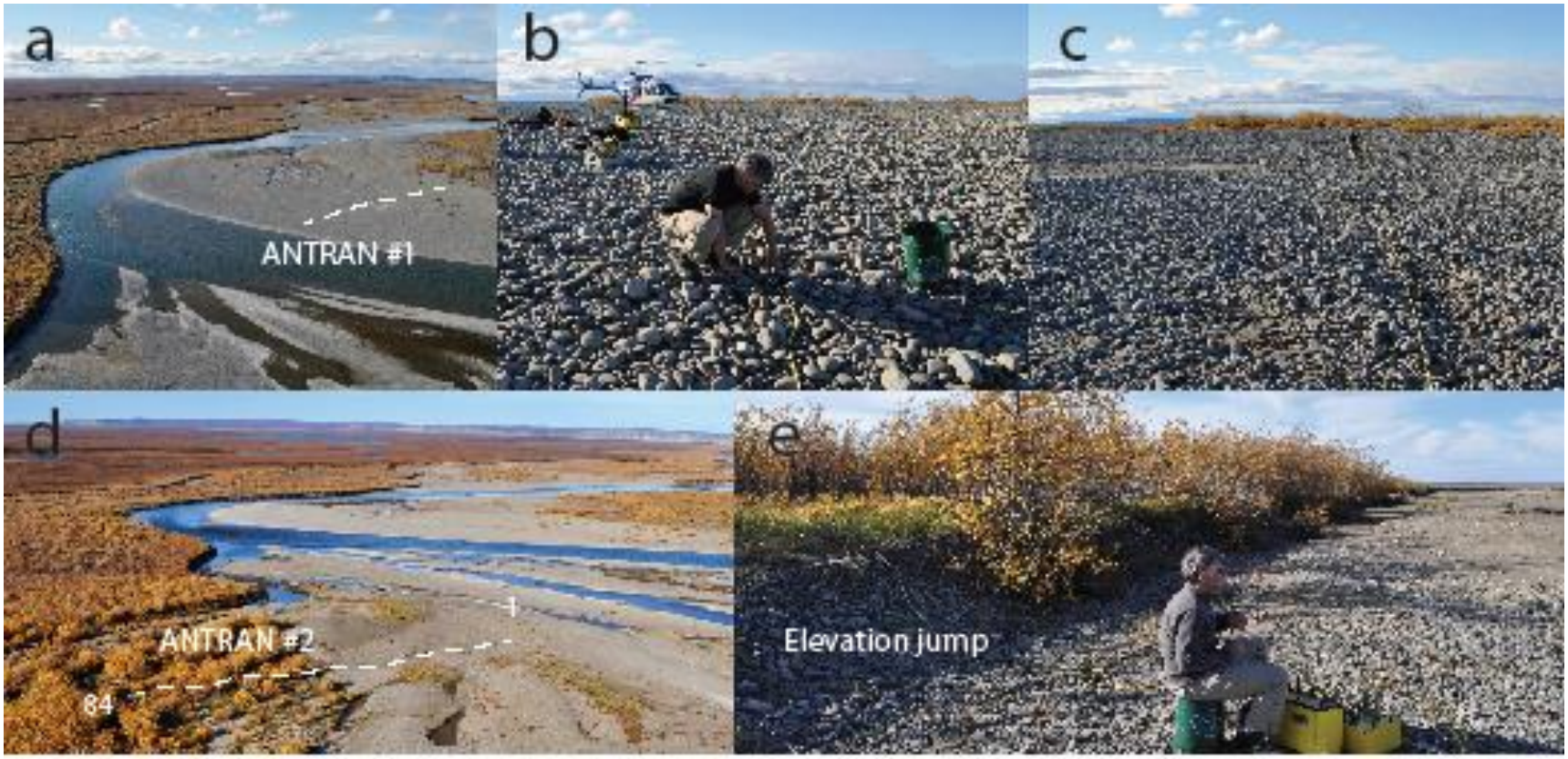


Figure 59. ANTRAN#1 site photos
a) Location of ANTRAN#1 looking toward Umiat bluffs; b) and c) Coarse gravelly surface; d) ANTRAN#2 across the Anaktuvuk River from ANTRAN#1; and e) Elevation jump on transect that was not captured in ASTER DEM due to 30 m resolution

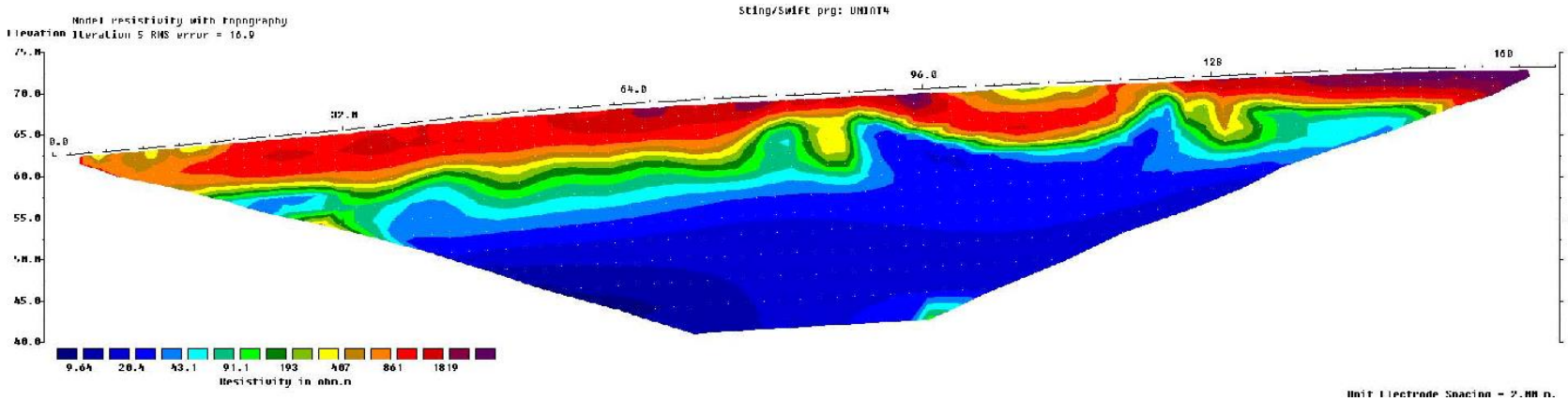


Figure 60. ANTRAN#1 results
DCR-ERT modeled resistivity (Ω m)

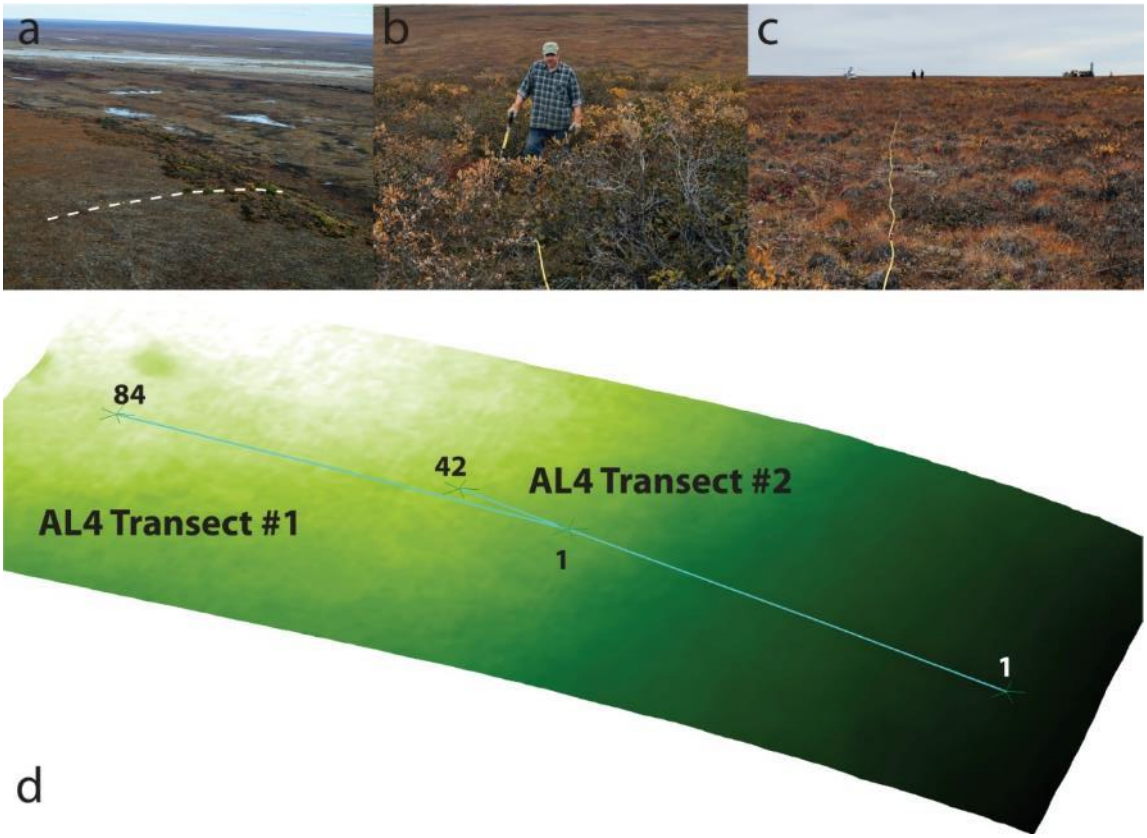


Figure 61. AL4TRAN#1 and #2 site photos
a) Location of AL4TRAN#1and AL4TRAN#2 indicated by dashed line; b) Large *Salix sp.* around transect on sloped portion; c) Looking toward end of transect (electrode 84) where DOT drilling site is visible on right horizon; and d) Transects draped on DEM with 5x vertical exaggeration

The second transect AL4TRAN#2 was an in-depth investigation of the ice-wedge polygons verified by boreholes AL4-2 and 3 over gently sloping tussock tundra. In comparison with ALTRAN#1, the average active layer depth was deeper at 51 cm, with a larger standard deviation of 20 cm. The modeled resistivities resolved a maximum depth of 3.25 m and mirrored the pattern of the active layer depths, albeit at a higher resolution. Shallower active layer depths corresponded to modeled resistivity values around 229 Ω m. Directly below 3.25 m were higher modeled resistivities of 7506 Ω m. These resistivity levels correspond to the distribution of ice-wedge polygons indicated by boreholes AL4-2 and 3. Direct comparisons between Figure 63 (a) and (b) indicate good agreement between the measured and modeled active layer.

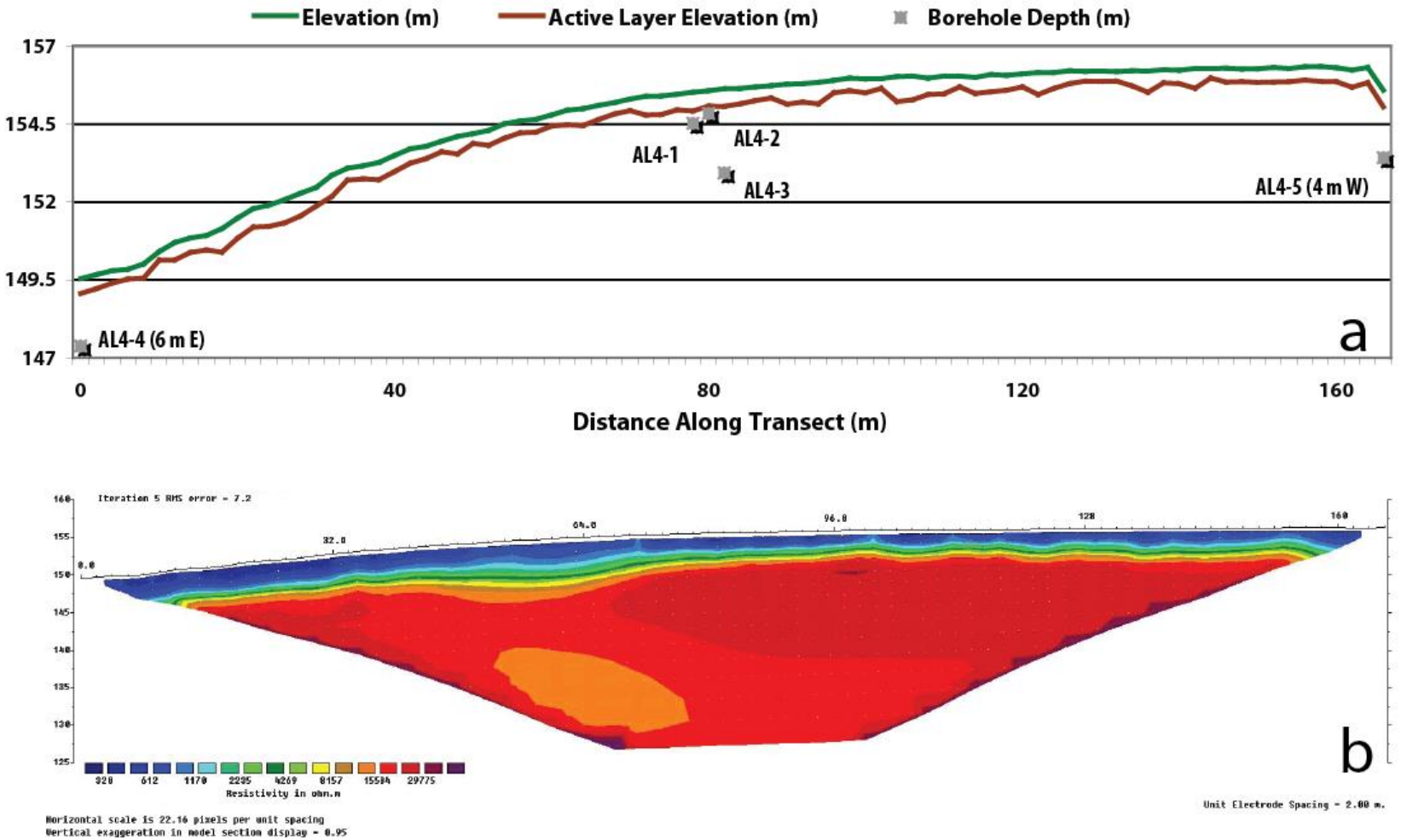


Figure 62. AL4TRAN#1 results
a) Surface and active layer elevation (m) and borehole location and depth (m); b) DCR-ERT modeled resistivity (Ω m)

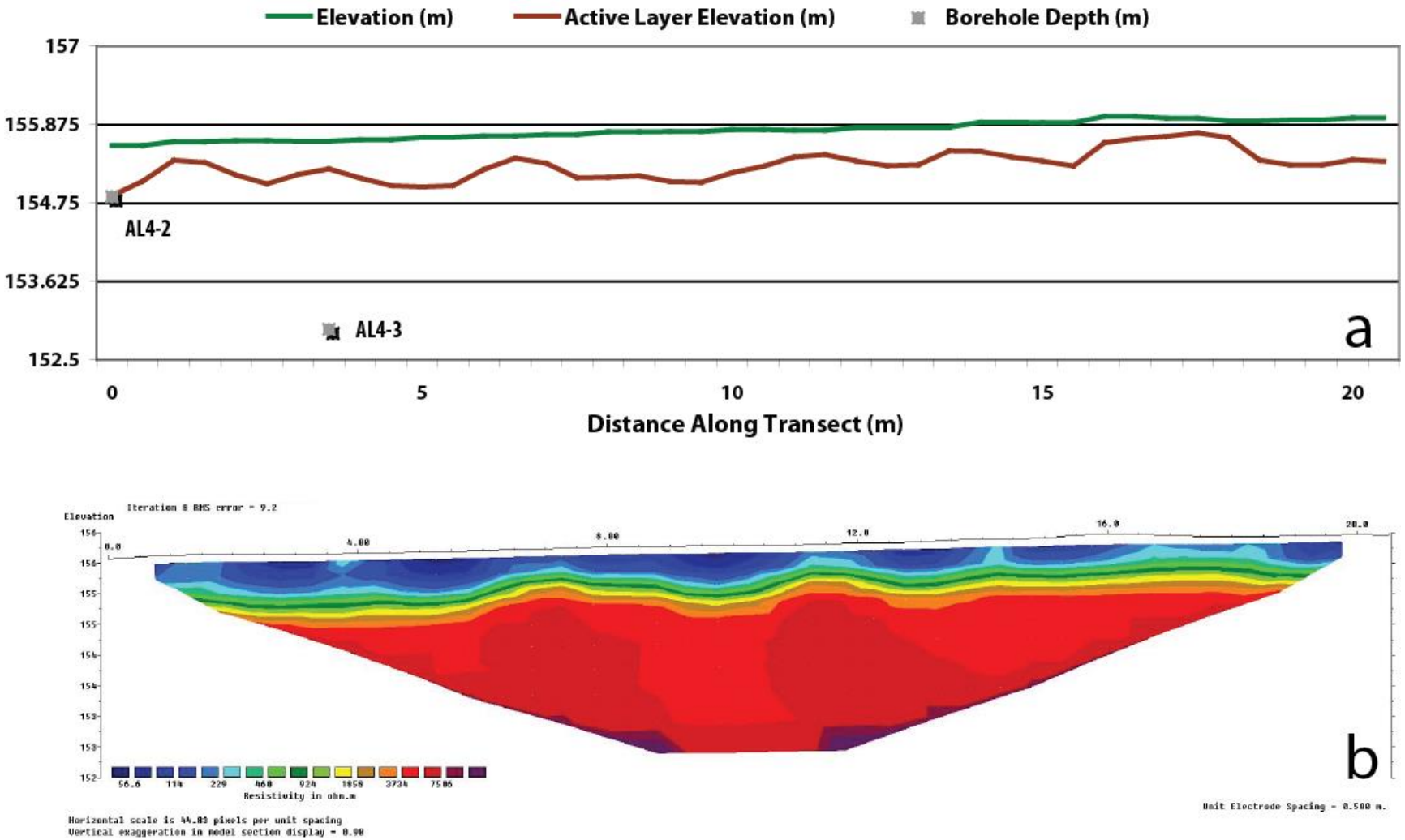


Figure 63. AL4TRAN#2 results
a) Surface and active layer elevation (m) and borehole location and depth (m); b) DCR-ERT modeled resistivity (Ω m)

**Anaktuvuk River Bridge Crossing – BRIDGETRAN**

On the east side of the Anaktuvuk River, BRIDGETRAN#1 bisected the large flat alluvial plain adjacent to the main channel (Figure 64). A sandy overburden supports shrubs over the underlying gravel bed. The presence of *Salix alaxensis* indicates a more recent history of active flooding. Multiple smaller subchannels contain coarser surficial gravels and cobbles. Surficial investigations indicated an active layer depth of greater than 1.5 m and no ice-rich permafrost. BRIDGETRAN#1 had modeled resistivities with minimum and maximum values of approximately 300 Ω m and 8.8 kΩ m (Figure 65). With 42 electrodes and 2 m spacing, maximum vertical resolution was 13 m. The surficial channels appear as lower modeled resistivities between 300 and 500 Ω m.

BRIDGETRAN#2 examined the transition between degrading high-centered ice-wedge polygons and the lower-lying floodplain (Figure 66 and Figure 67). Both areas are part of the larger alluvial plain, and gravel underlies the high-centered ice-wedge polygons. The polygons were severely burned during the tundra fire. The average active layer depth was 54 cm with a standard deviation of 13 cm. Under the alluvial shelf, active layer depths exceeded the maximum probing range in the channel between the plateau and the plain. The transect had a maximum resolution depth of 25 m, where the highest modeled resistivities of approximately 21 kΩ m were found under the ice-wedge polygons; the lowest were present under the alluvial plain with approximate values between 270 and 500 Ω m. All boreholes at this site indicated gravel at depth. BRIDGE-2 located in the trough above the ice wedge contained wedge ice from 30–90 cm with gravel below. Located further from the edge of the plateau, BRIDGE-1 contained ice-rich peat from 46–80 cm, sand that became coarser and ice-poor with depth from 90–180 cm, and gravel from 180 cm and below. Furthest from the floodplain, BRIDGE-3 had ice-rich peat/organic silt from 45–153 cm, ice-rich silty sand mixed with peat from 153–164 cm, ice-rich sand ranging from medium to very fine from 164–193 cm, and gravel below 193 cm. Modeled resistivities for all three boreholes at depth were approximately 3.2 kΩ m.

Coinciding with the second transect, BRIDGETRAN#3 investigated the burned high-centered ice-wedge polygons in detail (Figure 68). Average active layer depths were 48 cm with a standard deviation of 7 cm. With 42 electrodes and a spacing of 0.5 m, the maximum vertical resolution was 3.5 m. Minimum modeled resistivities between 117 and 220 Ω m were found on the surface in the centers of ice-wedge polygons. Higher values around 420 Ω m were found in the polygon depressions and in areas with severely cracked ground post-tundra fire. Gravel deposits established by the stratigraphy in BRIDGE-1 correspond to modeled resistivity values of 5.2 kΩ m. The highest modeled resistivity was found adjacent with nearly double values of 9.8 kΩ m.

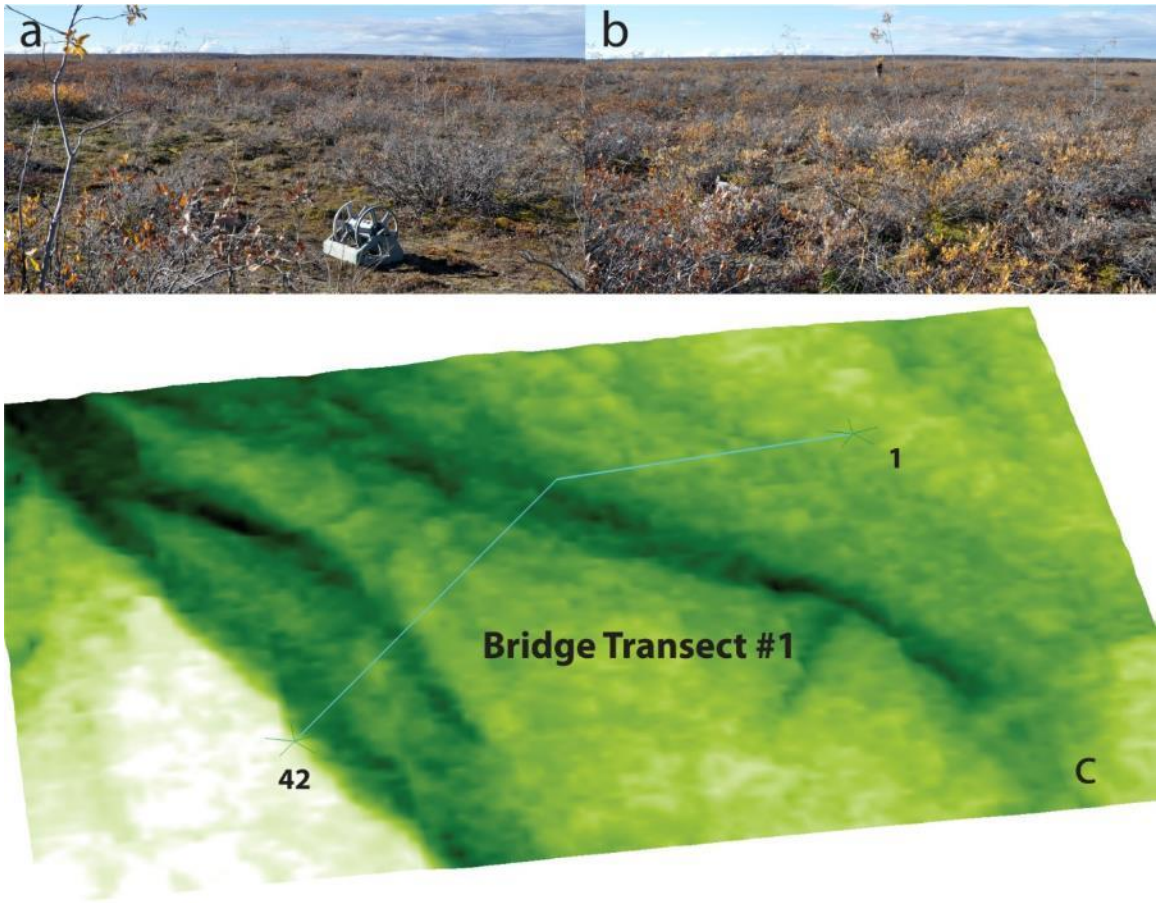


Figure 64. BRIDGETRAN#1 site photos
a) Looking toward the beginning of the transect at 0 m (electrode 1); b) Shrubby vegetation covering floodplain; c) Transect draped on DEM with 5× vertical exaggeration

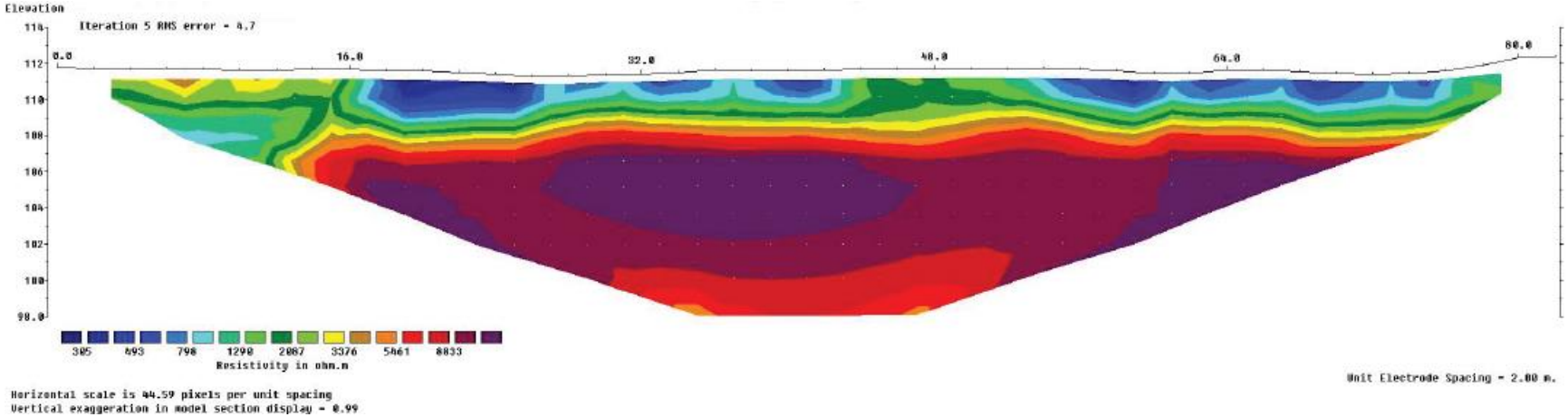


Figure 65. BRIDGETRAN#1 results
DCR-ERT modeled resistivity (Ω m)

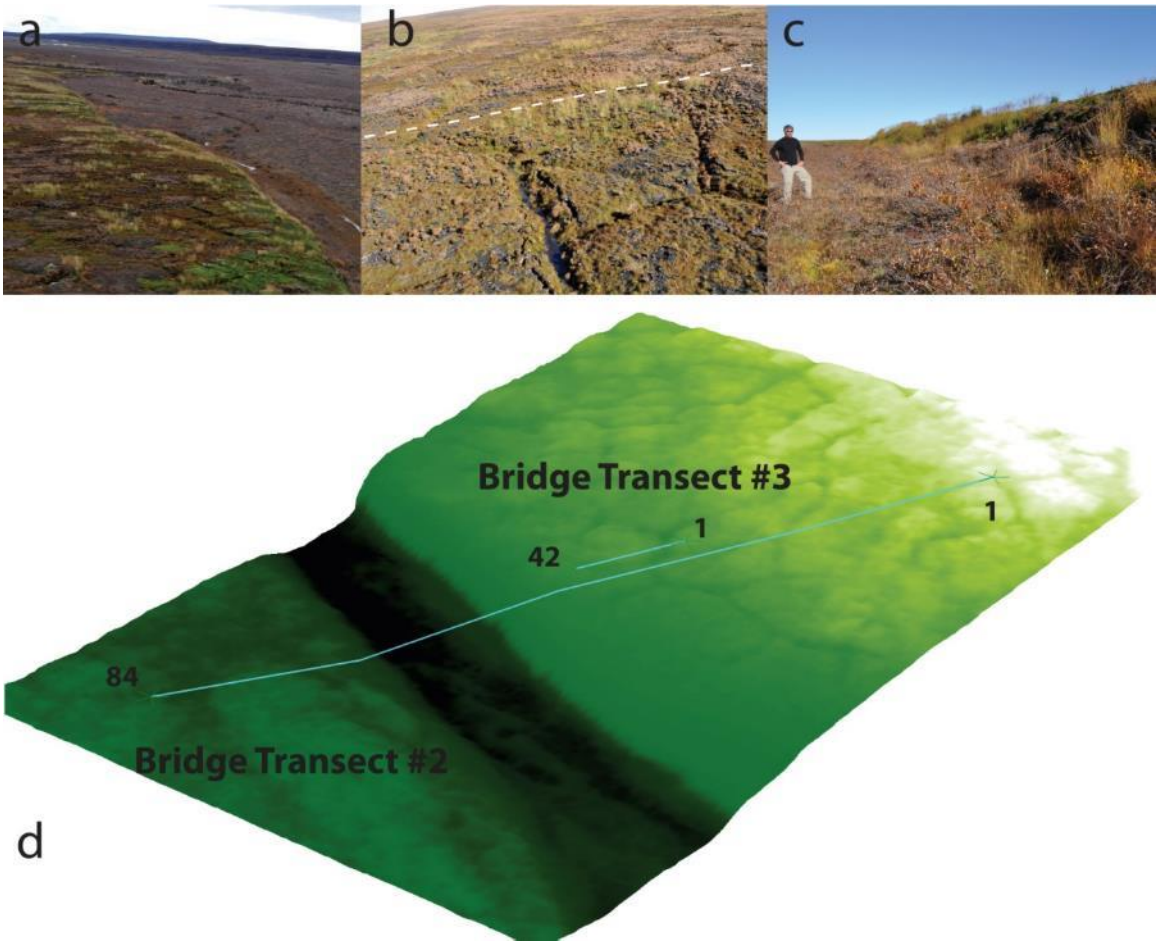


Figure 66. BRIDGETRAN#2 and #3 site photos
a) BRIDGETRAN#2 captured transition from burned high-centered ice-wedge polygons to floodplain; b) Burned high-centered ice-wedge polygons with degrading trenches; c) Elevation change from floodplain to the plateau; and d) Transects draped on DEM with 5× vertical exaggeration

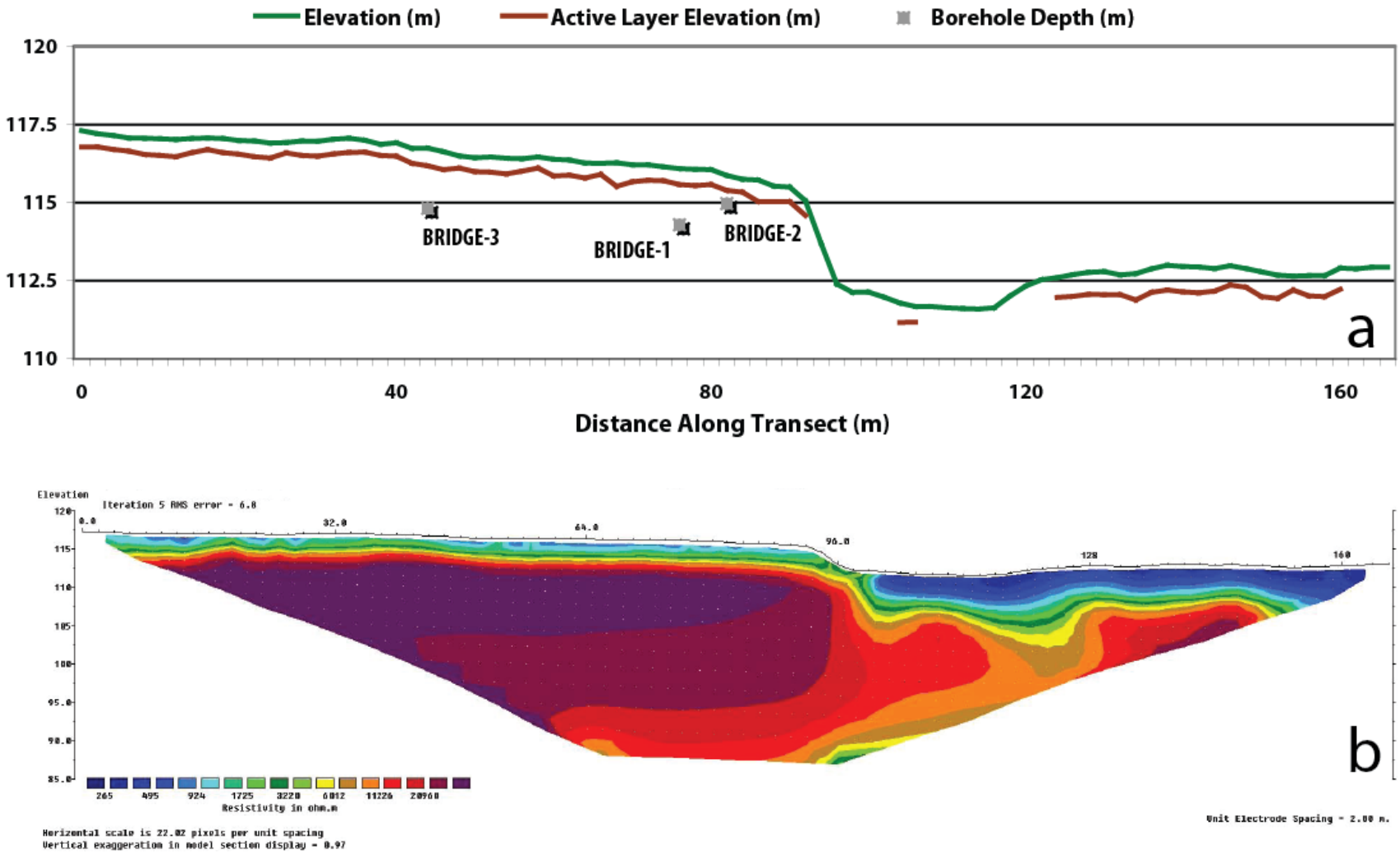


Figure 67. BRIDGETRAN#2 results
a) Surface and active layer elevation (m) and borehole location and depth (m); b) DCR-ERT modeled resistivity (Ω m)

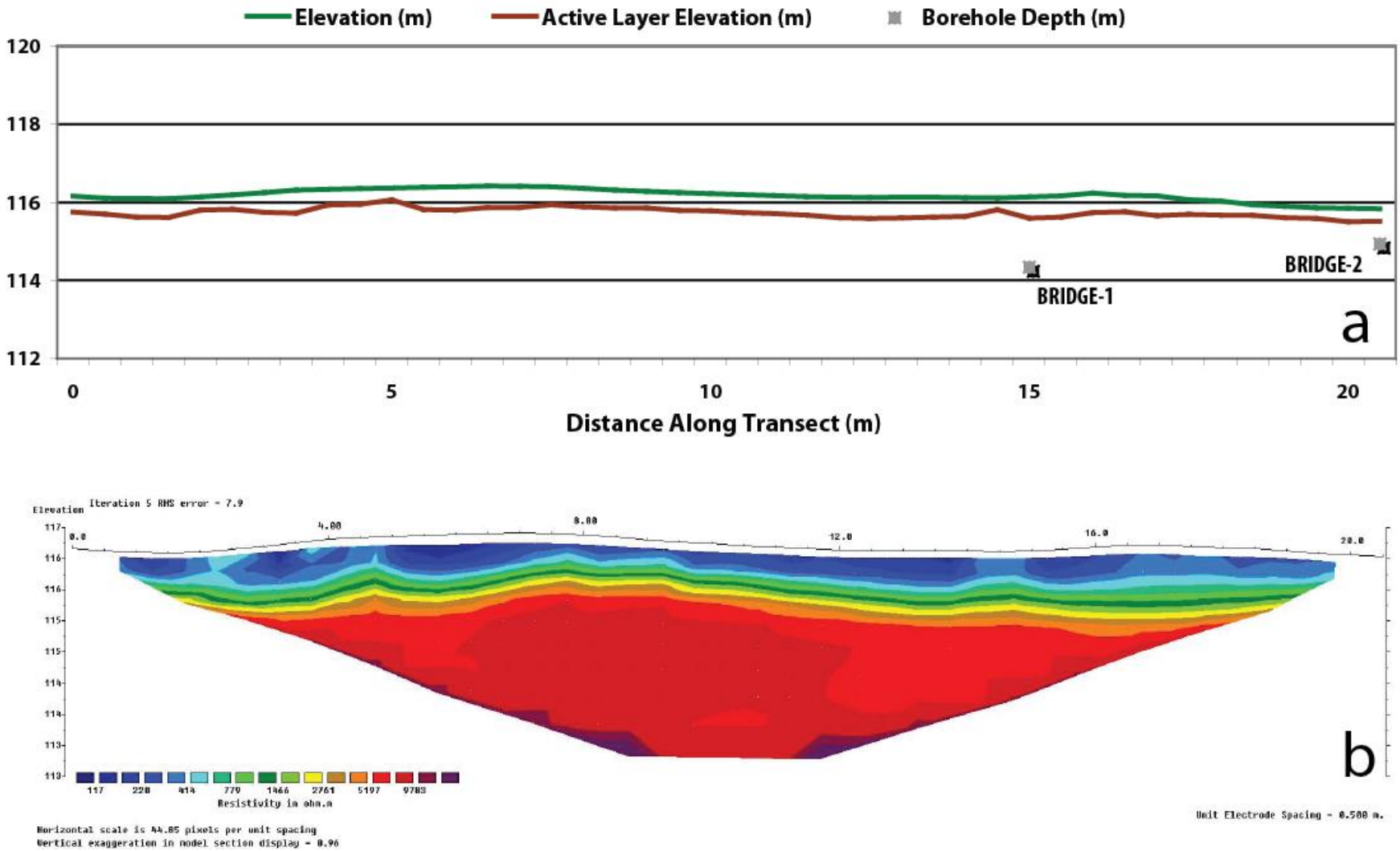


Figure 68. BRIDGETRAN#3 results
a) Surface and active layer elevation (m) and borehole location and depth (m); b) DCR-ERT modeled resistivity (Ω m)

**Alignment Hole #2 – AL2TRAN**

Representative of the Alignment Hole #2 area of burned tussock tundra, AL2TRAN#1 had varying amounts of combusted material and gently sloped toward the lake (Figure 69 and Figure 70). Active layer depths averaged 55 cm with a standard deviation of 10 cm. All three boreholes indicated the presence of buried ice wedges. In the center of the transect, AL2-1 contained ice-rich silt from 42–92 cm with wedge ice below. Toward the ridge borehole, AL2-2 contained peat/silt with vertical structure from 42–60 cm, ice-rich silt with vertical peat "veins" from 60–100 cm, ice-rich silt again from 100–217 cm, and wedge ice below 217 cm. AL-3, located in the direction of the adjacent lake, contained ice-rich silt with organics from 49–100 cm, interbedded ice-rich and ice-poor silt from 100–163 cm, and wedge ice below 163 cm. The DOT AL-2 borehole located to the northeast also contained wedge ice from 97–600 cm. Analysis of the draped DEM reveals subtle hillslope ice-wedge polygons. The lowest modeled resistivities of just under 300 Ω m were found on highly burned well-drained surfaces. High surface modeled resistivities of around 1.0 kΩ m were located in areas containing ponding and evidence of thermokarst troughs. Modeled resistivities of 19.8 kΩ m were found closer to the surface. Toward the maximum resolution depth of 25 m, resistivities decreased by approximately half to 10.8 kΩ m.

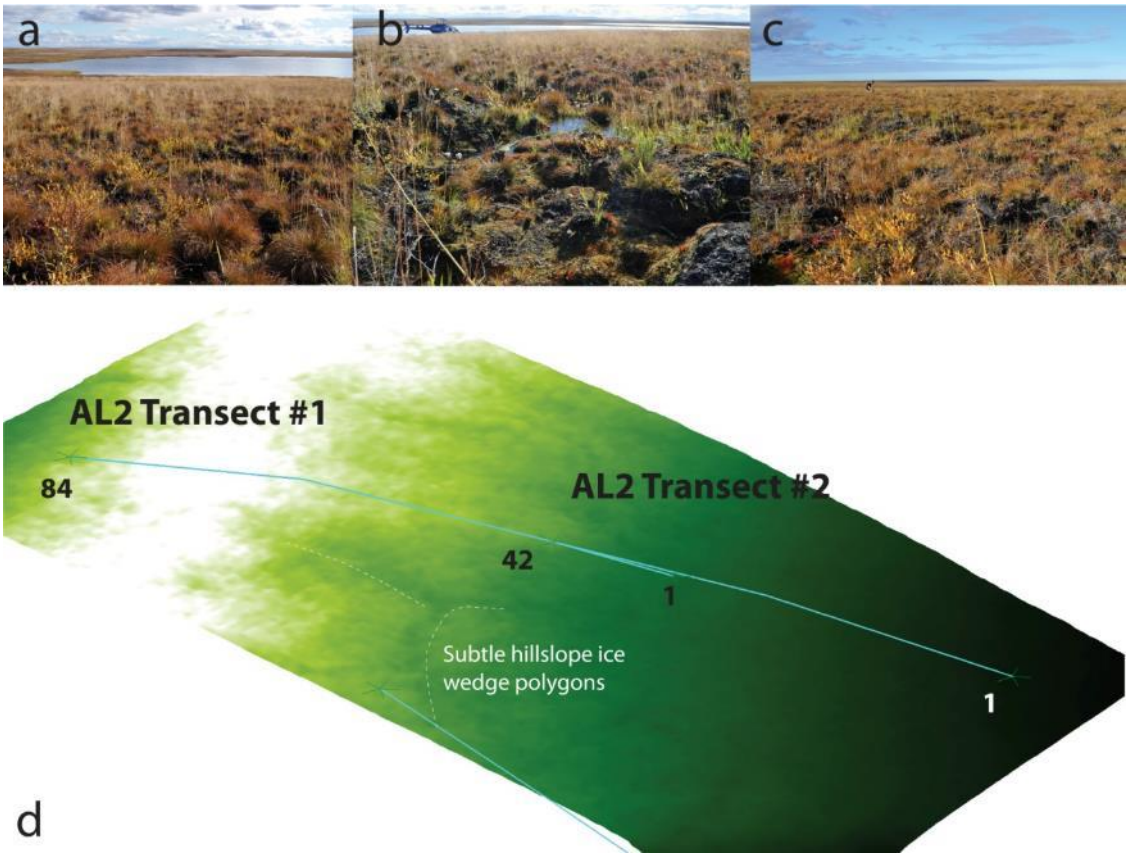


Figure 69. AL2TRAN#1 and #2 site photos
a) Facing south toward beginning of transect; b) Ponding on surface; c) Looking north to end of transect; and d) Transects draped on DEM with 5× vertical exaggeration

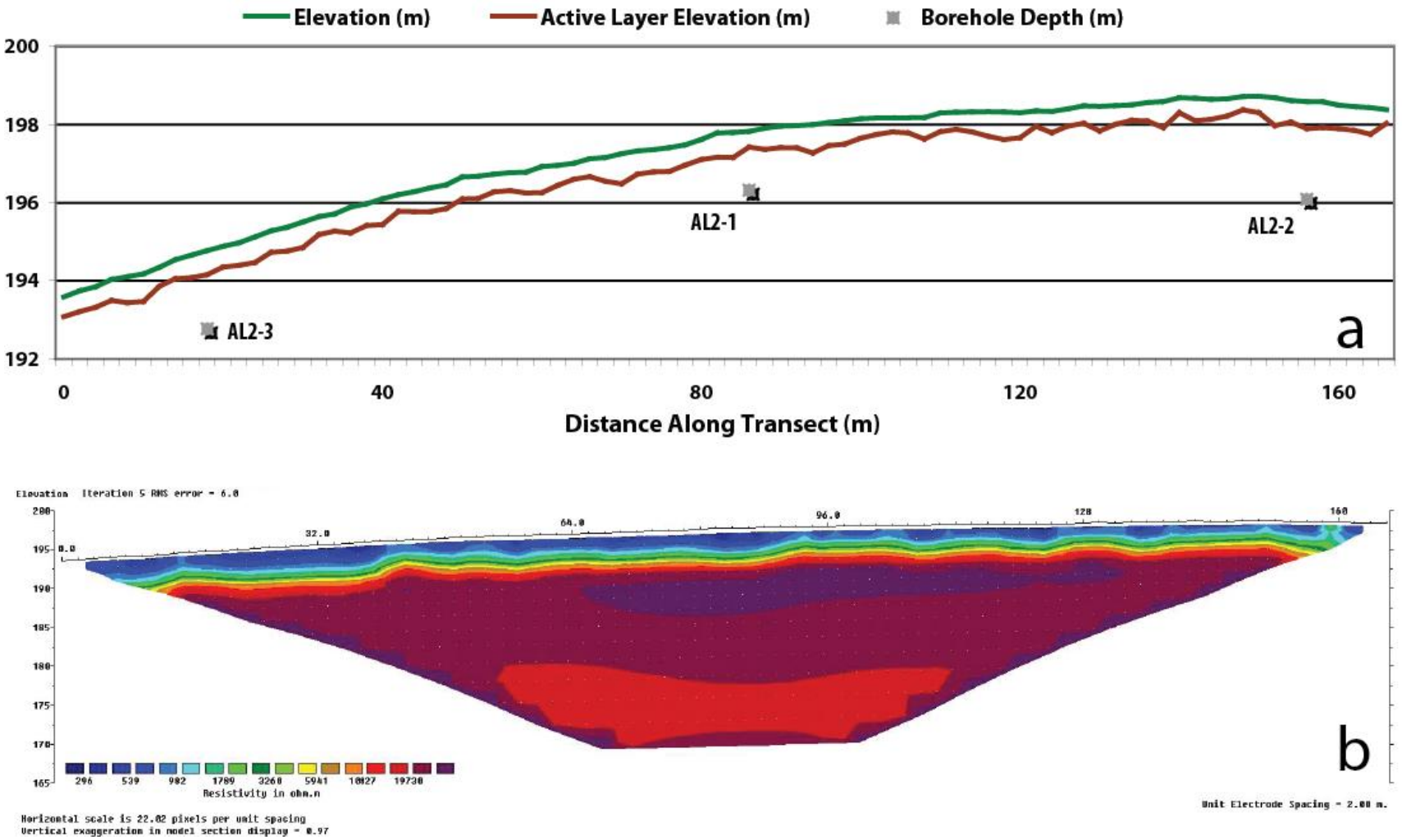


Figure 70. AL2TRAN#1 results
a) Surface and active layer elevation (m) and borehole location and depth (m); b) DCR-ERT modeled resistivity (Ω m)

Overlapping the first Alignment Hole #2 transect, AL2TRAN#2 investigated ice-wedge polygons on the burned tussock tundra in detail (Figure 71). As with AL4TRAN#2, the active layer depths and simulated resistivity profiles showed similar patterns. The average active layer was 58 cm, and the standard deviation was 9 cm. The deepest active layer depths were associated with lower modeled resistivity values of around 85 Ω m. Spacing the electrodes at 0.5 m produced a maximum vertical resolution depth of 3.5 m. Modeled resistivities increased with depth and reached average values around 2.6 kΩ m. These results are similar to those found for Holocene wedge ice in the AL4TRAN#2 and BRIDGETRAN#3 transects.

The next transect ALTRAN#3 was chosen to capture the transition between burned tussock tundra and an area of active thermokarst adjacent to the lake (Figure 72 and Figure 73). The middle of the survey was positioned next to the boundary between the burned tussock tundra and actively sliding material to maximize the DCR-ERT resolution to 14.5 m in this region. The average active layer was 62 cm, and the standard deviation was 20 cm due to large differences between the thermokarst and burned tundra areas.

Borehole AL2-4 contained relatively ice-poor silt to 127 cm, with gravimetric moisture content ranging from 58.8% from 70–77 cm to 81.5% from 93–100 cm. The lowest modeled resistivities of just over 60 Ω m were found where wet silt was exposed on the surface. On the slope with surficial thermokarst activity, modeled resistivity values of 5.8 kΩ m were found approximately 5 m below the surface. Much higher resistivities of 12.3 kΩ m were modeled at depth.

AL2TRAN#4 examined high- and low-centered ice-wedge polygons situated in an old lake bed (Figure 74 and Figure 75). A smaller electrode spacing of 1 m was used to better delineate the degree of ice-richness in the ground, with a maximum resolution depth of 13.5 m. Standing water and wetland conditions were present at this site. The average active layer depth was 50 cm, with a standard deviation of 11 cm. Borehole AL2-5, located in the center of a polygon, contained ice-rich silty peat from 48–137 cm, with silt and peat layers/inclusions from 137–389 cm. The sample was ice-rich until 245 cm and ice-poor underneath. AL-6 was located in the trough above an ice wedge and contained wedge ice from 47–110 cm.

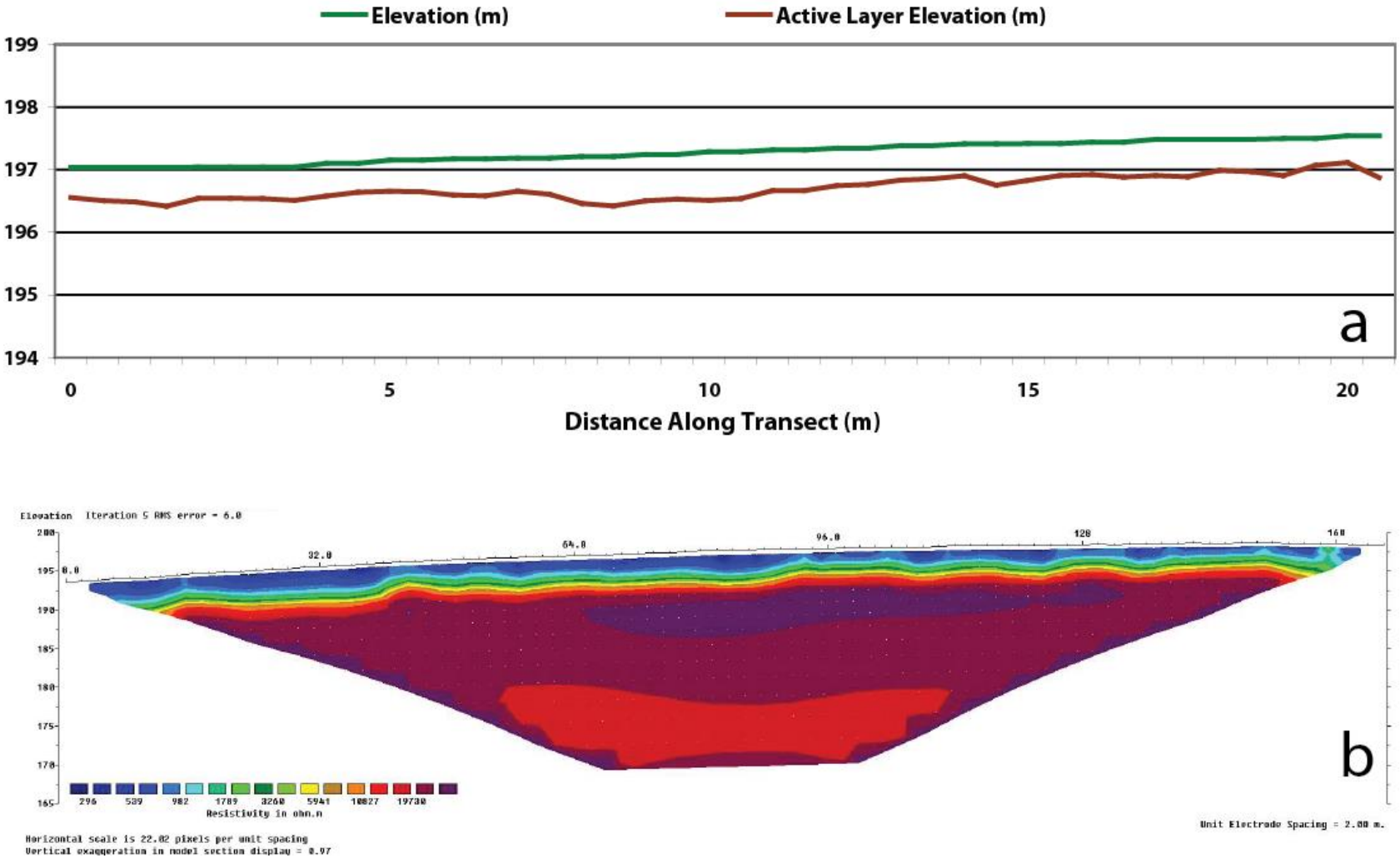


Figure 71. AL2TRAN#2 results
a) Surface and active layer elevation (m) and borehole location and depth (m); b) DCR-ERT modeled resistivity (Ω m)

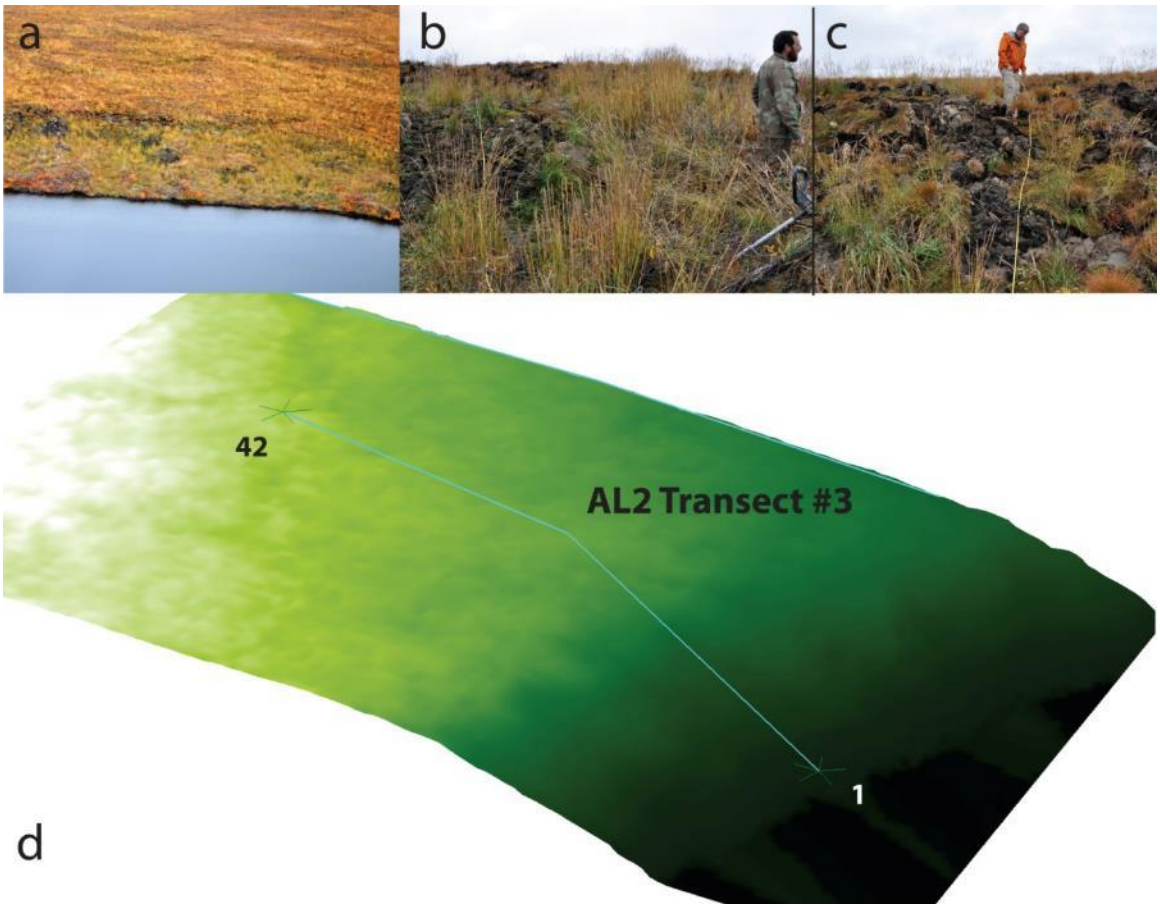


Figure 72. AL2TRAN #3 site photos
a) AL2TRAN#3 transect over thermokarst on edge of lake; b) View north at 0 m (electrode 1) looking uphill; c) Looking north at 22 m (electrode 22) near top of hill; and d) Transect draped on DEM with 5x vertical exaggeration

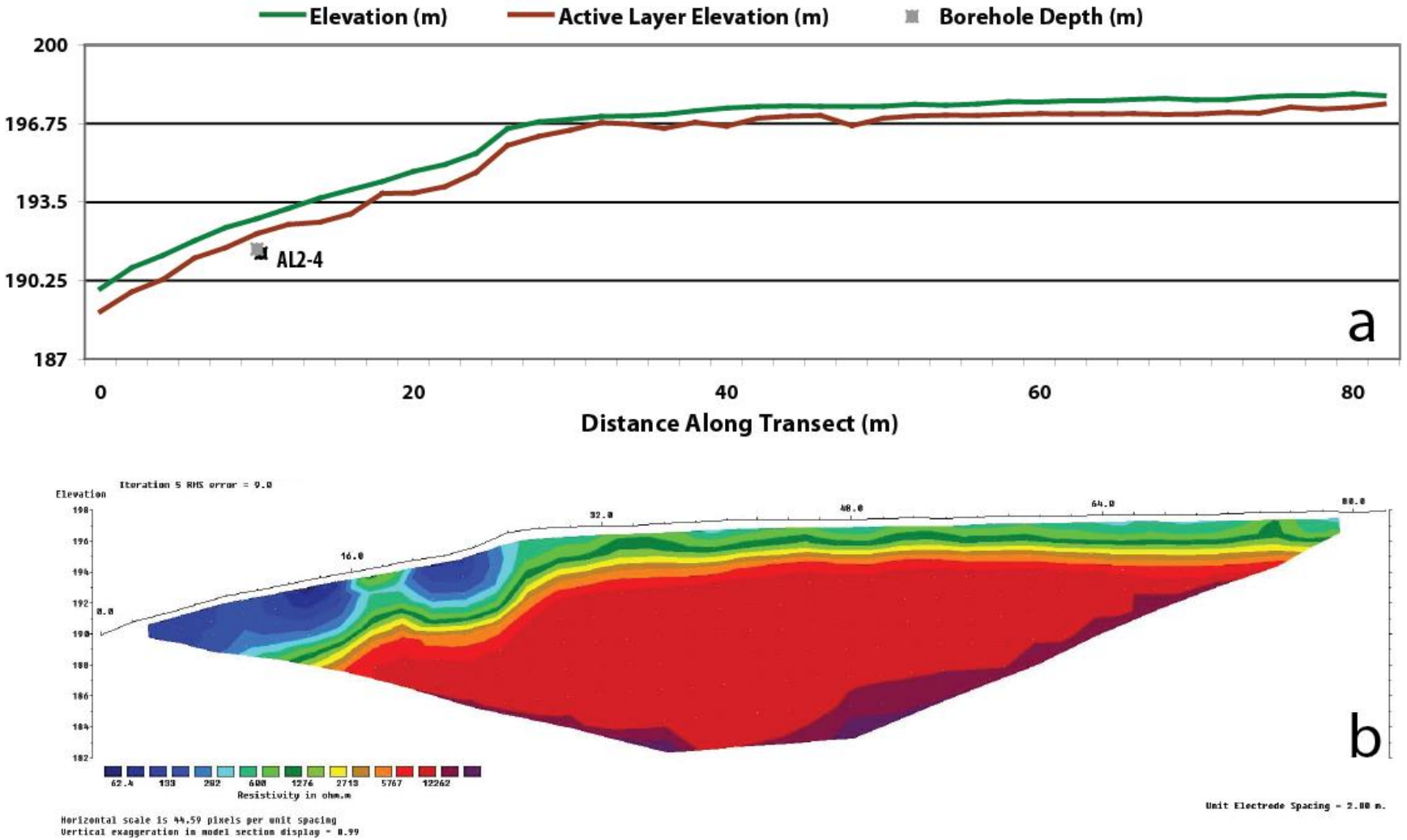


Figure 73. AL2TRAN #3 results
a) Surface and active layer elevation (m) and borehole location and depth (m); b) DCR-ERT modeled resistivity (Ω m)

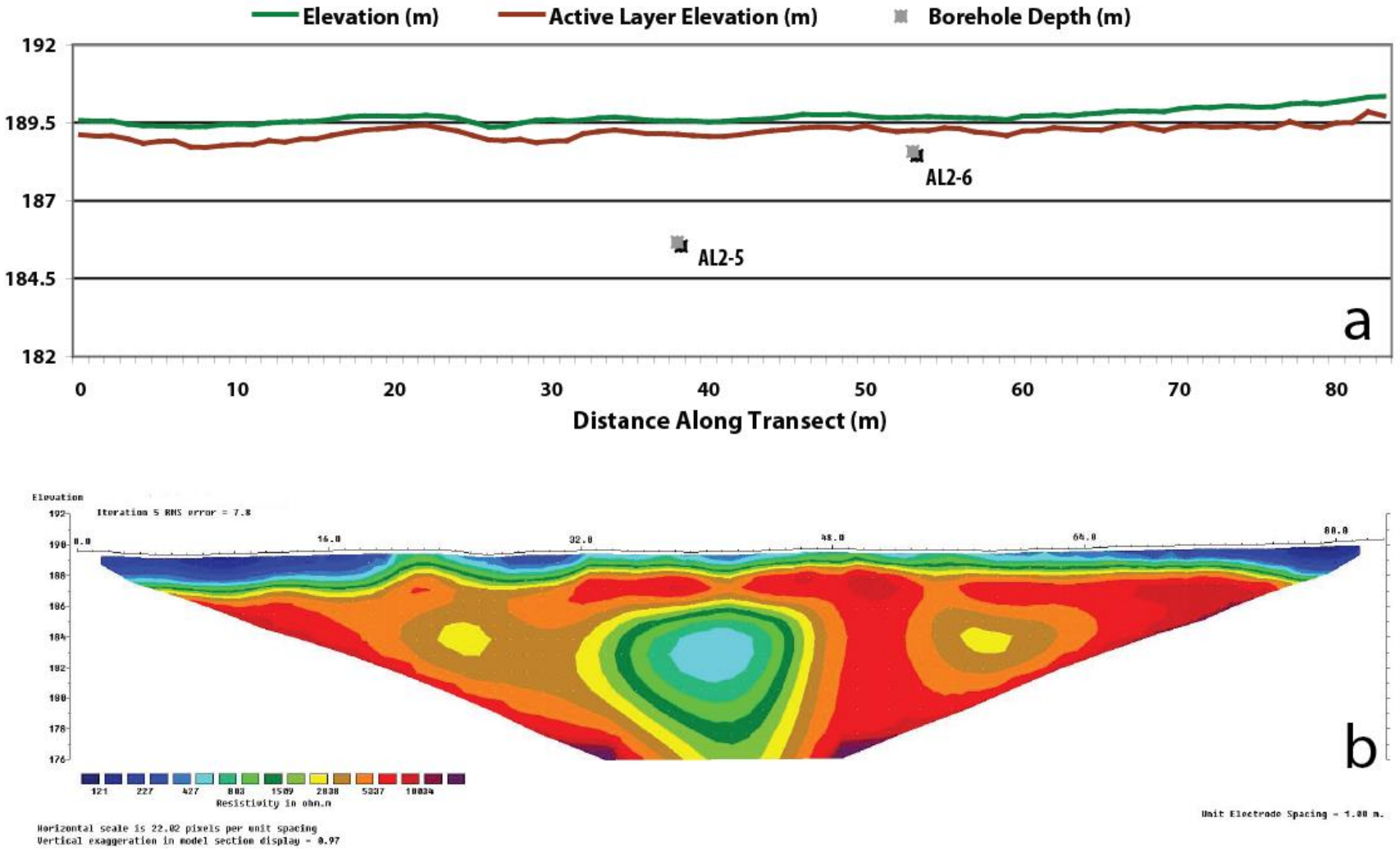


Figure 74. AL2TRAN #4 results
a) Surface and active layer elevation (m) and borehole location and depth (m); b) DCR-ERT modeled resistivity (Ω m)

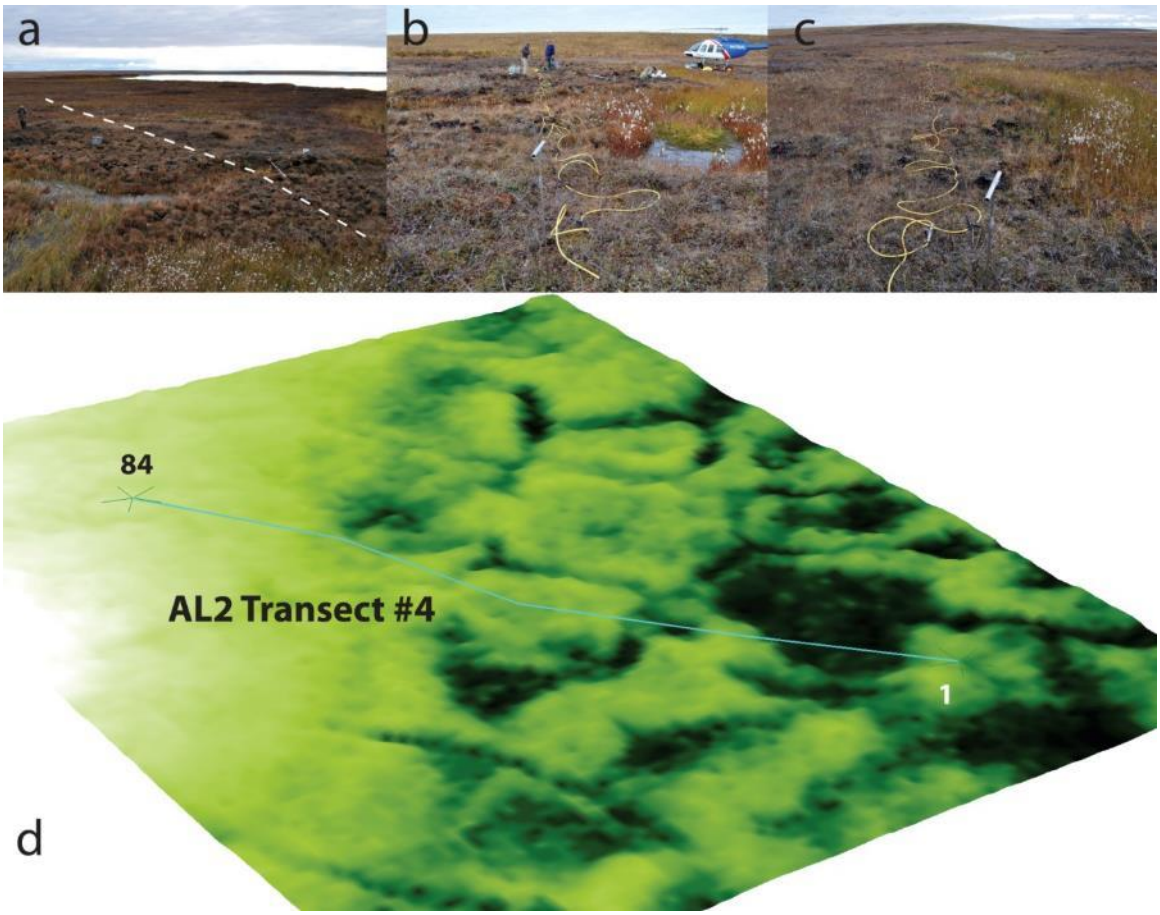


Figure 75. AL2TRAN#4 site photos
a) AL2TRAN#4 bisecting high-centered ice-wedge polygons; b) Looking northwest toward the end of the transect at 22 m (electrode 22); c) Facing southeast toward the beginning of the transect at 22 m (electrode 22); and d) Transect draped on DEM with 5× vertical exaggeration

Resistivities of just over 120 Ω m were modeled on the surfaces, where low-centered polygons occurred (around electrode 1) and toward electrode 84, where the surface was more severely burned during the tundra fire. Higher modeled resistivity values, around 20.0 kΩ m, were calculated at 2.5 m below the surface around both boreholes. These values decreased to around 430 Ω m at 6 m below the surface. This transect had two other predominant areas of lower modeled resistivity centered around the 2.8 kΩ m values located toward the margins of high-centered polygons.

**Interpretation of Geophysics with Respect to Soils Analysis**

The DCR-ERT method using a Wenner array was employed in the Anaktuvuk area to measure variations in the subsurface resistivity over six major terrain units there. These units included (1) low hills with gentle slopes and flat plateaus formed by ice-rich yedoma deposits, (2) flat thaw-lake basins connected by erosional patterns, (3) shallow thermokarst depressions connected by erosional patterns, (4) slopes of river valleys formed by alluvial gravel, (5) river terraces, and (6) modern floodplains.

Resistivity cross sections derived using DCR-ERT are consistent with respect to the unit, suggesting that terrain is a good indicator of the subsurface. DCR-ERT also proved useful in delineating frozen versus unfrozen subsurface soils. DCR-ERT using a Wenner array was relatively ineffective in delineating ice-rich from ice-poor regions, suggesting that a dipole-dipole array or CCR-ERT would be a more appropriate technique for this application.

## UAF FARM SURVEY RESULTS

### Site Description and Field Timeline

The UAF Farm survey site is adjacent to the main UAF campus and neighbors a predominant, large south-facing slope (Figure 76). The study site, part of the upper section of the Chena River floodplain, was cleared for agricultural purposes in 1940 and has been used continuously since. The fields are used mainly for testing various food and grain crops for production in Alaska. Permafrost thawed at the site after vegetation was cleared, and the current talik is approximately 11 m deep. Annually, winter refreezing occurs in the near surface, generally reaching 2.5 m.

Figure 76. CCR-ERT survey carried out at the UAF Farm on March 30, 2011
The OhmMapper system is visible behind the operator. The agricultural field is virtually flat

### UAF Farm Borehole Results and Soils Analysis

The sediment in the UAF Farm study area is described by Péwé (1958) as silt-composed alluvial fans over floodplain alluvium. This sediment has a small amount of organic matter and does not contain large masses of ground ice. In the borehole located approximately 400 m south of the study area (Péwé, 1958, site 148), the silt is 12.8 m thick and underlain by alluvial gravel

(12.8–56.5 m) and bedrock (from 56.5 m). Permafrost was detected at depths of 6.4 to 14.6 m. No thermokarst mounds or pits have developed since the field was cleared (Péwé, 1954), which indicates an absence of large masses of ground ice in this area. We expect the modern position of the permafrost table to be significantly lower than 6.4 m due to continuing permafrost degradation triggered by vegetation removal, if any permafrost still exists under cultivated fields.

**UAF Farm Geophysical Results**

The UAF Farm area has been closely monitored over the past several decades and provides a convenient location for direct comparison of DCR-ERT (direct-current resistivity) and CCR-ERT (capacitive-coupled resistivity). Figure 77 and Figure 78 show inverted resistivity cross sections obtained using the Wenner and dipole-dipole arrays, respectively, using the DCR-ERT system. Likewise, a comparison of cross sections obtained using the DCR-ERT and CCR-ERT systems are shown in Figure 78 and Figure 79, respectively, for a dipole-dipole configuration.

The cross sections illustrate similarities as well as differences between the three methodologies. All three data inversions are characterized by horizontal stratigraphy, with a highly conductive layer sandwiched between a more resistive surface and sub-subsurface layer. The DCR-ERT inversions are of particular interest, since measurements were made on the same day, using the same electrode placements. Hence, differences in the inverted cross sections are due solely to the array configuration. The cross sections illustrate the relative smoothness of the Wenner inversion when compared with the dipole-dipole inversion, and is particularly evident in the very near surface.

The CCR-ERT inversion results suggest a higher level of lateral sensitivity when compared with the DCR-ERT dipole-dipole results; this likely represents an artifact of the method (CCR-ERT), and results from fewer data points used in the inversion, resulting in each data point being more heavily weighted. Differences between the methodologies at the UAF Farm are consistent with those we observed on 9-Mile Road, where cross sections derived using CCR-ERT and DCR-ERT (Wenner only) show the same large-scale features, with the dipole-dipole derived cross section more highly resolved in the lateral direction. While CCR-ERT and DCR-ERT produce comparable results (particularly when using a dipole-dipole configuration), the CCR-ERT system allows for rapid data collection, since it does not require direct contact with the ground. As such, it can be implemented over highly resistive surfaces such as frozen ground, a condition that can prove difficult when doing a DCR-ERT survey. Advantages of the DCR-ERT system over the CCR-ERT system include slightly better resolution and, as a result of increased electrode spacing, imaging to greater depths. This is apparent when comparing Figure 78 and Figure 79.

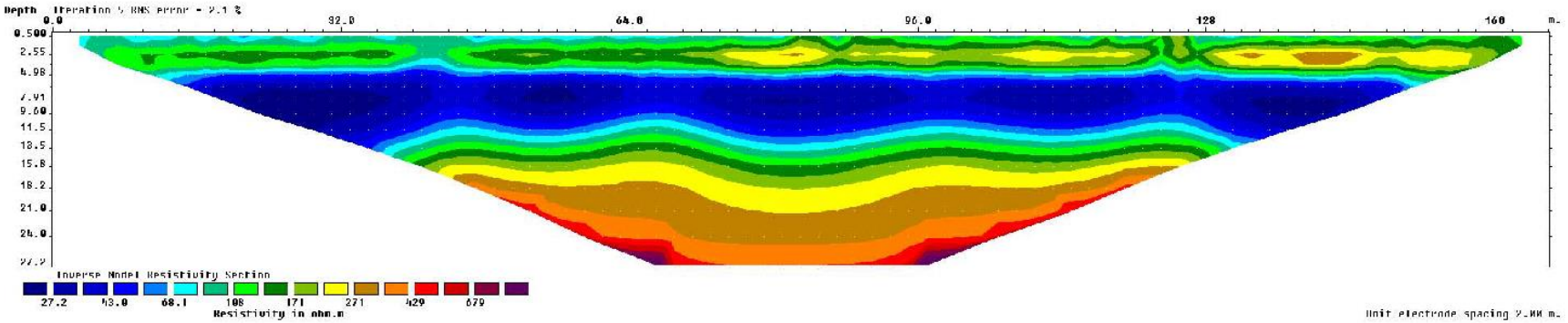


Figure 77. UAF Farm field Wenner array DCR-ERT survey results

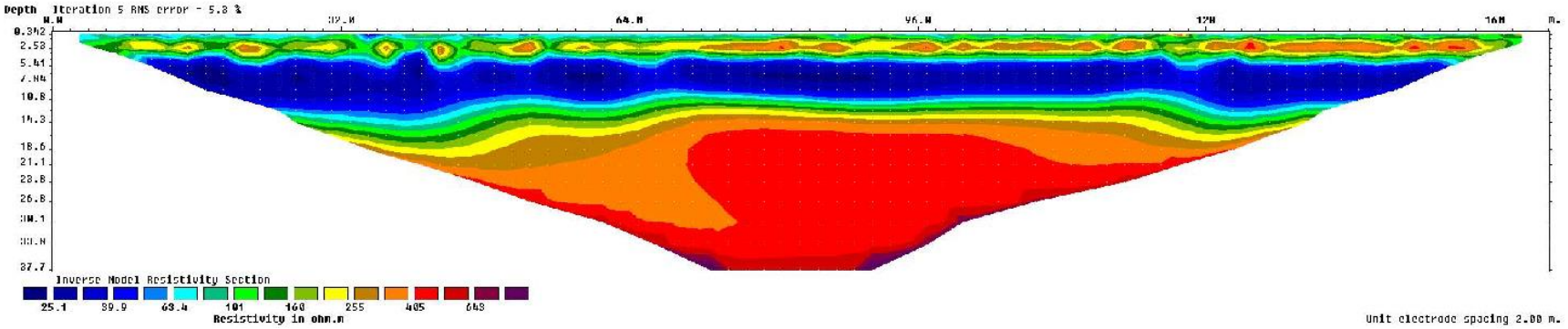


Figure 78. UAF Farm field dipole-dipole array DCR-ERT survey results

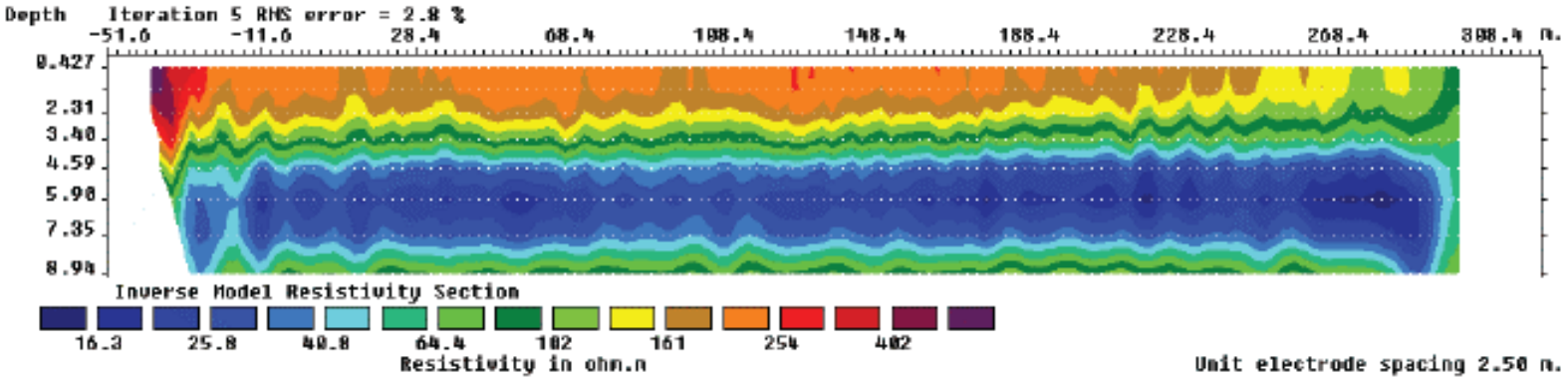


Figure 79. UAF Farm field CCR-ERT survey results

## GOLDSTREAM ROAD SURVEY RESULTS

### Site Description and Field Timeline

The Goldstream Road study area is located within the discontinuous permafrost zone (Péwé, 1975; Jorgenson et al., 2008). Permafrost in this part of Interior Alaska exists mostly in valley bottoms and on north-facing slopes; permafrost temperatures vary from -2°C to 0°C. High temperatures cause instability in permafrost, and any vegetation disturbance can cause its degradation (Douglas et al., 2008). Elevations of Goldstream Road vary from 200 to 300 m above sea level. Permafrost at this location consists mostly of yedoma silt (in many cases thawed and refrozen) underlain by gravel and/or weathered schist bedrock. Péwé (1958) described sediment in the Goldstream Valley as eolian silt that has been retransported from hills to lower slopes and valley bottom and that contains organic materials and large masses of ground ice. The thickness of silt in the boreholes drilled along the Goldstream Valley in the area of our survey varied from 13 to 34 m, and the thickness of permafrost varied from 37 to 60 m (no sites with a lowered permafrost table were detected) (Péwé, 1958).

### Borehole Results and Soils Analysis

Our knowledge of permafrost soils along Goldstream Road is based primarily on the logs of boreholes recently drilled and logged by ADOT&PF between Miles 1 and 3 and Miles 5 and 7. Six boreholes were drilled in September–October 2011, and 16 boreholes were drilled in January 2012 (Table 8, Figure 80 and Figure 81). In the table, the boreholes drilled in 2011 contain the prefix "11-" in the borehole number; the boreholes drilled in 2012 contain the prefix "12-." In the sections of the majority of boreholes, three units can be distinguished: (1) fill material (asphalt, gravel), thickness from 1.5 to 5.0 m; (2) unfrozen silty soil, thickness up to 4.6 m; and (3) frozen silty soil, thickness unknown. Bedrock was encountered only in one borehole at a depth of 5.2 m (Figure 80, borehole 12-5014). Two boreholes did not reach permafrost (Figure 80, boreholes 12-5008 and 11-7003). In all other boreholes, the permafrost table was located at depths of 3.1 to 7.9 m. The depth of winter freezing of soils in boreholes drilled in January 2012 varied from 2.6 to 4.1 m (Table 8). The lowered permafrost table was detected in almost all boreholes that encountered permafrost. We assume that the permafrost table coincides with the bottom of winter freezing of soils only around boreholes 12-0515, 11-7020, 11-7021, and 11-7022.

Table 8. Borehole results from Goldstream Road (courtesy of ADOT&PF)

| Borehole # | Coordinates | Fill thickness, (m) | Depth to permafrost table (m) | Depth of borehole (m) | Gravimetric moisture content of frozen soils | Notes |
|---|---|---|---|---|---|---|
| ***MP 1 to 3*** | | | | | | |
| 12-5007 | N64.94804°, W147.67841° | 3.4 | 5.5 | 8.5 | 6.5m – 116%<br>7.9m – 52% | 0-3.7 m – frozen active layer<br>3.4-3.8 m – peat |
| 12-5008 | N64.94858°, W147.68141° | 4.9 | - | 6.1 | | 0-3.5 m – frozen active layer |
| 11-7003 | N64.94927°, W147.68582° | 3.2 | - | 8.2 | | 3.2-3.4 m – peat<br>3.4-8.2 m – unfrozen silty sand w/gravel |
| 12-5009 | N64.95003°, W147.69083° | 4.3 | 7.3 | 7.6 | | 0-3.8 m – frozen active layer |
| 12-5010 | N64.95052°, W147.69357° | 2.4 | 5.5 | 6.4 | 6.0m – 39% | 0-3.1 m – frozen active layer<br>3.1-3.7 m – peat |
| 12-5012 | N64.95147°, W147.69981° | 4.1 | 7.9 | 9.2 | | 0-4.1 m – frozen active layer<br>4.3-4.4 m – peat |
| 12-5013 | N64.95191°, W147.7027° | 1.8 | 4.9 | 6.1 | 4.9m – 41% | 0-2.6 m – frozen active layer |
| 11-7006 | N64.95253°, W147.70678° | 4.0 | 7.0 | 8.2 | | 4.1-4.3 m – peat<br>7.0-7.9 m – silt, 10% visible ice<br>7.9-8.2 m – peat, 10% visible ice |
| 12-5011 | N64.95323°, W147.71121° | 2.1 | 7.2 | 7.6 | | 0-2.8 m – frozen active layer |
| 12-5014 | N64.95389°, W147.71487° | 2.3 | 5.0 | 7.0 | | 0-3.1 m – frozen active layer<br>5.2-7.0 – weathered schist |
| ***MP 5 to 7*** | | | | | | |
| 12-5015 | N64.9446°, W147.7982° | 3.1 | 4.4 | 7.3 | | 0-3.2 m – frozen active layer<br>3.1-4.0 m – sand with gravel |
| | | | | | 4.7m – 90%<br>5.1m – 90%<br>5.8m – 41%<br>7.2m – 80% | 4.0-4.3 m – peat<br>4.3-4.9 m – silt, ice lenses<br>4.9-5.2 m – peat<br>5.2-7.3 m – silt, 5-10% visible ice |
| 12-5022 | N64.94469°, W147.79858° | 4.6 | 7.0 | 9.2 | 7.0m – 27%<br>8.9m – 60% | 0-3.4 m – frozen active layer |
| 12-5016 | N69.94565°, W147.80194° | 3.7 | 6.7 | 7.3 | | 0-3.1 m – frozen active layer<br>3.8-4.0 m – peat |
| 12-5017 | N64.94648°, W147.80469° | 2.3 | 5.8 | 7.0 | 6.3m – 37%<br>6.9m – 113% | 0-2.8 m – frozen active layer<br>2.9-3.1 m – peat |
| 12-5018 | N64.9472°, W147.80725° | 1.7 | 6.3 | 7.0 | | 0-2.6 m – frozen active layer |
| 12-5019 | N64.94804°, W147.81322° | 4.3 | 7.6 | 9.0 | 8.9m – 46% | 0-3.1 m – frozen active layer |
| 11-7018 | N64.94809°, W147.81374° | 3.5 | 7.0 | 8.2 | | 3.5-3.7 m – peat<br>7.0-8.2 m – silt, 3-10% visible ice |
| 12-5020 | N64.94794°, W147.81667° | 4.0 | 6.3 | 7.2 | 6.5m – 58% | 0-3.1 m – frozen active layer<br>4.0-4.1 m – peat |
| 12-5021 | N64.94751°, W147.81947° | 2.1 | 6.4 | 7.6 | 7.2m – 35% | 0-2.8 m – frozen active layer |
| 11-7020 | N64.94661°, W147.82239° | 1.5 | 3.1 | 7.6 | | 3.1-6.1 m – silt, no visible ice<br>6.1-7.6 m – silt, 10% visible ice |
| 11-7021 | N64.94493°, W147.82691° | 4.0 | 4.0 | 7.6 | | 4.0-7.6 m – silt, with ice lenses |
| 11-7022 | N64.94397°, W147.82956° | 3.1 | 4.1 | 7.6 | | 4.1-7.3 m – silt, >25% visible ice<br>7.3-7.6 m – massive ice |

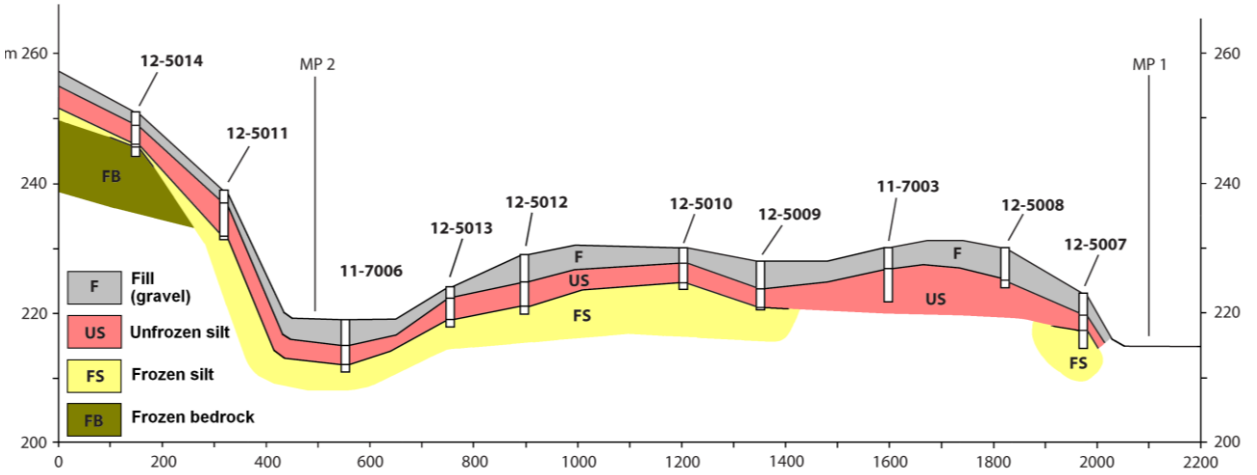


Figure 80. Cross section #1, Goldstream Road, Miles 1 to 3

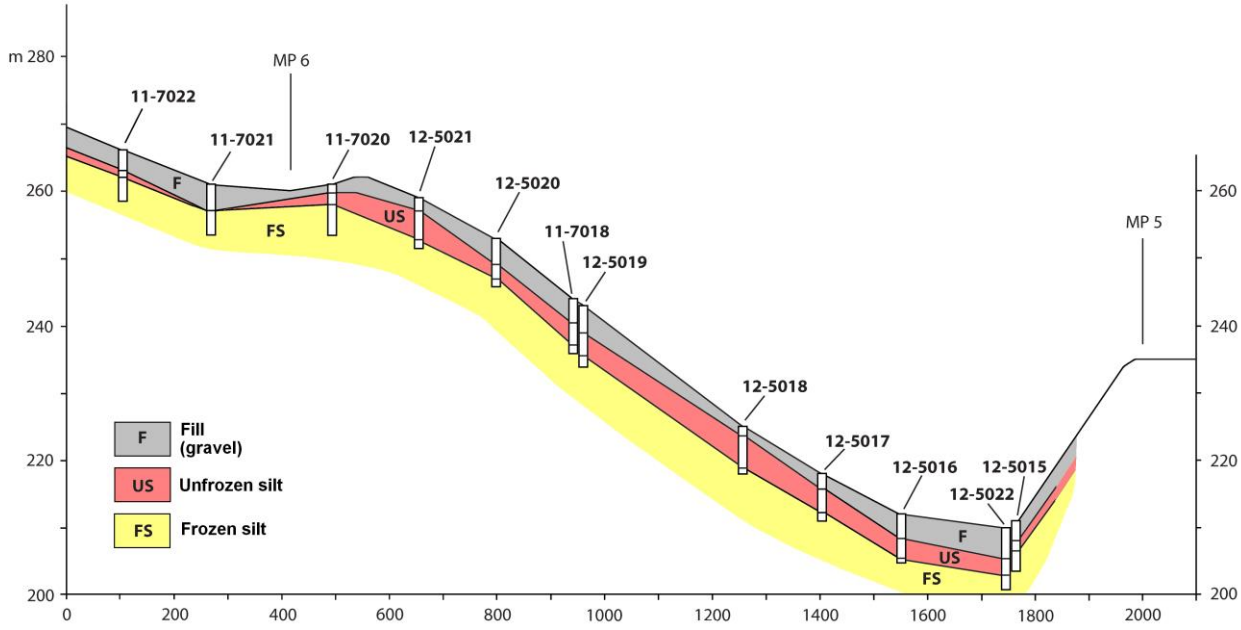


Figure 81. Cross section #2, Goldstream Road, Miles 5 to 7

Frozen and unfrozen silty soils are represented mostly by silts and sandy silts with a high content of organic matter (from 2.2 to 15.2%). In borehole 11-7003, unfrozen silty sand with gravel was encountered at a depth of 3.4 m. In borehole 11-7020, the silt layer was overlain by a 3 m thick layer of frozen and unfrozen gravelly silty clay with sand. In numerous boreholes, a peat layer up to 0.5 m thick was detected under the fill material (boreholes 12-5007, 11-7003, 12-5010, 12-5012, 11-7006, 12-5015, 12-5016, 12-5017, 11-7018, and 12-5020)

In several boreholes, ice-rich silty soils with gravimetric moisture content more than 50% and/or visible ice content more than 10% were detected (boreholes 12-5007, 11-7006, 12-5015, 12-5022, 12-5017, 12-5020, 11-7020, and 11-7022). Massive ground ice was detected only in

borehole 11-7022 at depths from 7.3 to 7.6 m (total thickness of the ice body is unknown). We believe that this massive ice body is a buried ice wedge. Unfortunately, the shallow depth of the boreholes and insufficient data on the ice content prevent us from drawing clear conclusions on permafrost structure and properties. However, evidence indicates a wide occurrence of ice-rich yedoma soils in the study area: (1) prevalence of silty soils with high organic content, (2) occurrence of ice-rich soils and massive ice bodies, and (3) occurrence of thermokarst mounds (baidzharakhs), which formed because of wedge-ice degradation in the areas adjacent to Goldstream Road. Ice-poor silt detected in several boreholes could have formed as a result of the thawing and refreezing of the ice-rich yedoma during the Holocene.

**Goldstream Road Geophysical Results**

The geophysical results for Milepost 5–6 of Goldstream Road are shown in Figure 82 and Figure 83; those for Milepost 6–7 of Goldstream Road are shown in Figure 84 and Figure 85. Note in Figure 82 and Figure 84 that GPR data are not to scale with respect to depth and are included only for comparison with CCR-ERT transects (b). A more detailed presentation of the GPR data is shown in Figure 83 and Figure 85, without the topography included.

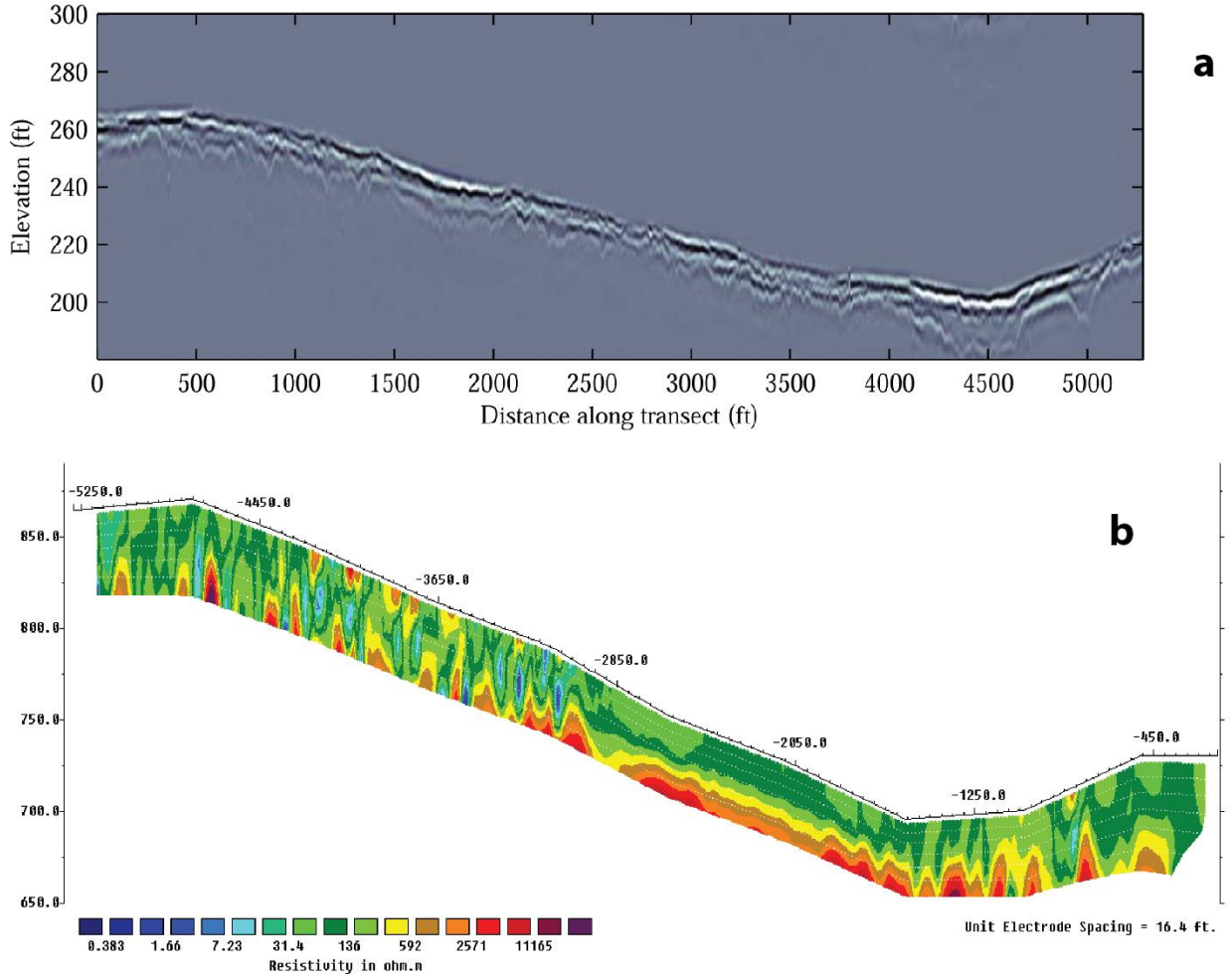


Figure 82. Goldstream Road geophysical results, MP 5–6
a) Topographically corrected GPR survey collected March 2011; b) CCR-ERT transect collected spring 2012 (courtesy of CRREL) on Goldstream Road Miles 5 to 6

In Figure 82, the data are presented in terms of depth versus distance (in feet), beginning at Milepost 6 and ending at Milepost 5. The penetration depth is determined by separating the antennae with respect to a common midpoint and by identifying and determining the velocity of the two "surface waves" in the data. The first wave component in the GPR record corresponds to "direct arrival," which travels along the surface at the speed of light ($3 \times 10^8$ m/s). A second, slower component has a time delay associated with a wave traveling in the slower subsurface material, which we determined to be approximately $1.5 \times 10^8$ m/s, or half the speed of light. Knowledge of this velocity allows one to convert the data, originally given in time, to the more useful unit of depth.

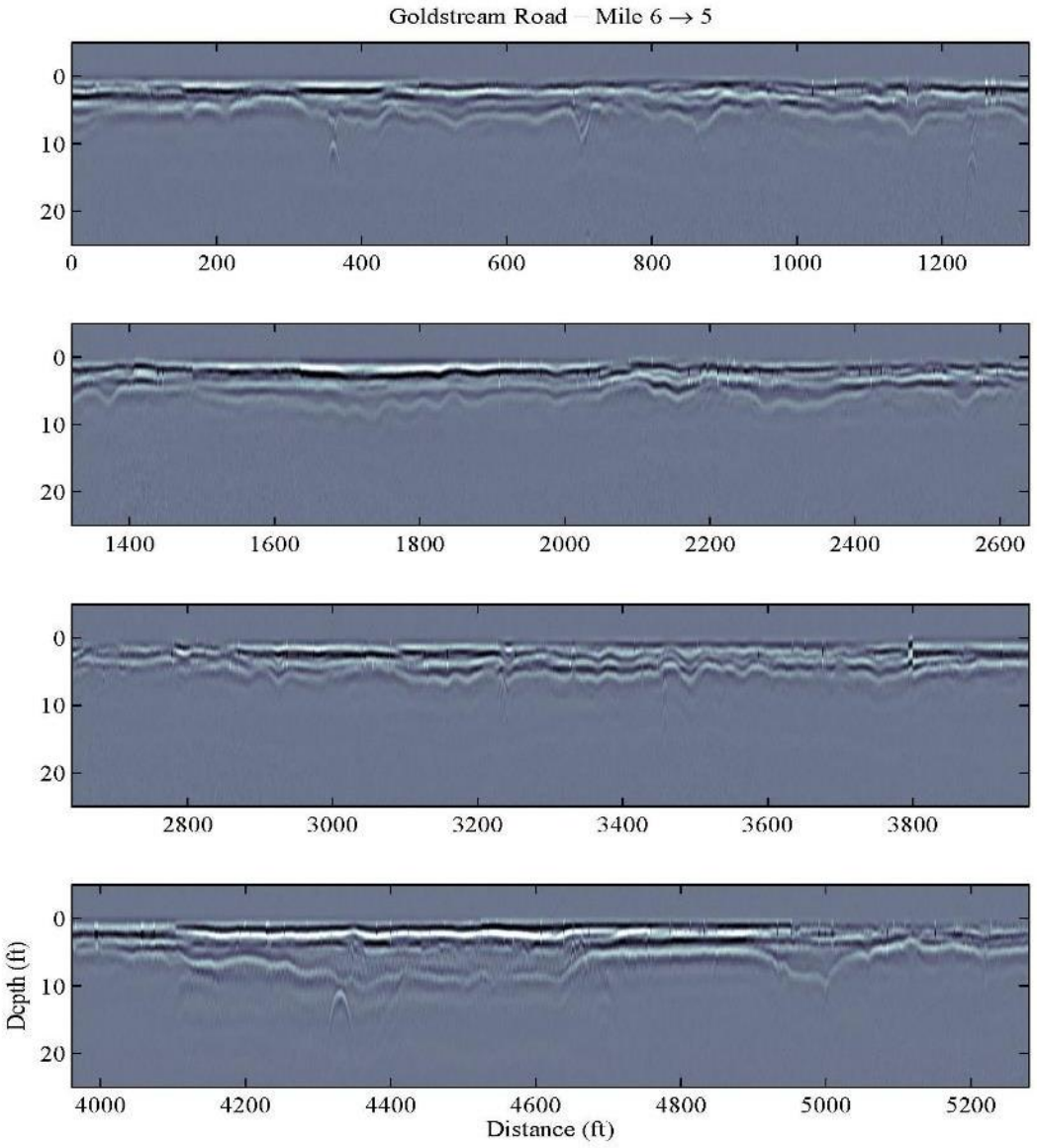


Figure 83. Goldstream Road geophysical results, MP 5–6
GPR survey collected March 2011, as shown in Figure 74a, without topography included

The GPR transects along Goldstream Road from Milepost 5 to 6 clearly show the presence of drainage conduits, and are easily identified by a hyperbolic shape in the GPR record. These conduits provide a strong electromagnetic reflector and provide some indication of the depth of penetration. Examples of these features can be seen in Figure 83 along this transect at 380 ft and 1250 ft, with an associated depth of 10 ft. The hyperbolic feature at 4350 ft corresponds to the much larger culvert used to channel the stream beneath the road. Also evident in the record is a continuous reflector, varying from several to 10 ft in depth, which we interpret as corresponding to the top of the foundation soils. The variability in the depth of this reflector suggests that this section of road has likely experienced significant frost heave and/or subsidence over time. This interpretation is consistent with what we observe in the CCR-ERT data, which hint at the presence of ice lenses throughout this record.

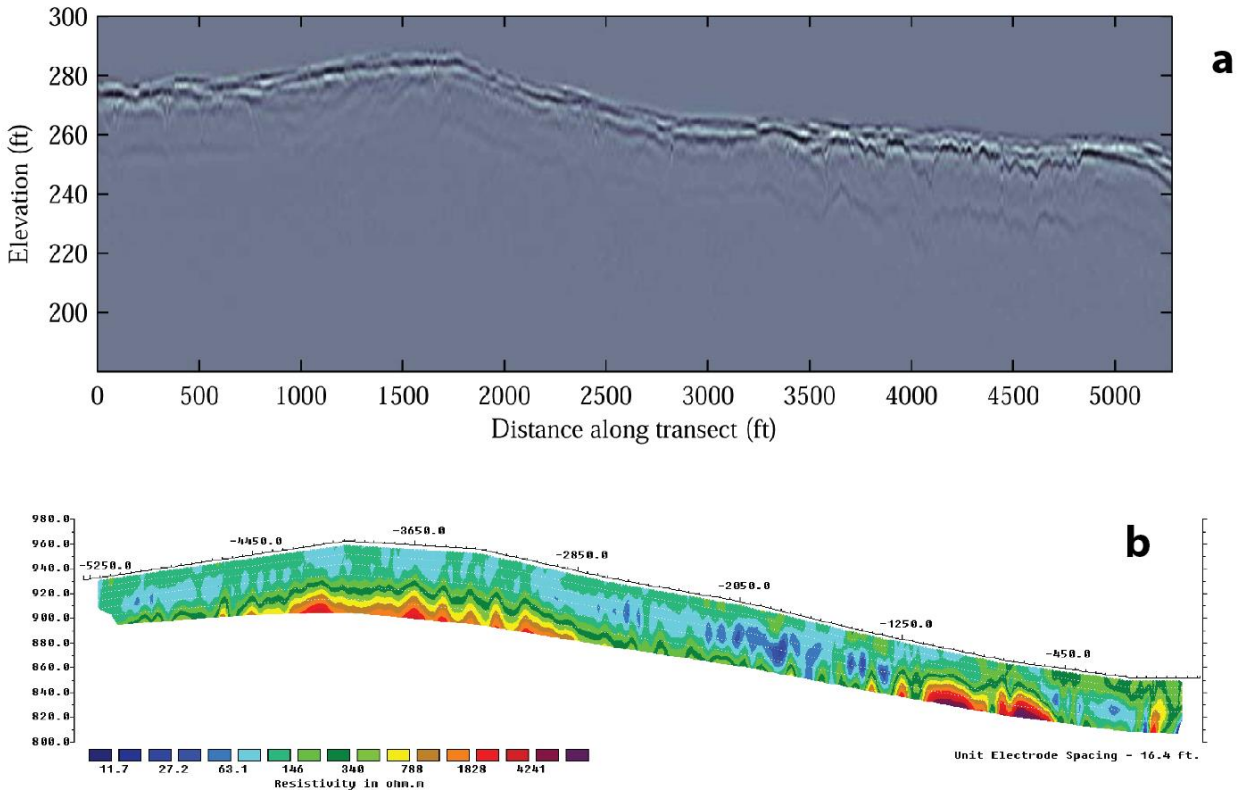


Figure 84. Goldstream Road geophysical results, MP 6–7
a) Topographically corrected GPR survey collected March 2011; b) CCR-ERT transect collected spring 2012 (courtesy of CRREL) on Goldstream Road Miles 6 to 7

In comparison with data from Milepost 5 to 6, CCR-ERT results for Goldstream Road from Milepost 6 to 7, shown in Figure 84a, show less lateral variability in the inverted cross section and lower overall resistivity values. These lower values may result from frozen ground, as opposed to massive ice. The associated GPR data, shown without topography in Figure 85, show the presence of a number of drainage conduits throughout the record, albeit at a more shallow depth than the drainage conduits observed along Miles 5 through 6. Typical examples can be seen at 1680 ft and 3400 ft along this transect. Also evident in the GPR record is a horizontal reflector, which begins at a depth of approximately 10 ft and extends throughout the

record, reaching a depth of over 18 ft at 4100 ft along the transect. The reflector may represent the transition from gravel to silt and/or the interface from unfrozen to frozen ground.

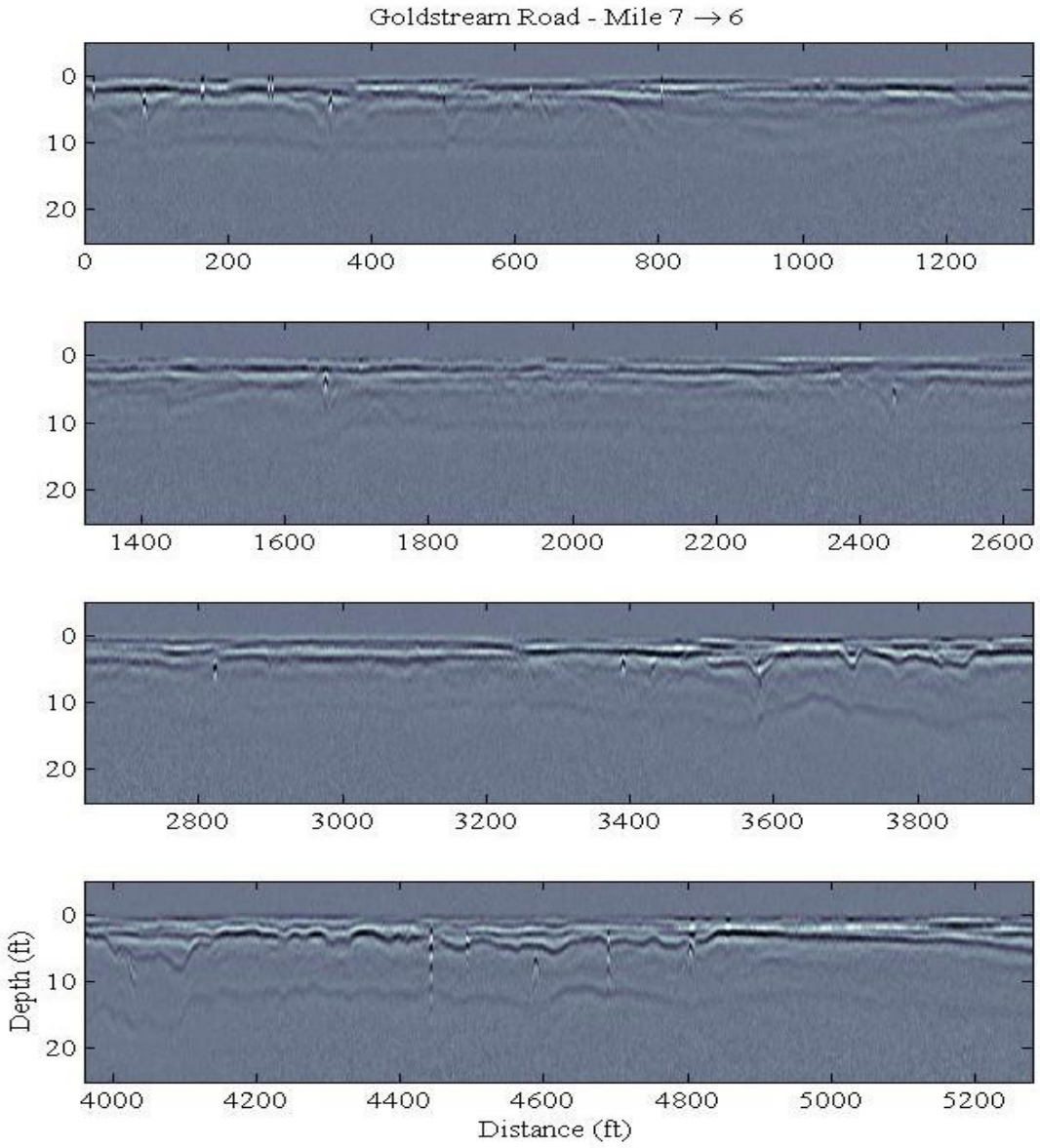


Figure 85. Goldstream Road geophysical results, MP 6–7
GPR survey collected March 2011, as shown in Figure 75a, without topography included

Compared with the GPR record from Miles 5 through 6, the data suggest a more stable section of road, with the exception of a 100 ft span, centered at around 4100 ft. The GPR data shown in Figure 85 are characterized by two roughly parallel reflectors, with the upper reflector varying in depth from near the surface to a maximum depth of 7–8 ft. A second deeper reflecting boundary averages a depth of 12 ft, with a maximum depth of 18 ft. The two reflectors are particularly evident in the final two panels spanning the range 3000–5200 ft along this transect.

We observed that the layer thickness separating the upper and lower reflectors is generally uniform with an approximate thickness of 10 ft. It is reasonable to suggest that the upper and lower reflectors correspond to the original road surface and top of the foundation soils, respectively. With this assumption, the GPR record indicates that sections of this road have experienced significant subsidence over time, with the origins occurring at a depth of at least 20 ft below the road surface. This is particularly so for the sections of road beginning at 3000 ft, and extending to 4800 ft along this transect, as shown in Figure 85.

## SUMMARY OF FIELD RESULTS: CORRELATING GEOPHYSICAL SURVEY RESULTS TO SUBSURFACE CONDITIONS

The four main field sites—9-Mile, Anaktuvuk, UAF Farm, and Goldstream—used a combination of three geophysical methods (DCR-ERT, CCR-ERT, and/or GPR) to characterize permafrost and subsurface conditions. In each of the sites, boreholes provided complementary knowledge of the subsurface conditions.

At 9-Mile, three geophysical methods (GPR, DCR-ERT, and CCR-ERT) were compared along a transect where the permafrost was well characterized by a dense array of boreholes. At this site, the CCR-ERT technique using dipole-dipole array was found to be an efficient method. This data were expediently collected using a tracked ATV on top of the seasonal snowpack. Although the DCR-ERT results were comparable, data collection required more effort. The main advantage of DCR-ERT is its greater flexibility with respect to array configuration once contact is established. The results indicated that the array choice was an important component in charactering ice-wedge distribution. Dipole-dipole was more effective for delineating vertical structures (used in CCR-ERT), while the Wenner was best suited for horizontal structures (DCR-ERT). The dipole-dipole results were a better representation, since ice wedges in this region were more strikingly vertical features. Ground-penetrating radar was not as useful at this site because the depth of penetration was limited to the near surface (1 to 2 m). This could be resolved by using a lower frequency antenna system (with the trade-off of lower resolution) and/or obtaining measurements over a frozen surface to minimize conductivity.

At Anaktuvuk, four main potential alignment areas associated with the ADOT&PF Foothills West project were examined using DCR-ERT. Each DCR-ERT transect used a Wenner array, while various spacing of electrodes was optimized to alter the spatial resolution and depth of penetration. Hollow-stem drilling was completed along the survey transects to ground truth the geophysical results. DCR-ERT was able to separate regions of permafrost versus nonpermafrost in and around floodplains and thermokarst areas. Coarser-resolution transects were not able to delineate individual areas of ice-rich permafrost in yedoma; this was also affected by the use of the Wenner array, which is less effective than dipole-dipole at resolving variations in the horizontal plane. At higher resolutions, where depth of penetration was the shallowest, isolating individual ice wedges is possible.

The UAF Farm site was a well-studied location, ideal for comparing CCR-ERT and DCR-ERT obtained simultaneously. At this site, DCR-ERT was acquired using both Wenner and dipole-dipole arrays. Both CCR-ERT and DCR-ERT (configured with a dipole-dipole array) had high lateral sensitivity, which would be useful for ice wedges.

Ground-penetrating radar data were collected in the Goldstream study area during spring 2012 and compared against drilling completed by ADOT&PF the previous winter. Drainage conduits could be discriminated in the GPR from Miles 5–6. In this section, the base of the asphalt concrete pavement could be inferred, and lack of linearity suggests frost heaving over time. This interpretation was consistent with CCR-ERT data obtained by CRREL in a parallel project. CCR-ERT also indicated the presence of ice lenses. Miles 6–7 had lower overall values, which were likely a result of frozen ground instead of massive ice. The GPR data revealed the distance between the road grade and the top of the original embankment. The nonconformity evident by differences between their relative positions suggests that subsidence has occurred over time.

Ideally, geophysics should be able to identify the following properties:

- Soil texture
- Soil moisture content
- Location and depth of groundwater
- Presence/absence of permafrost
- Location and depth of the active layer
- Ice content
- Location and depth of massive ice
- Salinity content

Geophysics can also be used to quantify the spatial and temporal variations that are critical for geotechnical investigations and the development of highway infrastructure. Ultimately, geophysical techniques including electrical profiling (which encompasses GPR, CCR-ERT, and DCR-ERT) are most sensitive to water content variations. These relationships are nonlinear with respect to soil texture and water content, and volumetric effect when comparing lab-derived measurements with measured apparent resistivity values from the field. Also, a feedback issue arises between understanding the heterogeneity of an area using boreholes and their placement versus selection of the appropriate geophysical technique and setup. As illustrated by our results, choosing the appropriate setup requires some prior knowledge of the underlying surface characteristics.

The reality is that there is a range of measured resistivity values that can represent similar subsurface conditions when using geophysical methods like DCR-ERT and CCR-ERT. Accurate interpretation and analysis are dependent on a solid understanding of geophysical principles and geomorphic processes and verified subsurface data. With these conditions in place, geophysics can be deployed successfully in various capacities including route exploration and development, facilities development, identification and quantification of borrow material, and route re-alignment. In areas of complex surface-water conditions and/or permafrost, geophysics can help establish baseline conditions and track changes over time.

With existing infrastructure, identification and mitigation of current conditions are the most important consideration. This can include using GPR to establish the physical extent of subsidence or CCR-ERT to monitor whether the extent of buried massive ice features are undisturbed over time. At present, no systematic guidelines are available during the planning and exploration phases for collecting geophysical data. Geophysics like DCR-ERT and CCR-ERT at best are used only in localized areas when problems arise. In addition, any geophysics data collected are not adequately archived, and projects are treated as stand-alone exercises.

Successful deployment of geophysics including GPR, DCR-ERT, and CCR-ERT for large projects will benefit from an organized approach to produce the most reliable interpretations. Geophysical values must be repeatedly verified with subsurface conditions to develop a regionalized understanding of the range of values that correspond to soil texture, water, and permafrost properties. The type and resolution of geophysics data should also be standardized and optimized to produce the best relationship to geotechnical properties.

# CHAPTER 3 – GUIDANCE FOR PRACTITIONERS

## THE ROLE OF GEOPHYSICS IN GEOTECHNICAL INVESTIGATIONS

In the context of a linear infrastructure project, a primary goal of the geotechnical investigation is to produce a terrain unit map containing cross sections depicting geotechnical properties. These maps are then used as the basis to provide engineering design recommendations. The objective of this study was to help understand whether and how geophysical techniques could be used to supplement, optimize, and perhaps reduce the overall cost of the geotechnical investigation. An example process for integrating geophysical techniques into a geotechnical investigation is presented in Figure 86. In this figure, we assume that the alignment is relatively long and the geophysical method is relatively fast (e.g., CCR-ERT).

As depicted in Figure 86, the first step in the example process is to compile and evaluate all existing information regarding the alignment in question. If no aerial photos are available, then they should be obtained in order to create a preliminary terrain unit map of the alignment. In the preliminary stage, boreholes should be drilled at key sites in representative terrain units to provide geotechnical information at discrete points. For long alignments especially, these boreholes should have low-density placement and be based on terrain unit information rather than placed at established intervals. In some instances, it may prove beneficial to conduct limited geophysical surveys prior to drilling to optimize borehole locations. With the preliminary terrain unit map completed, planners can then determine the level of information required to complete the final map. In the intermediate stage, planners should work to complete the final terrain unit map, supplemented by continuous subsurface cross sections that describe geotechnical properties. At this stage, continuous or extensive geophysical surveys may be used to help interpolate the cross sections between existing boreholes. In some instances, confirmation boreholes may be desired at this point to ground truth the geophysical results.

In practice, the scope and timing of supplemental geophysics will likely be highly project-dependent. On relatively short alignments, for example, it may make sense to conduct resistivity surveys along the entire alignment prior to drilling mobilization. This step would allow planners to make well-informed decisions about the number and locations of the boreholes required. On longer alignments, an iterative approach may be more appropriate, whereby widely spaced boreholes are selected based on terrain units, and then geophysics are used to help interpolate between the boreholes. In this scenario, geophysics would serve to determine whether additional boreholes are necessary.

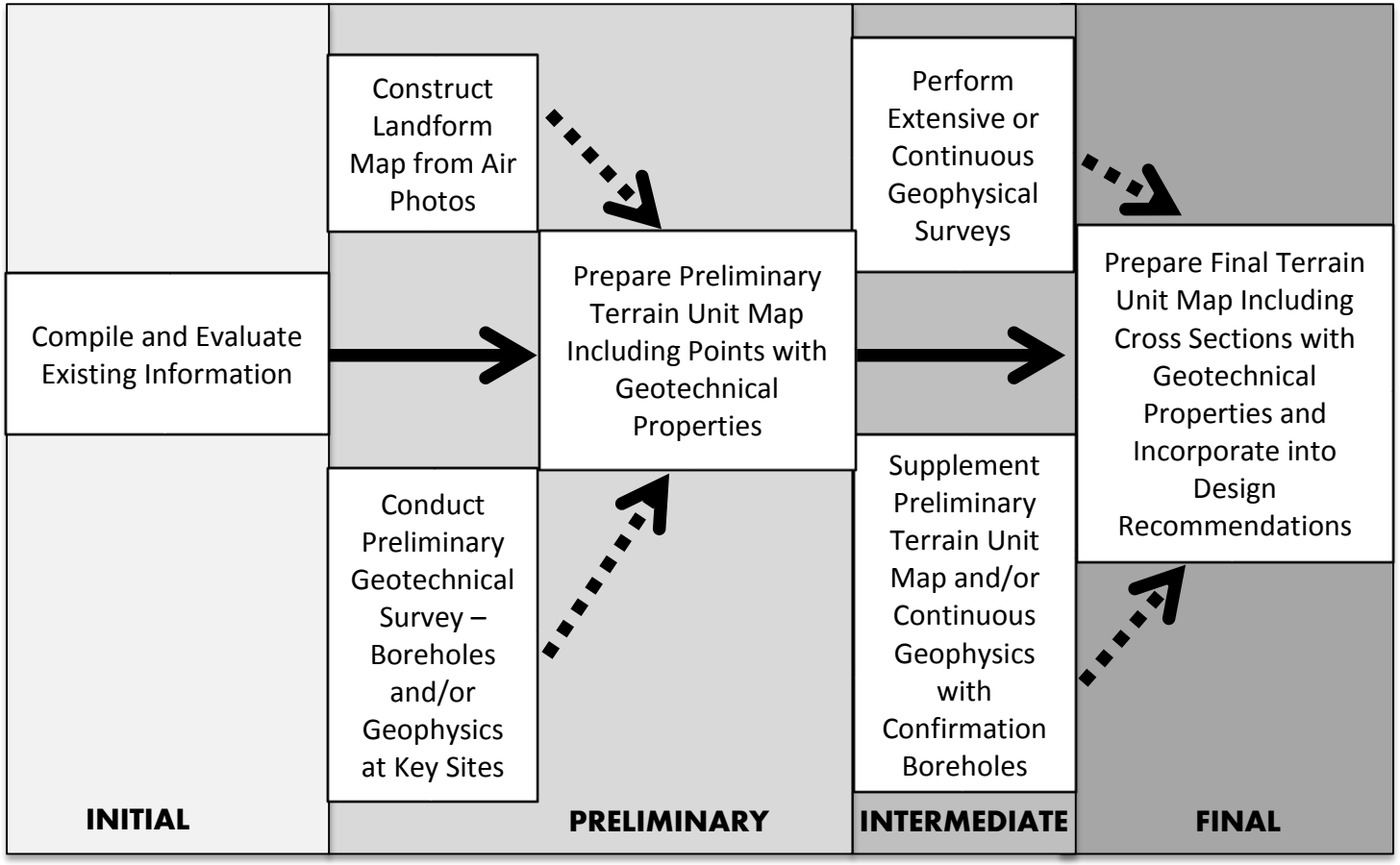


Figure 86. Proposed integration of geophysical techniques into geotechnical survey process.
Solid lines represent required steps. Dashed lines represent optional steps based on data requirements.

## SELECTING APPROPRIATE GEOPHYSICAL TECHNOLOGIES BASED ON MAPPED TERRAIN

Deployment of geophysics as a supplement to drilling can be an effective strategy in better understanding and characterizing mapped terrain. However, increased use of geophysics does not negate the role of boreholes. Geophysics can be used to better delineate the extent of bulk subsurface properties of boreholes drilled at regular intervals; it can also allow optimized borehole placement to capture subsurface irregularities. In many instances, this method could lead to a reduced number of boreholes required and improved characterization of phenomena. Geophysics can also be used to assist in interpolating between boreholes in an alignment, regardless of when or where the boreholes are drilled.

It is beneficial to consider any existing knowledge regarding a region's geomorphic features prior to conducting a geophysical evaluation. For example, does the area likely have yedoma and ice wedges? If so, then geophysics using electrical profiling with a dipole-dipole array could be most useful. CCR-ERT is more efficient for collecting large amounts of data. Ideally, CCR-ERT can be collected during winter, when snowpack facilitates the use of an ATV with tracks to tow equipment. The ATV allows a consistent speed, which allows the resolution of data to be consistent. This approach also allows the electrodes to create a groove in the snow so that during repeated passes data are collected in the same locations. The environmental impact of mechanized travel is mitigated in winter by the snowpack.

Alternatively, DCR-ERT using a dipole-dipole array is another option. The collection period for this technique is longer than that with CCR-ERT, as the cable and electrodes must be secured in place before data acquisition can begin. The advantage of DCR-ERT is that electrode locations can be more accurately recorded using differential GPS (D-GPS), and transects can be repeated at the same place. The resolution of the data is also easier to control with DCR-ERT, as this technique is dependent on electrode spacing. Another established data-collection technique with DCR-ERT is to pre-select the transect pattern to allow 3-D models to be produced. Lastly, DCR-ERT has the added advantage of flexibility with regard to array configurations.

Electrical resistivity tomography (ERT) configured in the Wenner array is more effective than dipole-dipole ERT for investigations of vertically stratified layers. In the Anaktuvuk River area, DCR-ERT configured in a Wenner array successfully mapped the depth of thaw associated with the floodplain. Thus, investigations evaluating horizontally oriented structures, such as the top of permafrost or the top of the groundwater table, are appropriate for DCR-ERT configured in a Wenner array.

When developing an initial understanding of basic mapped terrain units, CCR-ERT has great potential. Since it can be deployed quickly over large areas, CCR-ERT is an ideal technique for assessing the spatial variability of subsurface features. CCR-ERT allows the collection of solid baseline data so that seasonal and annual variations, or variations produced by infrastructure can be understood. Establishing a methodology that can easily delineate and track changes over time is a major advantage. As conditions change and problems arise with infrastructure, isolating the main controlling factors is easier. The situation can be more effectively monitored, and if necessary, resources may be deployed efficiently to engineer a solution.

## SELECTING APPROPRIATE GEOPHYSICAL TECHNOLOGIES BASED ON DATA SOUGHT

The most appropriate geophysical technique for geotechnical issues such as subsidence, route alignment and selection, quantifying alternative routes, and building supporting infrastructure may vary depending on site conditions. However, a combination of approaches will always produce the most robust analysis and interpretation. As such, the techniques employed in this study should not be viewed as competitive methods, but rather as complementary, each having distinct advantages and disadvantages.

Ground-penetrating radar (GPR) was demonstrated to be effective for identifying drainage conditions and the top of the road grade and foundation soils. As shown at the Goldstream Road site, areas of subsidence can be identified over time. The limitation to this technique is that depth of penetration is relatively shallow unless the soil is frozen (and conductivity maximized) and an appropriate antenna length is used. As with CCR-ERT, GPR surveys are easier to run in the winter using snowmachines or ATVs with tracks. In general, GPR should only be deployed for near-surface characterization.

During route alignment and selection, CCR-ERT is likely the more efficient geophysical method. Using a tracked ATV in the winter could allow miles of data to be collected in a day by a trained operator on an established trail. The technique can also be deployed during construction, if necessary, using ATVs in the winter or summer. If geospatial location information is collected simultaneously, then the processed data may be easily overlaid on as-built figures. This approach could be very useful in determining the final grades and amount of material that must be added or removed.

CCR-ERT would also likely be most effective when comparing alternative potential alignments. As discussed in the previous section, CCR-ERT is time- and cost-effective to deploy. Visualizing and interpreting the results are relatively easy with adequate knowledge and training in geophysics, geomorphology, and permafrost. Improvements in analysis of the data are possible by geo-spatially locating the data with respect to surface topography and variations. Since the data can be acquired repeatedly over time, conditions can be identified and monitored using a proactive approach.

An additional use of geophysics includes site selection and design of supporting infrastructure including buildings, camps, and pads. In circumstances where the spatial scope of the investigation is limited, the flexibility of DCR-ERT may outweigh the mobility of CCR-ERT. For example, DCR-ERT could be used for more-detailed surveys where the location of each electrode can be recorded and repeated as necessary. Also, since DCR-ERT can be easily deployed at different resolutions, it can evaluate for anomalies more thoroughly in the near surface, which might affect the amount of fill and/or insulation needed during construction. Other locations where DCR-ERT might be preferable over CCR-ERT include bridge approaches along a known alignment. In that instance, the ability of DCR-ERT to optimize vertical and horizontal resolution by performing surveys of different array configurations would be particularly useful, whereas the mobility proffered by CCR-ERT would not be as essential.

## ESTIMATING COSTS OF GEOPHYSICAL SURVEYS

Evaluating the potential exploratory cost savings from using geophysical methods is confounded by the high degree of variability between project objectives, available prior information, site accessibility, and field conditions. Nonetheless, managers must develop some criteria for estimating the costs and financial benefits in order to thoughtfully consider the use of geophysical methods.

As a rule, the cost of performing geophysics will be less than the cost of performing drilling, because geophysics is generally faster and requires less heavy equipment. Therefore, in instances where information provided by geophysics can substantially reduce the number of boreholes required, geophysics will likely reduce the overall investigation costs. Perhaps more importantly, if the information provided by geophysics allows investigators to optimize their borehole locations such that the informational value of the holes is maximized, then geophysics will reduce the life cycle cost of the project by producing a more effective design.

On the other hand, due to liability concerns, reducing the number of boreholes drilled for a project is not always possible. In this case, the addition of geophysics may increase the initial cost of the project. However, the use of geophysics has potential to significantly improve engineering design recommendations, and this may lead to lower maintenance costs and reduce the overall lifetime expense of projects.

While the costs of performing geophysics will vary significantly from project to project, the following observations made during this study may help managers to evaluate the potential costs of geophysics for future projects.

In general, the geophysical surveys described in this report can be conducted by teams of two to three trained individuals using mobile instrumentation. Thus, the mob/demob costs would be limited to getting the individuals and their hand-carried gear to and from the site. For longer CCR-ERT surveys, the team would also require onsite transport such as a snowmachine or ATV, which may incur additional mob/demob costs.

The time required to conduct the surveys themselves is ultimately dependent on the amount of data desired as well as the techniques used. Our team required approximately four hours to complete each DCR-ERT survey, thus providing subsurface information for survey lengths of approximately 550 ft (at 2 m electrode spacing). The CCR-ERT surveys performed at 9-Mile Hill required four to six hours to produce surveys of approximately 3000 ft. However, CCR-ERT surveys can be conducted more quickly than that, depending on the depth of the investigation and the means used to tow the array. We estimate that under optimal conditions, a CCR-ERT instrument towed over snow on an established trail could cover at least five miles per day. The GPR surveys conducted on Goldstream Road were collected at a slow walking speed. Thus, each mile of GPR data required approximately one hour to collect.

The time required to evaluate geophysical data is highly dependent on the quality of the output required. For example, a skilled operator could download, configure, assess, and draw preliminary conclusions from a resistivity survey within one to two hours of data collection. In many instances, this level of evaluation may be all that is required for assessing the homogeneity of a section or seeking specific anomalies. It can, however, take considerably longer (i.e., days)

to format geophysical data into geo-referenced, topographically scaled report-quality figures such as those presented in Figure 34. This level of effort and output quality is often required in order to effectively communicate geophysical results to managers or the public.

The ADOT&PF provided our team with a set of cost points to use when estimating the costs of drilling and logging activities. We have incorporated those numbers, together with our own estimates of geophysics costs, into a table designed to evaluate the costs of drilling programs with and without the inclusion of geophysics (Table 9). While these numbers are merely rough estimates, they can provide managers with a tool for evaluating the potential savings incurred through the inclusion of supplemental geophysics. Moreover, close examination of the table can help to illustrate those circumstances under which supplemental geophysics may have the highest relative value.

Table 9 provides cost estimates for three hypothetical drilling programs with and without the inclusion of supplemental geophysics. In this instance, we assumed that a supplemental resistivity survey was performed via CCR-ERT by a crew of two, similar to the technique employed at 9-Mile Hill. The objective of geophysics in all three scenarios was to survey the entire length of the section being investigated, and provide guidance with respect to borehole placement. We assumed that the availability of geophysical data reduced the overall number of boreholes required in each scenario. Finally, we assumed that the crew would survey at a rate of two miles per day.

In Scenario A, we estimated drilling costs for a five-mile highway alignment at a road-accessible site. In this scenario, we assumed a borehole density of 10 holes per mile, similar to the density for a fill section recommended in the Alaska Geological Field Investigations Guide (ADOT&PF 2007). By using supplemental geophysics, we assumed that the borehole density would decrease by half. As evidenced in the table, inclusion of geophysics in this scenario would be anticipated to reduce the cost of drilling by approximately 20%.

Scenario B assumes that the drilling was conducted in a community off the road system, with the drill rig transported to the site via barge. In this scenario, we assumed that the section under investigation was two miles long and that drilling costs per day were slightly higher than drilling costs at the highway-accessible site. Again, we assumed 10 holes per mile for conventional drilling, and we assumed that geophysics would decrease the number of required boreholes by half. Under these conditions, supplemental geophysics would decrease the drilling costs by approximately 6%.

In Scenario C, we assumed that the drilling was conducted in a remote location via helicopter, similar to the conditions experienced in the ADOT&PF Foothills West project. In this scenario, we assumed a much longer alignment (50 miles) and reduced borehole density for conventional drilling (1 hole/mile). Moreover, we assumed a much higher per-hole cost than the other scenarios, based on the data provided by ADOT&PF. In this scenario, we assumed that geophysics would reduce the conventional boreholes required to 25% of the original number. Under these conditions, the inclusion of supplemental geophysics would be expected to reduce drilling costs by 47%.

While the results presented in Table 9 do provide some rough numbers, perhaps the greater value of the table is to illuminate some general trends. With respect to CCR-ERT, for

example, the relative cost savings achieved through supplemental geophysics can be expected to increase with increasing per-hole costs of drilling. Other conditions expected to increase the relative cost savings of supplemental geophysics include longer alignment lengths and increased survey miles per day (i.e., more experienced crews, unobstructed trails). Factors that would tend to decrease the relative cost savings of supplemental geophysics include increased mobilization costs for the drill rig, and increased complexity of the subsurface (requiring more boreholes). Finally, the relative cost savings of supplemental geophysics would be expected to increase with time. As the geophysical technicians and drill managers accumulate experience working together in arctic and subarctic conditions, they will learn what to look for with geophysics and how to optimize their drilling based on those results.

Table 9. Cost estimates for drilling with and without supplemental geophysics

| Scenario | Traditional Drilling | | Geophysics | | Reduced Drilling | |
|---|---|---|---|---|---|---|
| **Scenario A: Road Accessible Site** | Total Miles | 5 | | | Total Miles | 5 |
| | Holes/Mile | 10 | Total Miles | 5 | Holes/Mile | 5 |
| | Holes/Day | 10 | Miles/Day | 2 | Holes/Day | 10 |
| | Drilling Costs/Day | $6,000 | Geophysics Cost/Day | $2,000 | Drilling Costs/Day | $6,000 |
| | Total Days Drilling | 5 | Total Days Geophysics | 2.5 | Total Days Drilling | 2.5 |
| | Mob/Demob Cost | $6,000 | Mob/Demob Cost | $3,000 | Mob/Demob Cost | $6,000 |
| | | | Geophysics Cost | $8,000 | Reduced Drilling Cost | $21,000 |
| | **Drilling Without Geophysics:** | **$36,000** | | **Drilling With Geophysics:** | **$29,000** | |
| **Scenario B: Off-road Community (Barge drill to location)** | Total Miles | 2 | | | Total Miles | 2 |
| | Holes/Mile | 10 | Total Miles | 2 | Holes/Mile | 5 |
| | Holes/Day | 10 | Miles/Day | 2 | Holes/Day | 10 |
| | Drilling Costs/Day | $8,000 | Geophysics Cost/Day | $2,000 | Drilling Costs/Day | $8,000 |
| | Total Days Drilling | 2 | Total Days Geophysics | 1 | Total Days Drilling | 1 |
| | Mob/Demob Cost | $20,000 | Mob/Demob Cost | $4,000 | Mob/Demob Cost | $20,000 |
| | | | Geophysics Cost | $6,000 | Reduced Drilling Cost | $28,000 |
| | **Drilling Without Geophysics:** | **$36,000** | | **Drilling With Geophysics:** | **$34,000** | |
| **Scenario C: Remote Work via Helicopter** | Total Miles | 50 | | | Total Miles | 50 |
| | Holes/Mile | 1 | Total Miles | 50 | Holes/Mile | 0.25 |
| | Holes/Day | 2 | Miles/Day | 2 | Holes/Day | 2 |
| | Drilling Costs/Day | $25,000 | Geophysics Cost/Day | $6,000 | Drilling Costs/Day | $25,000 |
| | Total Days Drilling | 25 | Total Days Geophysics | 25 | Total Days Drilling | 6.25 |
| | Mob/Demob Cost | $40,000 | Mob/Demob Cost | $5,000 | Mob/Demob Cost | $40,000 |
| | | | Geophysics Cost | $155,000 | Reduced Drilling Cost | $196,250 |
| | **Drilling Without Geophysics:** | **$665,000** | | **Drilling With Geophysics:** | **$351,250** | |

# CHAPTER 4 – CONCLUSIONS, RECOMMENDATIONS, AND SUGGESTED RESEARCH

We recommend that ADOT&PF integrate geophysical techniques more fully into their geotechnical investigations for arctic and subarctic linear infrastructure. In particular, this study revealed that data provided by electrical resistivity could be used to help optimize placement of boreholes and potentially reduce the number of boreholes required. We anticipate that this practice will save investigation costs, especially for long alignments.

The mechanism and schedule by which geophysics is incorporated into the investigation workflow will vary considerably from project to project. On short highway alignments or at the planned locations of stationary facilities, resistivity surveys conducted prior to borehole drilling would help to optimize borehole locations. On long alignments where borehole locations are selected based on terrain units, resistivity surveys conducted in the vicinity of boreholes would allow investigators to correlate geophysical results with borehole data. Again, conducting such surveys prior to borehole placement would aid in selecting specific borehole location. Long CCR-ERT surveys conducted primarily to help interpolate between widely spaced boreholes would likely be most effective if conducted after boreholes are drilled.

While we did not attempt to evaluate whether ADOT&PF should conduct future geophysical surveys in-house, we do recommend that ADOT&PF seek to develop in-house expertise in understanding and interpreting geophysical data. Understanding the origins, benefits, and limitations of geophysical data will ultimately lead to more-informed decisions regarding borehole placement and subsurface character.

Geophysics is best deployed when prior knowledge of expected permafrost and geotechnical site conditions is available. When using the most common electrical profiling techniques of CCR-ERT and DCR-ERT, the two different array setups have a significant influence on the results. The Wenner array (produced only via DCR-ERT) is recommended for horizontal structures like groundwater and assessment of general homogeneity. Dipole-dipole is most suitable for vertical structures like ice wedges. If knowledge of preexisting site conditions is insufficient, then an acceptable approach is to repeat surveys with both arrays in a designated test area. Once the data are interpreted, the array that produces the most applicable data should be applied to the remainder of the area.

Drilling must be located in areas where the site locations maximize the information derived from the borehole. Terrain unit mapping is an important step in guiding drilling and geophysical surveys. The availability of better geospatial data is highly beneficial to this process. The addition of high-resolution LIDAR and multispectral optical and near-infrared imagery produces a much more detailed description of the landscape. All data must be accurately geospatially referenced to aid in interpretation. Proximity and spatial relationships are critical in both horizontal and vertical planes and allow more-thorough analysis.

Education, training, and development of expertise is critical in selecting the most appropriate geophysical technique, and for correct analysis and interpretation. One potential form is a three-step process consisting of (1) an international workshop, (2) a graduate-level course on applications of geophysics, and (3) master’s degree students collaborating with UAF faculty and ADOT&PF.

Geotechnical issues in Alaska are similar to those in other parts of the Arctic. Organization of an international workshop that includes engineers and scientists from Canada and Europe would provide a cutting-edge review of geophysical applications in permafrost regions, with a focus on highway infrastructure. Currently, Danish researchers are working in Greenland to develop and apply geophysical techniques specific to monitoring active layer development and massive ice degradation. A workshop should include hands-on field exercises to observe and understand various local permafrost processes and geophysical methods (CCR-ERT, DCR-ERT, and GPR). Future research and data analysis needs could be discussed including geophysical data storage, visualization, and analysis of borehole data combined with geophysical interpretation in 3-D, more sophisticated software to process geophysical data, and a streamlined data processing system for greater efficiency.

A graduate-level course on using geophysics for geotechnical applications should be developed in cooperation with UAF. This course should be targeted at working professional engineers and scientists (similar to the UAF graduate course Arctic Engineering). Remote participation should be facilitated through online lectures to encourage attendance by all interested parties. Faculty with a range of expertise should be included as guest lecturers to maximize knowledge transfer and illustrate quality case studies.

Future geophysics research based at UAF should include the participation of master's students on the projects. Ideally, students would be junior engineers with ADOT&PF who would like to gain experience and develop expertise in geophysics. This practice would allow more direct collaboration between UAF faculty and ADOT&PF during the project and in future relations; it would also open more opportunities for external professional development and provide incentives for internal growth and retention.

Evaluations of future geophysical research projects should recognize the progression of approaches within interdisciplinary studies over time as shown in Figure 79. At this time, analysis and interpretation of geophysical data are based on expert knowledge from a variety of fields including geophysics, geocryology, environmental engineering, and physical geography. As studies become larger and more complex, it will be possible to integrate statistical approaches to increase the robustness and repeatability of data interpretation. Good statistical analysis is based on appropriate sampling design and standardization of data. Approaches can include clustering of patterns as well as an understanding of the correlations between datasets in space and time. This approach acts as a solid platform for the development of physically based models that explicitly connect geophysical results to subsurface conditions. Presently, this approach is computationally expensive, but in the future, this might be less of a technological limitation. Physically based models depend on good input data to validate model predictions and could build on appropriately archived data used in previous approaches and studies.

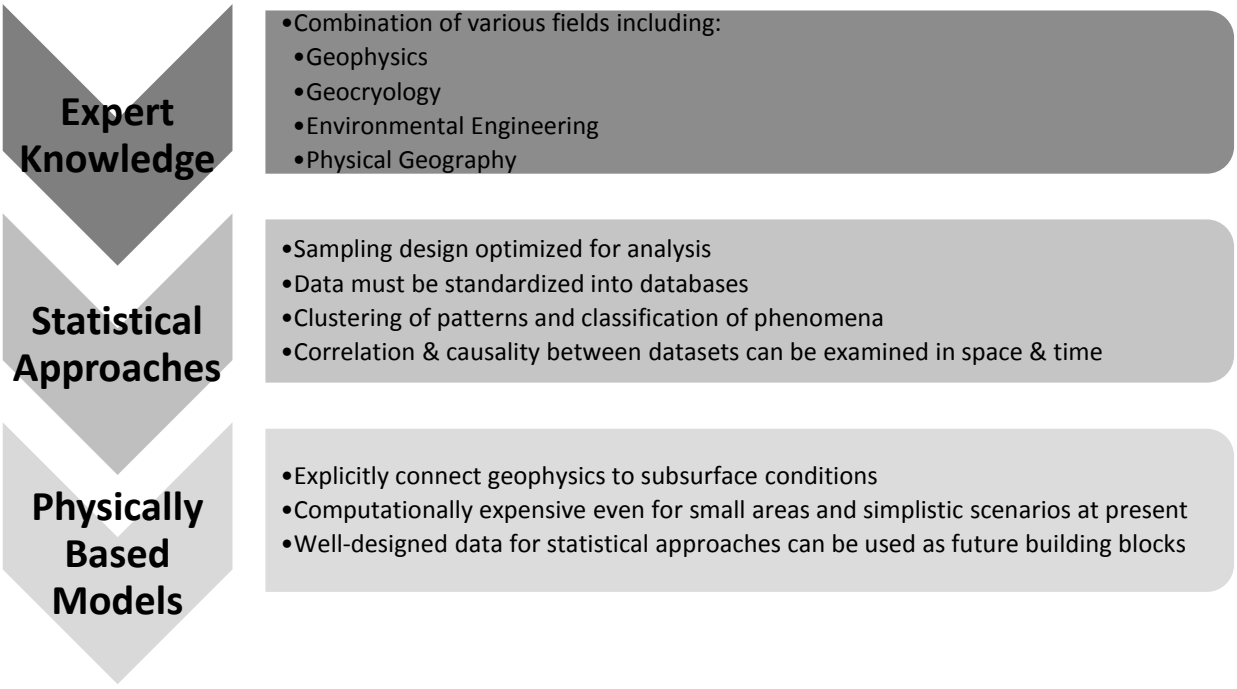


Figure 87. Applications of geophysics for geotechnical applications based on future developments.

## REFERENCES


AASHTO, 1988. Manual on Subsurface Investigations, American Association of State Highway and Transportation Officials, Washington DC (accessed online).

ADOT&PF, 2007. Alaska Geological Field Investigations Guide, Alaska Department of Transportation and Public Facilities.

ASTM D422, 1998. Standard test method for particle-size analysis of soils. American Society for Testing and Materials, West Conshohocken, PA.

Black, R.F., 1978. Fabrics of ice wedges in central Alaska. *Proceedings of the Third International Conference on Permafrost, Edmonton, July 10–13, 1978.* Ottawa: National Research Council of Canada, 248–253.

Blott, S.J., and Pye, K., 2001. Gradistat: A grain size distribution statistics package for the analysis of unconsolidated sediments. *Earth Surface Processes and Landforms* 26: 1237–1278.

Bray, M.T., French, H.M., and Shur, Y., 2006. Further cryostratigraphic observations in the CRREL permafrost tunnel, Fox, Alaska. *Permafrost and Periglacial Processes* 17(3): 233–243.

Brown, J., and Kreig, R.A. (Eds.), 1983. *Guidebook to Permafrost and Related Features along the Elliott and Dalton Highways, Fox to Prudhoe Bay, Alaska*. 230 pp.

Brewer, M.C., Carter, L.D., and Glenn, R., 1993. Sudden drainage of a thaw lake on the Alaskan Arctic Coastal Plain. *Proceedings of the Sixth International Conference on Permafrost, July 5–9, Beijing, China.* South China University of Technology Press, pp. 48–53.

Cantwell, J.C., 1887. A narrative account of the exploration of the Kowak River, Alaska, under the direction of Capt. Michael A. Healy, commanding U.S. Revenue steamer Corwin. In: Healy, M.A. Report of the cruise of the Revenue Marine steamer Corwin in the Arctic Ocean in the year 1885. Washington, DC: Government Printing Office, 21–52.

Carter, L.D., 1988. Loess and deep thermokarst basins in Arctic Alaska. *Proceedings of the Fifth International Conference on Permafrost*. Trondheim, Norway: Tapir Publishers, pp. 706–711.

De Pascale, G.P., Pollard, W.H., and Williams, K.K., 2008. Geophysical mapping of ground ice using a combination of capacitive coupled resistivity and ground-penetrating radar, Northwest Territories, Canada. *Journal of Geophysical Research: Earth Surface*, 113(F2): F02S90.

Douglas, T.A., Jorgenson, M.T., Kanevskiy, M.Z., Romanovsky, V.E., Shur, Y., Yoshikaw, K., 2008. Permafrost dynamics at the Fairbanks Permafrost Experimental Station near Fairbanks, Alaska. In: Kane, D.L. and Hinkel, K.M. (eds.), *Proceedings of the Ninth International Conference on Permafrost. Institute of Northern Engineering University of Alaska Fairbanks, Fairbanks, Alaska*, pp. 373–378.

Fortier, R., and Savard, C., 2010. Engineering geophysical investigation of permafrost conditions underneath airfield embankments in Northern Quebec (Canada). In: *Proceedings, Sixth Canadian Permafrost Conference, Calgary, Alberta*, pp. 1307–1316.

Fortier, D., Kanevskiy, M., and Shur, Y., 2008. Genesis of reticulate-chaotic cryostructure in permafrost. In: *Proceedings of the Ninth International Conference on Permafrost, June 29–July 3, 2008, Fairbanks, Alaska.* Kane, D.L. and Hinkel, K.M. (eds.). Institute of Northern Engineering, University of Alaska Fairbanks, Vol. 1: 451–456.

Fortier, R., Leblanc, A.-M., and Yu, W., 2011. Impacts of permafrost degradation on a road embankment at Umiujaq in Nunavik (Quebec), Canada. *Revue Canadienne de Géotechnique*, 48: 720–740.

French, H.M., 2007. *The Periglacial Environment*, 3rd Ed. Chichester, UK: John Wiley and Sons Ltd., 458 pp.

French, H., and Shur, Y., 2010. The principles of cryostratigraphy. *Earth-Science Reviews* 110, 190–206. doi: 10.1016/j.earscirev.2010.04.002.

Frolov, A.D., 2005. Electrical and elastic properties of frozen soils and ice. Pushchino, ONTI PNC RAN.

Gasanov, S.S., 1963. *Morphogenetic classification of cryostructures of frozen sediments*. Trudy SVKNII, Vol. 3, Magadan (in Russian).

Golder, 2002. Evaluation of Geophysical Methods: Field Program. *FHWA-AK-RD-02-07,* Alaska Department of Transportation and Public Facilities, Fairbanks.

Hamilton, T.D., 1979. Geologic road log, Alyeska haul road, Alaska, June–August 1975. *U.S. Geological Survey Open-File Report 79-227*, 64 pp.

Hamilton, T.D., Ager, T.A., and Robinson, S.W., 1983. Late Holocene ice wedges near Fairbanks, Alaska, USA: Environmental setting and history of growth. *Arctic and Alpine Research* 15(2): 157–168.

Hamilton, T.D., Craig, J.L., and Sellmann, P.V., 1988. The Fox permafrost tunnel: A late Quaternary geologic record in central Alaska. *Geological Society of America Bulletin* 100: 948–969.

Hamilton, T.D., 1994. Late Cenozoic glaciation of Alaska. In: *The Geology of Alaska*. Plafker, G., and Berg, H.C. (eds.), Boulder, Colorado, Geological Society of America, The Geology of North America, Vol. G-1, 813–844.

Hopkins, D.M., 1963. Geology of the Imuruk Lake area, Seward Peninsula, Alaska. *U.S. Geological Survey Bulletin 1141-c*, 101 pp.

Hopkins, D.M., and Kidd, J.G., 1988. Thaw lake sediments and sedimentary environments. *Proceedings of the Fifth International Conference on Permafrost.* Trondheim, Norway: Tapir Publishers, 790–795.

Jafarov, E.E., Marchenko, S.S., and Romanovsky, V.E., 2012. Numerical modeling of permafrost dynamics in Alaska using a high spatial resolution dataset. *The Cryosphere Discuss.*, 6(1): 89–124.

Jones, B.M., Kolden, C.A., Jandt, R., Abatzoglou, J.T., Urban, F., and Arp, C.D., 2009. Fire behavior, weather, and burn severity of the 2007 Anaktuvuk River tundra fire, North Slope, Alaska. *Arctic Antarctic and Alpine Research*, 41(3): 309–316.

Jorgenson, M.T., and Heiner, M., 2008. *Ecosystems of Northern Alaska*. ABR Inc. and the Nature Conservancy.

Jorgenson, T., Yoshikawa, K., Kanevskiy, M., Shur, Y., Romanovsky, V., Marchenko, S., Grosse, G., Brown, J., and Jones, B., 2008. Permafrost characteristics of Alaska. In: *Proceedings of the Ninth International Conference on Permafrost*, extended abstracts. June 29–July 3, 2008, Fairbanks, Alaska. Kane, D.L. and Hinkel, K.M. (eds.), Institute of Northern Engineering, University of Alaska Fairbanks, pp. 121–122.

Kanevskiy, M.Z. 1991. The role of quasi-syngenesis in formation of Quaternary sediments cryogenic structure in Northern Yakutia. In: Melnikov, P. and Shur, Y. (eds.), *The Upper Horizon of Permafrost.* Moscow: Nauka, pp. 47–63 (in Russian).

Kanevskiy, M., 2003. Cryogenic structure of mountain slope deposits, northeast Russia. In: Phillips, M., Springman, S., and Arenson, L. (eds.), *Proceedings of the Eighth International Conference on Permafrost*, 21–25 July 2003, Zurich, Switzerland, Swets and Zeitlinger B.V., Lisse, The Netherlands, Vol. 1, pp. 513–518.

Kanevskiy, M., Fortier, D., Shur, Y., Bray, M., and Jorgenson, T., 2008. Detailed cryostratigraphic studies of syngenetic permafrost in the winze of the CRREL permafrost tunnel, Fox, Alaska. In: *Proceedings of the Ninth International Conference on Permafrost, June 29–July 3, 2008, Fairbanks, Alaska.* Kane, D.L. and Hinkel, K.M. (eds.), Institute of Northern Engineering, University of Alaska Fairbanks, Vol. 1, pp. 889–894.

Kanevskiy, M., Shur, Y., Fortier, D., Jorgenson, M.T., and Stephani, E., 2011a. Cryostratigraphy of late Pleistocene syngenetic permafrost (yedoma) in northern Alaska, Itkillik River exposure. *Quaternary Research*, 75: 584–596. doi:10.1016/j.yqres.2010.12.003.

Kanevskiy, M., Shur, Y., Jorgenson, M.T., Ping, C.-L., Fortier, D., Stephani, E., and Dillon, M., 2011b. Permafrost of Northern Alaska. In: *Proceedings of the Twenty-first International Offshore and Polar Engineering Conference Maui, Hawaii, USA, June 19–24, 2011*: 1179–1186, ISBN 978-1-880653-96-8 (Set); ISSN 1098-6189 (Set).

Kanevskiy, M., Shur, Y., Connor, B., Dillon, M., Stephani, E., and O'Donnell, J., 2012a. Study of the ice-rich syngenetic permafrost for road design (Interior Alaska). In: *Proceedings of the Tenth International Conference on Permafrost, June 25–29, 2012, Salekhard, Russia.* The Northern Publisher, Salekhard, Russia, Vol. 1: International contributions. Hinkel, K.M. (ed.): 191–196.

Kanevskiy, M., Shur, Y., Jorgenson, M.T., Ping, C.-L., Michaelson, G.J., Fortier, D., Stephani, E., Dillon, M., and Tumskoy, V., 2012b. Ground ice in the upper permafrost of the Beaufort Sea coast of Alaska, *Cold Regions Science and Technology.* doi: 10.1016/j.coldregions.2012.08.002.

Katasonov, E.M., 1969. Composition and cryogenic structure of permafrost. National Research Council of Canada, Ottawa, *Technical Translation 1358*, pp. 25–36.

Katasonov, E.M., 1978. Permafrost-facies analysis as the main method of cryolithology. *Proceedings of the Second International Conference on Permafrost, July 13–28, 1973. USSR Contribution*. Washington: National Academy of Sciences, 171–176.

Kawasaki, K., and Osterkamp, T.E., 1984. Electromagnetic induction measurements in permafrost terrain for detecting ground ice and ice-rich soils. Final Report, Alaska Department of Transportation and Public Facilities.

Kotzebue, O. von, 1821. A voyage of discovery into the South Sea and Beering's straits, for the purpose of exploring a north-east passage, undertaken in the years 1815–1818, at the expense of His Highness the Chancellor of the Empire, Count Romanzoff, in the ship Rurick, under the command of the lieutenant in the Russian imperial navy, Otto von Kotzebue. London: Longman, Hurst, Rees, Orme, and Brown, 3 vols.

Kreig, R.A., and Reger, R.D., 1976. Preconstruction terrain evaluation for the Trans-Alaska Pipeline project. In: Coates, D.R. (ed.), *Geomorphology and Engineering*. Stroudsburg, Dowden, Hutchinson and Ross, 55-76.

Kreig, R.A., and Reger, R.D., 1982. *Air-photo analysis and summary of landform soil properties along the route of the Trans-Alaska Pipeline System*. DGGS, College, *Alaska, Geologic Report 66*, 149 pp.

Krynine, D.P., and Judd, W.R., 1957. *Principles of Engineering Geology and Geotechnics.* New York: McGraw-Hill Book Company, 730 pp.

Kudryavtsev, V.A. (ed.), 1978. *General Permafrost Science (Geocryology),* 2nd Ed., Moscow: Moscow University Press, 463 pp. (in Russian).

Kuras, O., Beamish, D., Meldrum, P.I., and Ogilvy, R.D., 2006. Fundamentals of the capacitive resistivity technique. *Geophysics*, 71(3): G135–G152.

Lachenbruch, A.H. 1962. *Mechanics of thermal contraction cracks and ice-wedge polygons in permafrost*. Geol. Soc. of Am. Special Paper 70.

Lawson, D.E., 1982. Long-term modifications of perennially frozen sediment and terrain at East Oumalik, northern Alaska. *CRREL Report 82–36*, 33 pp.

Lawson, D.E., 1983. Ground ice in perennially frozen sediments, northern Alaska. In: *Proceedings of the Fourth International Conference on Permafrost*. National Academy Press, Washington, DC: 695–700.

Lawson, D.E., 1986. Response of permafrost terrain to disturbance: A synthesis of observations from Northern Alaska, USA. *Arctic and Alpine Research*, 18(1): 1–17.

Leffingwell, E. de K., 1915. Ground-ice wedges, the dominant form of ground-ice on the north coast of Alaska. *Journal of Geology*, 23: 635–654.

Livingstone, D.A., Bryan, K., Jr., and Leahy, R.G., 1958. Effects of an Arctic environment on the origin and development of freshwater lakes. *Limnology and Oceanography*, 3: 192–214.

Loke, M.H., and Barker, R.D., 1995. Least-square deconvolution of apparent resistivity pseudosections. *Geophysics*, 60(6): 1682–1690.

Maddren, A.G., 1905. *Smithsonian Explorations in Alaska in 1904*. Smithsonian Misc. Coll., Vol. 49, 1–117.

Matheus, P., Begét, J., Mason, O., and Gelvin-Reymiller, C., 2003. Late Pliocene to Late Pleistocene environments preserved at the Palisades Site, central Yukon River, Alaska. *Quaternary Research,* 60: 33–43.

Melnikov, E.S., and Dubikov, G.I. (eds.), 1986. *Methods of Regional Permafrost-Engineering Investigations.* Moscow: Nedra (in Russian), 207 pp.

Melnikov, V.P., and Spesivtsev, V.I., 2000. *Cryogenic Formations in the Earth's Lithosphere.* Novosibirsk: Siberian Publishing Center UIGGM, Siberian Branch, Russian Academy of Sciences, 343 pp.

Meyer, H., Yoshikawa, K., Schirrmeister, L., and Andreev, A., 2008. The Vault Creek Tunnel (Fairbanks Region, Alaska) – A late Quaternary palaeoenvironmental permafrost record. In: *Proceedings of the Ninth International Conference on Permafrost, June 29–July 3, 2008, Fairbanks, Alaska.* Kane, D.L. and Hinkel, K.M. (eds.), Institute of Northern Engineering, University of Alaska Fairbanks, Vol. 2: 1191–1196.

Miller, D.E., and Johnson, L.A., 1990. Pile settlement in saline permafrost: a case history. In: *Proceedings 5th Canadian Permafrost Conference*, Quebec City, Quebec, 371-378.

Murton, J.B., and French, H.M., 1994. Cryostructures in permafrost, Tuktoyaktuk coastlands, western arctic Canada. *Canadian Journal of Earth Sciences,* 31: 737–747.

O'Donnell J.A., Harden, J.W., McGuire, A.D., Kanevskiy, M.Z., Jorgenson, M.T., and Xu, X., 2011. The effect of fire and permafrost interactions on soil carbon accumulation in an upland black spruce ecosystem of interior Alaska: Implications for post-thaw carbon loss. *Global Change Biology,* 17: 1461–1474. doi: 10.1111/j.1365-2486.2010.02358.x.

Osterkamp, T.E., and Payne, M.W., 1981. Estimates of permafrost thickness from well logs in northern Alaska. *Cold Regions Science and Technology*, 5(1): 13–27.

Péwé, T.L., 1954. Effect of permafrost on cultivated fields, Fairbanks Area, Alaska. *Geological Survey Bulletin* 989-F, pp. 315–351.

Péwé, T.L., 1958. Geology of the Fairbanks (D-2) quadrangle, Alaska. United States Geological Survey, Quadrangle Map GQ-110, scale 1:63,360.

Péwé, T.L., 1975. Quaternary geology of Alaska. *U.S. Geological Survey, Professional Paper 835,* 145 pp.

Popov, A.I., 1967. *Cryogenic Phenomena in the Earth Crust (Cryolithology)*. Moscow: Moscow University Press, 304 pp. (in Russian).

Popov, A.I., Rozenbaum, G.E., and Tumel, N.V., 1985. *Cryolithology*. Moscow: Moscow University Press, 239 pp. (in Russian).

Porter, L., 1986. Jack Wade Creek: An in situ Alaskan late Pleistocene vertebrate assemblage. *Arctic,* 39: 297–299.

Porter, L., 1988. Late Pleistocene fauna of Lost Chicken Creek, Alaska. *Arctic,* 41: 303–313.

Prindle, L.M., 1913. A geologic reconnaissance of the Fairbanks Quadrangle, Alaska. *USGS Bulletin 525*. Government Printing Office, Washington, 220 pp.

Quackenbush, L.S., 1909. Notes on Alaskan mammoth expeditions. *Am. Mus. Nat. Hist. Bul.*, Vol. 26: 87–130.

Romanovskii, N.N., 1993. *Fundamentals of Cryogenesis of Lithosphere*. Moscow: Moscow University Press, 336 pp. (in Russian).

Rowland, J., 2010. *Geotechnical report – supplemental, Dalton Highway 9 mile North, Federal Project No. NH-F-06502(3) / State Project No. 64899*. Alaska Department of Transportation and Public Facilities, Northern Region Material Section.

Sazonova, T.S., and Romanovsky, V.E., 2003. A model for regional-scale estimation of temporal and spatial variability of active layer thickness and mean annual ground temperatures. *Permafrost and Periglacial Processes,* 14(2): 125–139.

Schlichting, S.J., Darrow, M.M., and Masterman, S., 2006. *Geotechnical Report. Dalton Highway 9 Mile Hill North. Federal Project No. NH-F-065-2(3), State Project No. 64899*. Northern Region, Department of Transportation and Public Facilities, State of Alaska, 96 pp.

Sellmann, P.V., 1967. Geology of the USA CRREL permafrost tunnel, Fairbanks, Alaska. *U.S. Army CRREL Technical Report 199*, Hanover, New Hampshire, 22 pp.

Shur, Y.L., 1988a. *Upper Horizon of the Permafrost Soils and Thermokarst.* Novosibirsk: Nauka, Siberian Branch, 210 pp. (in Russian).

Shur, Y.L., 1988b. The upper horizon of permafrost soils. In: *Proceedings of the Fifth International Conference on Permafrost*, Vol. 1. Trondheim, Norway: Tapir Publishers, 867–871.

Shur, Y., and Jorgenson, M.T., 1998. Cryostructure development on the floodplain of the Collville River Delta, northern Alaska. In: *Proceedings of the Seventh International Conference on Permafrost. Yellowknife, Canada*, 993–999.

Shur, Y., and Kanevskiy, M., 2010. Geotechnical Investigations for the Dalton Highway Innovation Project as a Case Study of the Ice-Rich Syngenetic Permafrost. Alaska University Transportation Center, 153 pp.

Shur, Y., French, H.M., Bray, M.T., and Anderson, D.A., 2004. Syngenetic permafrost growth: cryostratigraphic observations from the CRREL Tunnel near Fairbanks, Alaska. *Permafrost and Periglacial Processes*, 15(4): 339–347.

Shur, Y., Hinkel, K.M., and Nelson, F.E., 2005. The transient layer: implications for geocryology and climate-change science. *Permafrost and Periglacial Processes,* 16(1): 5–17.

Shur, Y., Kanevskiy, M., Dillon, M., Stephani, E., and O'Donnell, J., 2010. Geotechnical investigations for the Dalton Highway innovation project as a case study of the ice-rich syngenetic permafrost. *Report # FHWA-AK-RD-10-06,* prepared for ADOT & PF, AUTC assigned project #207122.

Smith, P.S., 1913. The Noatak-Kobuk region, Alaska. *U.S. Geological Survey Bulletin 536*, 160 pp.

Taber, S., 1943. Perennially frozen ground in Alaska: Its origin and history. *Bulletin of the Geological Society of America*, 54: 1433–1548.

Timofeev, V.M., Rogozinski, A.W., Hunter, J.A., and Douma, M., 1994. A new ground resistivity method for engineering and environmental geophysics. *Proceedings of the Symposium on the Application of Geophysics to Engineering and Environmental Problems*, EEGS: 701–715.

Tuck, R., 1940. Origin of the muck-silt deposits at Fairbanks, Alaska. *Bulletin of the Geological Society of America*, 51: 1295–1310.

Tumel, 1945. On permafrost survey. *Proceedings of USSR Academy of Sciences, Series of Geophysics and Geography Volume IX, Issue 2*, 137–144 (in Russian).

van Everdingen, R.O. (Ed.), 1998. *Multi-language Glossary of Permafrost and Related Ground-Ice Terms.* Calgary: Univ. of Calgary Press.

Wahrhaftig, C., 1965. Physiographic divisions of Alaska. *USGS Professional Paper 482*. Washington: United States Government Printing Office, 52 pp.

Wilkerson, A.S., 1932. Some frozen deposits in the goldfields of interior Alaska. *American Museum Novitates*, 525, 22 pp.

Williams, J.R., 1962. Geologic reconnaissance of the Yukon Flats district, Alaska. *U.S. Geological Survey Bulletin 111-H*, Washington, DC: 290–311.

Williams, J.R., and Yeend, W.E., 1979. Deep thaw lake basins in the inner Arctic Coastal Plain, Alaska. U.S. Geological Survey in Alaska: Accomplishments during 1978. Johnson, K.M., and Williams, J.R. (eds.). *USGS Circular 804-B*, B35–B37.

Yanovsky, V.K., 1933. Expedition to Pechora River to determine the position of the southern permafrost boundary. In *Reports of the Committee for Permafrost Investigations*, Vol. 5(2). Moscow-Leningrad: Akademiia Nauk SSSR, 65–149 (in Russian).

Zhestkova, T.N., 1982. *Formation of the Cryogenic Structure of Ground*. Moscow: Nauka, 209 pp. (in Russian).

Zhestkova, T., and Shur, Y., 1982. Impact of cryostructure on electrical resistivity of frozen soils. In: *Permafrost Investigations*, Vol. 20. Moscow, Moscow State University, 157–164 (in Russian).

Zykov, Y.D., 2007. *Geophysical Methods of Permafrost Investigations*. Moscow: Moscow State University (in Russian).